

# Mathematical modelling and brain dynamical networks



Awatf Alwiya

A thesis submitted for the degree of  
*Doctor of Philosophy*

Department of Mathematical Sciences  
University of Essex

January 2020

*Dedicated to  
Intidhar, Saber, Maryam and Mohammed*

## Acknowledgements

The author has the pleasure to thank Dr Chris Antonopoulos and Prof. Hadi Susanto (PhD Supervisors) for their precious guidance, patience and support throughout my PhD studies. Their guidance helped me in all the time of research and writing of this thesis.

I would also like to thank both Prof. Berthold Lausen and Dr Vanni Noferini for their numerous useful comments during supervisory panel meetings.

My thanks due to the academic and administrative staff of the Department of Mathematical Sciences at Essex university, for creating a friendly and well-organised environment for postgraduate studies. Special thank is due to Graduate Administrators.

Finally, special feeling of gratitude and appreciation to members of my family Intidhar, Saber, Maryam and Mohammed. Your endless love and support never let me feel, I am away from home.

## Abstract

In this thesis, we study the dynamics of the Hindmarsh-Rose (HR) model which studies the spike-bursting behaviour of the membrane potential of a single neuron. We study the stability of the HR system and compute its Lyapunov exponents (LEs). We consider coupled general sections of the HR system to create an undirected brain dynamical network (BDN) of  $N_n$  neurons. Then, we study the concepts of upper bound of mutual information rate (MIR) and synchronisation measure and their dependence on the values of electrical and chemical couplings. We analyse the dynamics of neurons in various regions of parameter space plots for two elementary examples of 3 neurons with two different types of electrical and chemical couplings. We plot the upper bound  $I_c$  and the order parameter  $\rho$  (the measure of synchronisation) and the two largest Lyapunov exponents  $\lambda_1$  and  $\lambda_2$  versus the chemical coupling  $g_n$  and electrical coupling  $g_l$ . We show that, even for small number of neurons, the dynamics of the system depends on the number of neurons and the type of coupling strength between them. Finally, we evolve a network of Hindmarsh-Rose neurons by increasing the entropy of the system. In particular, we choose the Kolmogorov-Sinai entropy:  $H_{KS} = \sum_{\lambda_i > 0} \lambda_i$  (Pesin identity) as the evolution rule. First, we compute the  $H_{KS}$  for a network of 4 HR neurons connected simultaneously by two undirected electrical and two undirected chemical links. We get different entropies with the use of different values for both the chemical and electrical couplings. If the entropy of the system is positive, the dynamics of the system is chaotic and if it is close to zero, the trajectory of the system converges to one of the fixed points and loses energy. Then, we evolve a network of 6 clusters of 10 neurons each. Neurons in each cluster are connected only by electrical links and their connections form small-world networks. The six clusters connect to each other only by chemical links. We compare between the combined effect of chemical and electrical couplings with the two concepts, the information flow capacity  $I_c$  and  $H_{KS}$  in evolving the BDNs and show results that the brain networks might evolve based on the principle of the maximisation of their entropies.

---

## Abbreviations

IVP	Initial Value Problem
ODE	Ordinary Differential Equation
BVP	Boundary Value Problem
MLE	Maximal Lyapunov Exponent
SDIC	Sensitive Dependence on Initial Conditions
LCEs	Lyapunov Characteristic Exponents
GS	Gram-Schmidt orthonormalisation process
LTE	Local Truncation Error
RK4	Fourth-order Runge-Kutta method
RK45	Runge-Kutta-Fehlberg method
BFS	Breadth First Search
ER	Erdős-Rényi model
WWW	World Wide Web
BA	Barabási-Albert model
WS	Watts-Strogatz model
SW	Small-World network
NW	Newman-Watts model
pdf	probability distribution function
BDNs	Brain Dynamical Networks
HH	Hodgkin-Huxley model
HR	Hindmarsh-Rose model
LEs	Lyapunov Exponents
CPU	Central Processing Unit
MI	Mutual Information
MIR	Mutual Information Rate
K-S	Kolmogorov-Sinai entropy
BEN	Brain ENtropy
fMRI	functional Magnetic Resonance Imaging
rsfMRI	resting-state fMRI
BOLD	Blood Oxygenation Level-Dependent

EEG	Electroencephalogram
GABA	Gamma-Aminobutyric Acid
RS	Regular Spiking
FS	Fast-Spiking
AdEx	Adaptive Exponential integrate-and-fire model
SampEn	Sample Entropy
SPE	Shannon Permutation Entropy
DistEn	Distribution Entropy
ApEn	Approximate Entropy

# Contents

	<b>Page</b>
<b>Acknowledgement</b>	<b>ii</b>
<b>Abstract</b>	<b>iii</b>
<b>Abbreviations</b>	<b>iv</b>
<b>Contents</b>	<b>vi</b>
<b>1 Introduction</b>	<b>1</b>
<b>2 Dynamical systems, complex systems and complex networks</b>	<b>9</b>
2.1 Dynamical systems . . . . .	9
2.1.1 Phase space . . . . .	11
2.1.2 Stability of dynamical systems . . . . .	14
2.1.2.1 Equilibria . . . . .	14
2.1.3 Bifurcation theory . . . . .	17
2.1.3.1 Local bifurcations . . . . .	18
2.1.3.2 Global bifurcations . . . . .	24
2.2 Nonlinear chaotic systems . . . . .	25
2.2.1 Sensitivity to initial conditions . . . . .	26
2.2.2 Lyapunov exponents . . . . .	26
2.2.3 The Lorenz system . . . . .	30
2.2.4 The Rössler system . . . . .	34
2.3 Numerical integration methods . . . . .	36
2.3.1 The Euler method . . . . .	36
2.3.2 The fourth-order Runge-Kutta method . . . . .	38

---

2.4	Complex systems . . . . .	39
2.4.1	Emergence . . . . .	41
2.4.2	Self-organisation . . . . .	42
2.5	Complex networks . . . . .	44
2.5.1	Shortest path-length . . . . .	49
2.5.2	Clustering coefficient . . . . .	51
2.5.3	Random networks . . . . .	52
2.5.4	Scale-free networks . . . . .	57
2.5.5	Small-world networks . . . . .	60
2.5.6	Quantifying Watts-Strogatz small-world networks . . . . .	64
<b>3</b>	<b>Biological neuron models</b>	<b>66</b>
3.1	The neuron . . . . .	66
3.2	The brain . . . . .	70
3.3	Brain plasticity . . . . .	71
3.4	Brain dynamical networks (BDNs) . . . . .	73
3.5	Biologically inspired neuron models . . . . .	75
3.6	The Hindmarsh-Rose model . . . . .	78
3.6.1	Lyapunov exponents of the Hindmarsh-Rose system . . . . .	83
3.6.2	Bifurcations in biological neuron models . . . . .	86
<b>4</b>	<b>Dynamics in networks of coupled HR systems</b>	<b>89</b>
4.1	Electrical and chemical couplings . . . . .	89
4.2	Coupled Hindmarsh-Rose systems . . . . .	91
4.2.1	Expanding the coupling terms in two coupled Hindmarsh-Rose neurons . . . . .	92
4.2.2	Lyapunov exponents of three and four coupled Hindmarsh-Rose neurons . . . . .	93
4.3	Synchronisation measures in brain dynamical networks . . . . .	96
4.4	Upper bound for Mutual Information Rate . . . . .	97
4.5	Conclusions . . . . .	104

---

<b>5</b>	<b>Evolution of networks of Hindmarsh-Rose neurons (by increasing the KS entropy)</b>	<b>107</b>
5.1	Entropy . . . . .	108
5.1.1	Clausius entropy . . . . .	108
5.1.2	Entropy in Statistical Mechanics . . . . .	112
5.1.3	Shannon entropy . . . . .	113
5.1.4	Kolmogorov-Sinai entropy . . . . .	114
5.1.5	Pesin identity . . . . .	116
5.2	Brain entropy . . . . .	118
5.3	Evolution of brain dynamical networks . . . . .	120
5.4	Evolution of Hindmarsh-Rose neurons in brain dynamical networks . . .	121
<b>6</b>	<b>Conclusions and future work</b>	<b>131</b>
6.1	Conclusions . . . . .	131
6.2	Future work . . . . .	133
	<b>References</b>	<b>138</b>

# Chapter 1

## Introduction

In this chapter, an introduction to the thesis' research subject, its objectives and approach are presented followed by brief descriptions of the content of each chapter.

The brain is by far the most complex structure in the known universe [188]. It produces our thoughts, feelings, actions, memories and experiences of the world. It contains a staggering number of nerve cells, or neurons. The neuron is the functional unit of the brain. A typical neuron consists of the soma or cell body, the dendrites, and the axon. It is a specialised cell designed to receive signals at its dendrites and transmit them to other neurons or cells through its axons [188]. Neurons communicate with one another at junctions called synapses, the site of transmission of electric nerve impulses between two neurons or between a neuron and a gland or muscle cell. The patterns of connections between neurons form the physical basis for communication in the brain.

Of the countless unexplained phenomena in the universe, the brain is the most important challenge for humanity to resolve. We need to study the brain to understand the human behaviour and mental processes. Understanding the brain is a challenge that is attracting a growing number of researchers, from many research areas. The knowledge of the brain development and functioning are shared across many disciplines such as physiology, computer science, physics, biology, mathematics, engineering, psychology, etc. Researchers are now focusing on how much the brain influences the course of health and diseases in humans. Much of what we call them degenerative disorder diseases and mental illnesses are the result of the malfunctioning of regions in the brain. In addition, many scientists are studying the relation between brain and mind. The brain is a physiological structure which produces the more abstract functioning of the mind. They try to explain the functions and processes of the brain which produce concepts related to the

mind through individual learning experiences [204]. The development of human cognition can be represented as a journey taken by the brain, from an organ of organised cells, blood vessels, and chemicals at birth, through its shaping by experiences and environment into potentially the most powerful and exquisite force in the universe, the human mind. The brain is built for sensory and motor functions and humans need to explore and make discoveries (perception), a step that leads to new thoughts or capabilities (action). Regions of the brain such as frontal cortex is associated with decision-making, problem-solving, creating images, predicting events and more, all are highly satisfying behaviours. Resources for the development of intelligence are found in the integrative regions of the brain [204].

In the past few decades, advances in science and technology have led to the development of innovative models to study the activity of neurons and how they communicate with one another. The process that incorporates the biophysical and geometrical characteristics of biological neurons and represents it by a mathematical structure is called *neuronal modelling*. This mathematical structure or model is referred to as *the model of the neuron* [128]. The objective of the neuronal modelling is to provide a quantitative description of the behaviour of the membrane potential at the neuron as it is shaped by injected currents and synaptic inputs. A good neuron models inspire new experiments and provide new insights, they can suggest what variables are most important to investigate in an experiment [96]. The variables and parameters of the model must be defined with their associated limiting assumptions to express the model properties [128]. Still, while these models have led to remarkable insights about the brain in both health and in diseases, they do have their limitations in explaining the behaviour and inner workings of neurons.

The combination of excitatory and inhibitory synaptic inputs allows neurons to perform complex information processing tasks, while brain regions which each consists of a large number of neurons can perform tasks of extraordinary complexity. In this thesis, we use simplified models of brain networks by reducing the amount of detailed information [147]. The simplified neuron models are fundamental for studying the emergent properties of neural networks. The studies of detailed neuron dynamics in simplified models at different levels of biological details provide insights into neuronal functions and allow to analyse physiological and pathological phenomena of spiking networks in simulations. Therefore, it is essential to obtain simplified neuronal models that could be at the same

---

time biologically meaningful and computationally efficient [80]. Despite decades of intense research efforts investigating the brain at the molecular, cell, circuit and system levels, the operating principles of the human brain, or any brain, remain largely unknown due to the level of complexity of the brain functions. In broad terms, we can say that we now have a fairly good understanding of how individual neurons operate and process information, but still the behaviour of networks of such neurons is poorly understood [67]. At the level of networks, most studies have focused on generic properties of models with a single or a handful of neuronal populations consisting of identical neurons with statistically identical connection properties. Such studies have given invaluable qualitative insights into the wide range of possible network dynamics. However, real brain networks have heterogeneous neural populations and more structured synaptic connections. For small networks, excellent models aiming to mimic real neural networks have been developed and many brain initiatives and projects are focusing now on creating large-scale network models for mathematical exploration of brain network dynamics [67].

The main purpose of this thesis is to study the dynamics of biological neurons. We focus on the Hindmarsh-Rose (HR) equations which model the spike-bursting behaviour of the membrane potential of a single neuron. The HR model not only simplifies the Hodgkin-Huxley (HH) model but it also mimics almost all the behaviours of real, biological neurons [110, 185]. After reviewing the development history of the model, we study and plot the spike-bursting behaviour which is exhibited by the system for specific initial conditions and parameter values.

We couple the HR system to create an undirected brain dynamical network (BDN) of  $N_n$  neurons connected simultaneously by electrical (linear coupling) and chemical (non-linear coupling) synapses. We use the coupled HR system with same parameter values and slightly different initial conditions to study the dynamics of elementary examples of three and four neurons and plot the Lyapunov exponents of the dynamics of these examples. Then, we study the concepts of upper bound of mutual information rate (MIR) and synchronisation measure and their dependence on the values of electrical and chemical couplings. The resulting dynamics of the basic HR neuron examples indicates that the two types of coupling produce different patterns of dynamics. Even for small number of neurons, it has been shown that dynamics depends on the number of neurons and the type of coupling strength between them.

---

Brain is a dynamic network which evolves over time, our goal is to evolve a network of Hindmarsh-Rose neurons by increasing the entropy of the system. In particular, we choose the Kolmogorov-Sinai entropy:  $H_{KS} = \sum_{\lambda_i > 0} \lambda_i$  (Pesin identity) as the evolution rule. We ran six realisations of the code for evolving 6 networks of coupled HR system with different pairs of chemical and electrical couplings to compare between the combined effect of chemical and electrical couplings with the two concepts, the upper bound  $I_c = \lambda_1 - \lambda_2$  and  $H_{KS}$  in evolving the BDNs and show results that brain networks might evolve based on the principle of the maximisation of their entropies.

In Chapter 2, we present the key concepts of dynamical systems. The chapter starts with a brief review of the system states, state space and evolution rules. A continuous and finite-dimensional state space is called the phase space. Then, we review two important concepts related to dynamical systems, stability of equilibria and bifurcation theory. When analysing dynamical systems, the stability of equilibria determines the dynamics of the system. On the other hand, the system's long-term behaviour depends on its parameter values. When a slight change in parameter values causes a drastic, qualitative change in the system's behaviour, this change is called a bifurcation. For systems of nonlinear differential equations, numerical integration methods are used to find numerical approximations to the analytical solutions (which exist or not). We present two time-integration schemes, namely the Euler's forward method and the fourth order Runge-Kutta method. After that, we discuss in detail two main features of nonlinear chaotic systems, the sensitive dependence on initial conditions and Lyapunov exponents. We discuss the computation of the Lyapunov exponents for continuous flows of differential equations by using the Gram-Schmidt orthonormalisation method. Two of the classical examples of chaotic systems, the Lorenz and Rössler are presented. Then, we review the concept of complex systems and two of their main features, namely emergence and self-organisation. This chapter also covers a literature review of complex networks. It explains in detail the main characteristics of complex networks; the node-degree, average node-degree, degree distribution, shortest path-length and clustering coefficient. Finally, the main three complex network types; random, scale-free and small-world networks are discussed. We review the main structural properties of each network type focusing on small-world networks and then we discuss a mathematical approach to quantify small-world networks.

In Chapter 3, we present some properties of biological neuron models. It starts by

---

reviewing briefly the anatomy of both nerve cells (neurons) and the brain. We discuss the structure of the two types of synapses: chemical and electrical and their specialised functions. The initiation of action potential, the rapid rise and subsequent fall in membrane potential is also discussed in detail. Then, we explain the concept of brain dynamical networks as complex networks and in particular, as small-world networks. We show that the topology of small-world networks can support both segregated (specialised) and distributed (integrated) information processing in brain networks. Brains perform sophisticated information processing tasks and quantitative mathematical models are tools which describe the neural dynamics and, transmission and processing of information. We briefly review the two categories of biological neuron models. Then, we discuss the Hindmarsh-Rose (HR) system which models the spike-bursting behaviour of the membrane potential of a single neuron and provide us with a good mathematical description of neuronal activity. We review the two HR models, HR 1982 and HR 1984 and then compute the Lyapunov exponents using two different time-integration schemes, the Runge-Kutta (RK4) and Euler's forward method. Finally, we briefly discuss the bifurcations appearing in biological neuron models.

In Chapter 4, we present a detailed study on the characteristics and dynamics of neurons that are connected by electrical and chemical links. First, we discuss briefly the mechanisms of information transfer and the structural organisation of the main types of synaptic transmission; chemical and electrical. Coupling strengths play a crucial role in information transmission and synchronous activities in neural systems. We couple the HR system to create an undirected brain dynamical network (BDN) of  $N_n$  neurons connected simultaneously by electrical (linear coupling) and chemical (nonlinear coupling) synapses. Then, we examine the dynamics of coupled HR neurons through elementary examples of 2, 3 and 4 neurons connected simultaneously by undirected chemical and electrical links. Synchronisation is a common feature in biological systems and plays an important role in information processing in neuronal networks. It depends on the network structural properties, dynamics of individual neurons and on coupling strengths. After that, we discuss the concepts of mutual information, mutual information rate (MIR) and the upper bound for MIR. We study the upper bound for MIR and the effect of synchrony on the dynamics of three interacting bursting neurons depending on the values of the coupling strengths. To further examine the dynamics of the system, we select three dif-

---

ferent values of chemical and electrical coupling strengths and plot the trajectories for all neurons at each value.

In Chapter 5, we review the development of the concept of entropy. In the first section, we describe the work of two physicists, Sadi Carnot and Rudolf Clausius. Carnot envisaged an ideal engine in which any heat converted into work could be reinstated by reversing the motion of the cycle. Building on the work of Carnot, Rudolf Clausius presented the first-ever mathematical formulation of entropy. His work stated the second law of thermodynamics. In 1877, the Austrian physicist Ludwig Boltzmann developed a statistical mechanics approach to define entropy. Later, Josiah Gibbs extended Boltzmann's entropy formula to cases where the microstates of the system that realise the macrostate may have different probabilities of occurring. Information entropy which represents a fundamental concept in information theory, was developed by Claude Shannon during his work to quantify mathematically the statistical nature of "lost information" in phone-line signals in 1948. After that, we review the metric entropy also known as Kolmogorov-Sinai entropy which is based on Shannon entropy. The entropy in dynamical systems was originally studied by the Russian mathematician Andrei Kolmogorov and later improved by his student, Yakov Sinai. The Pesin identity relates the Kolmogorov-Sinai entropy to positive Lyapunov exponents. Then, we briefly review the concept of brain entropy which can provide an informative tool to assess brain states and functions. We also explain the use of two entropy-derived measures, functional magnetic resonance imaging and electroencephalogram which have been used in mapping brain entropy for evaluating the physiological complexity in neuroscience. Finally, we discuss the topic of the evolution of brain dynamical networks. In evolving dynamical networks; topology, dynamics and evolution are all affecting one another. The dynamical processes that take place over the network structure are coupled to the evolutionary rules of the network itself. We used the Kolmogorov-Sinai entropy,  $H_{KS}$ , which is equal to the summation of the positive Lyapunov exponents (Pesin identity) as the evolutionary rule to evolve a network of coupled Hindmarsh-Rose neurons. We ran six realisations of the code evolving 6 networks of coupled HR system with different pairs of chemical and electrical couplings to compare between the combined effect of chemical and electrical couplings with the two concepts, the upper bound  $I_c$  and  $H_{KS}$  in evolving the BDNs and show results that brain networks might evolve based on the principle of the maximisation of their entropies.

In Chapter 6, we discuss the main results of the thesis regarding the dynamics of Hindmarsh-Rose neuronal model and the evolution of HR neuron networks. In the Future Work section, we review briefly the neuronal models which we have suggested for future work: the fractional-order Hindmarsh-Rose model, the time-delay Hindmarsh-Rose model, the simple model of spiking neurons and the adaptive exponential integrate-and-fire model. In addition, the study of the entropy-based metrics represents another interesting approach in studying brain dynamical networks.

The work in this thesis offers an overview of this challenging, stimulating and yet promising field of research, putting the main subject of BDN into perspective. Most of the research papers on BDNs are dealing with two important concepts related to biological neuron models, synchronisation and bifurcations. In this research, we explore other important concepts, namely mutual information rate (MIR) and entropy. In Ref. [27], the authors derived the upper bound of mutual information rate,  $I_c$  which is equal to the difference between the largest and the second largest Lyapunov exponents. This work inspired us to concentrate our work on studying Lyapunov exponents of Hindmarsh-Rose model and the two concepts which depend on its LEs, the upper bound of MIR:  $I_c = \lambda_1 - \lambda_2$  and the Kolmogorov-Sinai entropy:  $H_{KS} = \sum_{\lambda_i > 0} \lambda_i$  (Pesin identity). In Ref. [20], the authors have used the upper bound for MIR to propose a working hypothesis that brain networks evolve based on the principle of the maximisation of their internal information flow capacity. We proposed that the amount of the increase of the entropy of the system can be another approach that we used to evolve HR networks in this thesis. We investigate the relation between  $I_c$  and  $H_{KS}$  during the evolution process of the networks of HR neurons. The main novelties of this thesis are

- Detailed study of Lyapunov exponents of HR model.
- Most research papers depend on one type of coupling strength. We used both coupling strengths, the chemical and the electrical in basic examples of HR neurons to show that dynamics of the system depends on the number of neurons and the type of coupling strength between them.
- Researchers use entropy-based metrics in mapping brain regions. We construct networks of 60 HR neurons with small-world properties and compute the  $H_{KS}$  entropy for the HR networks. Then, we investigate the relation between entropy and

the evolution of HR networks.

- Proposing another approach for evolving HR networks by increasing the entropy of the system.
- Evolving networks of HR neurons by increasing the entropy of the system and investigating the relation between  $I_c$  and  $H_{KS}$  during the evolution process.

The results from the work with six realisations of the code evolving 6 networks of coupled HR system with different pairs of chemical and electrical couplings, show that brain networks might evolve based on the principle of the maximisation of their entropies. The relation between the upper bound and entropy during the evolution of brain networks can provide new insights on how BDNs evolve and it needs further research with much larger size networks.

# Chapter 2

## Dynamical systems, complex systems and complex networks

### Introduction

In this chapter, we will present basic concepts of dynamical systems, complex systems and complex networks. We briefly review the states, state space, phase space and evolution rules which describe a system that evolves in time. Then, we review two important concepts related to dynamical systems, stability of equilibria and bifurcation theory. We discuss in more details the main features of nonlinear chaotic systems and the Lorenz and Rössler are presented. We review the concept of complex systems and their two main features, emergence and self-organisation. After that, we explain the characteristics of complex networks and reviewing the three main complex network models; random, scale-free and small-world networks.

### 2.1 Dynamical systems

A *dynamical system* is a system whose states are uniquely specified by a set of variables and whose behaviour is described by predefined rules which describe its temporal evolution. Dynamical systems can be described over either discrete-time steps or along a continuous-time line. Such systems consist of their *states*, an abstract *state space* or *phase space*, whose coordinates describe a state at any instant, and an *evolution rule* that specifies the immediate future of all state variables, given only their present values.

The state space of a dynamical system is an abstract space where every state of the system is mapped to a unique spatial location [172]. It is the set of all possible values of the state variables that completely describe the state of the dynamical system. The state

space can be either discrete, consisting of isolated points such as when the state variables can only take on integer values or it can be continuous, consisting of a smooth set of points, such as when the state variables can take on any real value. In the case where the state space is continuous and finite-dimensional, it is often called the phase space. The state space can also be infinite-dimensional. The number of state variables in a dynamical system represents the dimension of the system.

Dynamical systems describe the evolution with respect to time of all points of a given space  $S$ . Mathematically,  $S$  can be an Euclidean space or an open subset of an Euclidean space or some other space such as a surface in  $\mathbb{R}^n$ ,  $n \in \mathbb{Z}$  [99]. The rule of the time evolution of the dynamical system must be defined to make the state variables completely describe the state of the system. Our world is modelled with dynamical systems; population growth, weather systems, epidemics, traffic jams and economies at all scales are examples of dynamical systems.

Given an initial position  $x \in \mathbb{R}^n$ , a dynamical system on  $\mathbb{R}^n$  tells us where  $x$  will be located 1 unit of time later, 2 units of time later, and so on. At time zero,  $x$  is located at position  $x_0$ . One unit after time zero,  $x$  is at  $x_1$ , etc. In general, the “trajectory” of  $x$  is given by  $x_t$ . The function that takes  $t$  to  $x_t$  yields either a sequence of points or a curve in  $\mathbb{R}^n$  which represents the life history of  $x$  as time runs from  $x_0$  to infinity. If we measure the positions of  $x_t$  using only integer time values, we have an example of a discrete dynamical system. If time is measured continuously with  $t \in \mathbb{R}^n$ , we have a continuous dynamical system. If the system depends on time in a continuously differentiable manner, then we have a smooth dynamical system. These are the three principal types of dynamical systems that arise in the study of systems of differential equations [99].

### Definition 1

*Let  $x = (x_1, \dots, x_n)$  be a point in the  $n$ -dimensional space  $\mathbb{R}^n$  that traces out a curve through time. We can describe it as*

$$x \equiv x(t) = (x_1(t), \dots, x_n(t))$$

*Often we do not know  $x(t)$  directly, but we know the rate and direction of change in some region of  $\mathbb{R}^n$ . Thus, we have*

$$\dot{x} = f(x), \quad x \in \mathbb{R}^n,$$

where  $\dot{x}$  indicates the derivative with respect to  $t$  as we always assume that  $f$  has partial derivatives. We call  $x(t)$  a solution to the dynamical system if it satisfies such a set of ordinary differential equations, in the sense that  $\dot{x}(t) = f(x(t))$  for  $t$  in some (possibly infinite) interval.

A dynamical system is *deterministic* if there is a unique consequence to every change of the system variables or initial states that uniquely determine its past and future trajectories [162], or *stochastic* (or *random*) if there is more than one possible consequence for a change in its variables or initial states according to some probability distribution. In deterministic dynamical systems, trajectories never intersect in its phase space (though they could merge), because if they did, that would mean having multiple future states and that is a violation to the deterministic nature of the system. Once we specify an initial state of the system, the trajectory that follows is uniquely determined [172].

### 2.1.1 Phase space

In studying the behaviour of a dynamical system, we use the concept of a *phase space*, which is informally defined as a theoretical space where every state of the system is mapped to a unique spatial location. The number of state variables needed to uniquely specify a state of the system is called the *degrees of freedom* in the system. By having an axis for each degree of freedom, one can construct a phase space of a system, i.e. by taking each state variable as one of its orthogonal axes. Therefore, the system's degrees of freedom equal the dimensions of its phase space [172]. A 1-dimensional system is called a *phase line*, while a 2-dimensional system is called a *phase plane*. For every possible state of the system a point is included in the multidimensional space. The system's evolving state over time traces a path through the high-dimensional space and is called the *trajectory* or *orbit*,  $x(t)$  of the system's phase space. Consider an autonomous system (i.e. it does not explicitly depend on the independent variable  $t$ ) of first-order ordinary differential equations of the form

$$\dot{x} = F(x), \tag{2.1.1}$$

where  $x(t) \in \mathbb{R}^n$  is a vector of dependent variables and  $F : \mathbb{R}^n \rightarrow \mathbb{R}^n$  is a vector field. The trajectories are integral curves of the vector field  $F$  and each point in the vector field has a tangent to an integral curve. The existence and uniqueness theorem for *Initial Value*

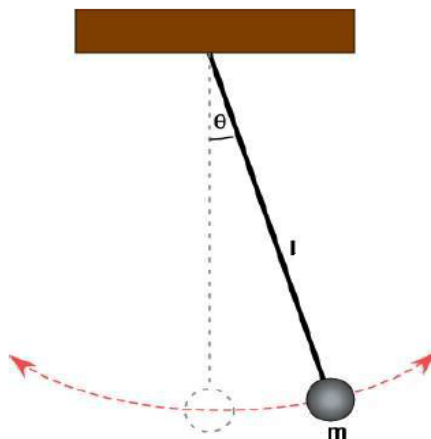


Figure 2.1: A diagram of undamped pendulum.  $l$  is the length,  $m$  the mass and  $\theta$  the angle of the pendulum [9].

*Problems* (IVPs) implies that if the vector field  $F(x)$  is smooth (i.e. every one of its  $n$  defining functions,  $f_1, \dots, f_n$ , has derivatives of any order with respect to any variables, at any point in the domain of  $f_i$ ), then a unique trajectory passes through each point of phase space and that trajectories cannot cross themselves [106].

A phase space trajectory represents by set of states starting from one particular initial condition. An undamped pendulum consists of a single particle mass that swings in a plane and represents an example of a phase space. The differential equation which describes the motion of the undamped pendulum is

$$\frac{d^2\theta}{dt^2} + \frac{g}{l} \sin \theta = 0, \quad (2.1.2)$$

where  $\theta$  is the angular displacement,  $g$  the gravitational acceleration and  $l$  the length of the pendulum [18] (see Fig. 2.1). The dynamical system describing an undamped pendulum requires two state variables; the angle  $\theta$  of the pendulum and its angular velocity  $v = \frac{d\theta}{dt}$ . These two variables completely describe the state of the pendulum. The initial angle and angular velocity of the system is  $(\theta_0, v_0) = (\theta(0), v(0))$  and its trajectory which indicates the state at time  $t$  is  $(\theta(t), v(t))$ . The phase state  $(\theta, v)$  is periodic in  $\theta$  and the range is  $-\pi \leq \theta < \pi$  (see Fig. 2.2). If one draws the system's states in a Cartesian plane coordinate system, one can get an ellipsis or a circle that fully describes all possible states of the pendulum.

A plot of the system's variables as a function of time is sometimes called a *phase plot* or a *phase diagram*. One of the benefits of plotting a phase space is that it allows us to

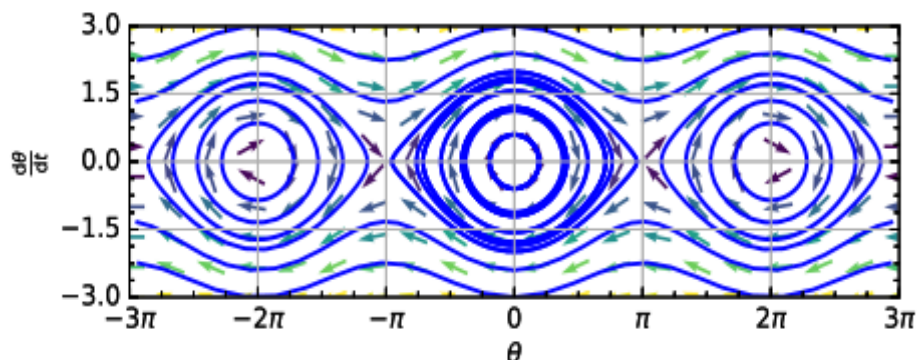


Figure 2.2: The phase space of the motion of undamped pendulum.  $\theta$  is the angular displacement and  $v = \frac{d\theta}{dt}$  is the angular velocity [11].

represent visually the dynamical behaviour of a system as a static trajectory. From phase space visualisations, one can learn about what will eventually happen to a system's state in the long run.

Trajectories may diverge to infinity, converge to a certain point, or remain dynamically changing yet staying in a confined region in the phase space from which no outgoing trajectories are running out. This converging point or a region is called an *attractor*. The set of all the initial states which will eventually end up falling into that attractor is called the *basin of attraction* of that attractor [18]. The concept of attractors is particularly important for understanding the behaviour of the system. If the system has more than one attractor in the phase space, one can divide the phase space into several different regions and that reveals how sensitive the system is to its initial conditions. Otherwise, if one region is dominating in the phase space, the system's fate doesn't depend much on its initial condition. The system's state is stable in a specific area if trajectories are converging to that area and it is unstable if trajectories are diverging from it [172].

Historically, Carl Gustav Jacobi and Ludwig Boltzmann invented the concept of the phase space and discovered the conserved volumes in it, but in his lectures, Boltzmann gave French mathematician Joseph Liouville the credit as the first one who used it. The view of a dynamical system as a single trajectory is made by analogy to a curve rather than made explicitly, first appeared in Boltzmann's "*Lectures on Gas Theory*" in 1896 [39]. The explicit reference to the trajectory of the phase point in a high-dimensional space, later appeared in Josiah Gibbs "*Elementary Principles in Statistical Mechanics*" in

1902 [83]. Henri Poincaré carried out much of the work in phase space. He introduced new tools and geometric approaches that have become essential topics of modern dynamics. Among his contributions are *Poincaré maps* which plot where trajectories intersect a specified section of phase space and equilibria classifications that categorise various types of equilibrium behaviour [150].

## 2.1.2 Stability of dynamical systems

When we talk about the *stability of a dynamical system*, we talk about the stability of its solutions (trajectories) under small perturbations of their initial conditions. In general, perturbing the initial state in some directions can change the behaviour of the trajectory. Stability means that the trajectories do not change too much under small perturbations. The qualitative behaviour of trajectories under perturbations can be analysed by using the *linear stability analysis* of nonlinear systems. The linear stability analysis is an analytical method to determine the stability of the system at or near its equilibrium point by approximating its dynamics around that point as a linear dynamical system [172]. The simplest kind of behaviour of a trajectory is exhibited by equilibrium points. An *equilibrium point* (also known as the *critical point* and the *stationary solution*) is a constant solution to a differential equation, whose derivative is zero for all times  $t$ .

### 2.1.2.1 Equilibria

The study of equilibria plays a central role in nonlinear systems of ordinary differential equations and their applications [99]. The stability of equilibria determines the dynamics of the system. Trajectories around a stable equilibrium point remain close even with small perturbations. On the other hand, trajectories around an unstable equilibrium point move away from it for small perturbations [133]!

Let us consider a general, 2-dimensional, autonomous system,

$$\begin{aligned}\dot{x} &= f(x, y), \\ \dot{y} &= g(x, y),\end{aligned}\tag{2.1.3}$$

with a given initial conditions  $(x_0, y_0)$  at time  $t = t_0$ , where  $f$  and  $g$  are smooth nonlinear functions. The path travelled by the solution of the system starting from the initial state  $(x_0, y_0)$  is a trajectory, or the orbit of the system [55]. To distinguish a solution from

the system state that produces it, and indicate its dependence on the initial condition, we denote it by  $\varphi_t(x_0, y_0)$  where  $\varphi_{t_0}(x_0, y_0) = (x_0, y_0)$ . In  $x - y$  plane, any solution  $\varphi_t(x, y)$  of an autonomous system which is considered as a family of trajectories with different initial conditions, is called a *flow*. *Equilibria*, or *fixed points*, if exist, are the solutions  $(x, y)$  that satisfy simultaneously the following two homogeneous equations:

$$f = 0 \text{ and } g = 0. \quad (2.1.4)$$

Equilibria are often among the most important solutions of any dynamical system. They are time-independent, constant solutions. We can determine the stability of dynamical systems by examining the behaviour of their solutions nearby equilibria. An equilibrium point, which is usually denoted by  $(x^*, y^*)$  and is a solution of Eq. (2.1.4), can be *stable*, if all nearby trajectories approach it and *unstable*, if nearby trajectories drift away from it [55].

In particular, let  $\lambda_1$  and  $\lambda_2$  be the eigenvalues of the Jacobian matrix of the dynamical system (2.1.3)

$$J = \begin{pmatrix} f_x & f_y \\ g_x & g_y \end{pmatrix}, \quad (2.1.5)$$

where  $f_x$  is the derivative of  $f$  with respect to  $x$ , etc. All the derivatives of the matrix must be evaluated at the equilibrium point  $(x^*, y^*)$ , and the dominant eigenvalue  $\lambda_d$  determines the overall stability of the equilibrium point, although it would generally require a nonlinear analysis to show that the equilibrium point is truly neutral (Lyapunov stable) [172]. Figures 2.3 and 2.4 show several types of equilibrium points for both discrete- and continuous-time dynamical systems. For the continuous dynamical systems (2.1.3), we can classify the types of its equilibria depending on the values of the real parts of  $\lambda_1$  and  $\lambda_2$ , the two eigenvalues of the Jacobian matrix (2.1.5) which represent the roots of the characteristic equation of the system

$$\lambda^2 - tr(J)\lambda + det(J) = 0, \quad (2.1.6)$$

where  $tr(J)$  is the trace and  $det(J)$  is the determinant of the Jacobian matrix.

For distinct nonzero real eigenvalues, we have the following cases [18]:

- If  $\lambda_1 < 0$  and  $\lambda_2 < 0$ , the equilibrium point is a *stable node* and all trajectories that

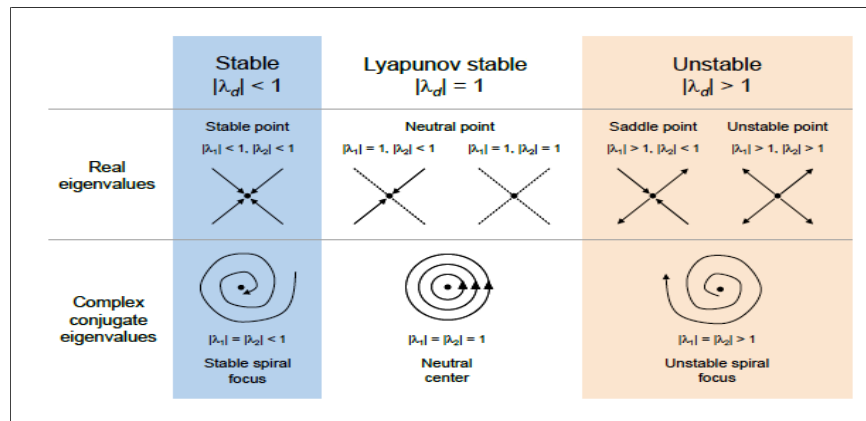


Figure 2.3: Stability of equilibrium points in discrete-time dynamical systems [172].

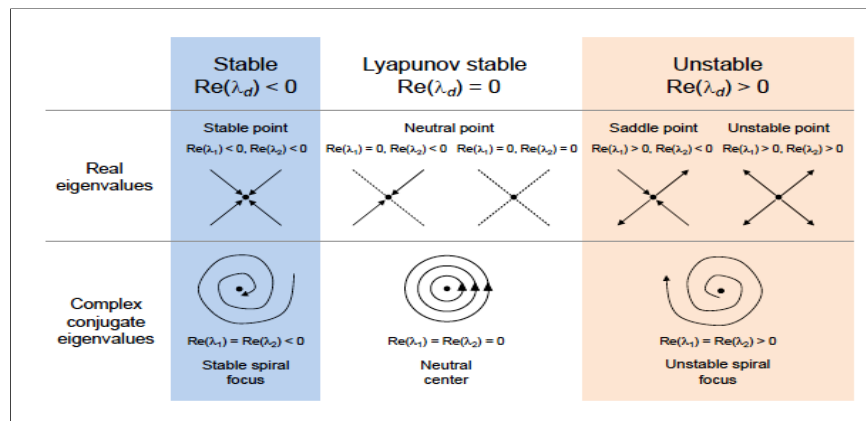


Figure 2.4: Stability of equilibrium points in continuous-time dynamical systems [172].

start near it move toward the attracting equilibrium point as  $t \rightarrow \infty$ .

- If  $\lambda_1 = 0$  and  $\lambda_2 = 0$ , for the linear systems the equilibrium point is a *neutral point* and all trajectories that start sufficiently close to it remain close to it for all times. However, for the nonlinear systems it requires a nonlinear analysis to show that the equilibrium point is truly neutral (Lyapunov stable) [172].
- If  $\lambda_1 > 0$  and  $\lambda_2 > 0$ , the equilibrium point is an *unstable node* and all trajectories that start near it move away from the repelling equilibrium point as  $t \rightarrow \infty$ .
- If  $\lambda_1 > 0$  and  $\lambda_2 < 0$ , the equilibrium point is a *saddle point*. The trajectories that start near it move toward the equilibrium point in one direction and move away from it in the other direction as  $t \rightarrow \infty$ .

In case of repeated nonzero real eigenvalues (*degenerate case*), we have two other

types of equilibria, *star* and *singular nodes*. Both equilibria can be stable and unstable depending on the values of the real parts of the eigenvalues.

For complex conjugate eigenvalues, we have three other cases:

- If  $Re(\lambda_1) = Re(\lambda_2) < 0$ , the equilibrium point is a *stable spiral* and all trajectories spiral toward the equilibrium point.
- If  $Re(\lambda_1) = Re(\lambda_2) = 0$ , the equilibrium point requires a nonlinear analysis to show that it is a *neutral centre*. Trajectories neither approach the centre nor move away from it. They move in closed curves or cycles around it.
- If  $Re(\lambda_1) = Re(\lambda_2) > 0$ , the equilibrium point is an *unstable spiral* and all trajectories spiral away from the equilibrium point [18, 55, 99].

If the system has an eigenvalue with zero real part, then there exists a line of equilibrium points. The behaviour of trajectories depends on the sign of  $\lambda_i$ , they may move toward or get away from the line of equilibrium points [31].

### 2.1.3 Bifurcation theory

In analysing any dynamical system, one of the most important questions that need to be answered is how the system's long-term behaviour depends on its parameter values. Most of the time, one can assume that a slight change in their values causes only a slight quantitative change in the system's behaviour with the essential structure of the system's phase space unchanged. However, sometimes we may witness that a slight change in parameter values causes a drastic, qualitative change in the system's behaviour and the structure of its phase space topologically altered. This change is called a *bifurcation*, and the parameter values at which a bifurcation occurs are called the *critical thresholds* or *bifurcation points*. In many real-world systems, bifurcations play important roles as a switching mechanism. Examples include excitation of neurons, pattern formation, complex circuits, networks, and catastrophic transition of ecosystem states, to name a few [172]. Various types of bifurcations exist in nonlinear dynamical systems and they can be important and beneficial if they are under appropriate control. However, not all nonlinear dynamical systems have bifurcations [54]. There are two categories of bifurcations: local and global, and we will discuss them briefly next.

### 2.1.3.1 Local bifurcations

A *local bifurcation* can be characterised and analysed entirely through changes in the local stability properties of an equilibrium point. It is called local because it can be detected and analysed only by using localised information around the equilibrium point. The local bifurcations occur when the eigenvalues  $\lambda_i$  of the Jacobian matrix of the linearised system, evaluated at an equilibrium point satisfy the following properties:

- For discrete-time models:  $|\lambda_i| = 1$  for some  $i$ , while  $|\lambda_j| < 1$  for  $j \neq i$ .
- For continuous-time models:  $Re(\lambda_i) = 0$  for some  $i$ , while  $Re(\lambda_j) < 0$  for  $j \neq i$ .

The previous conditions describe a critical situation when the equilibrium point is about to change its stability. We can formulate these conditions in equations and then solve them in terms of the parameters to obtain their critical thresholds [172]. Near a bifurcation point, the dynamical system can be reduced to a generic mathematical form by a change of variables and a reduction of its dimension in order to keep only the directions implied in the bifurcation. Those reduced mathematical expressions are called *normal forms* [66, 158] and each one of them is associated to a type of bifurcation. This normal form reduction proves to be convenient for a discussion of local bifurcation as the reduction in dimensionality proves especially helpful in the bifurcation analysis of high-dimensional systems.

Bifurcations are classified according to how the stability of an equilibrium solution changes. There are two ways in which this can occur, either an eigenvalue of the system linearised about the equilibrium solution can pass through zero, or a pair of non-zero eigenvalues may cross the imaginary axis [177]. Types of local bifurcations include:

- Saddle-node bifurcations.

A *saddle-node* bifurcation is represented by the collision and disappearance of two equilibria at the bifurcation point. In systems generated by autonomous ODEs, this occurs when the critical equilibrium has only one zero eigenvalue. This phenomenon is also called *fold* or *tangent* bifurcation. The name saddle-node comes from the corresponding 2-dimensional bifurcation in the phase plane,

$$\begin{aligned}\dot{x} &= \mu - x^2, \\ \dot{y} &= -y,\end{aligned}\tag{2.1.7}$$

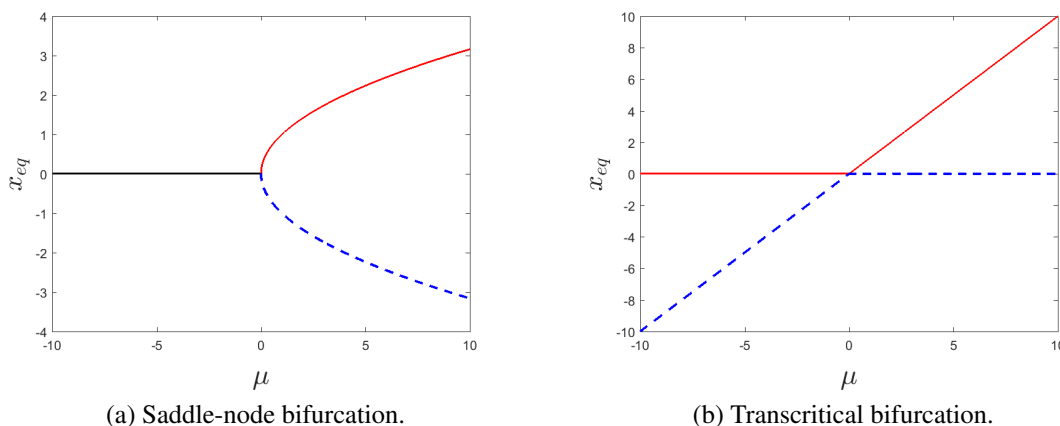


Figure 2.5: Saddle-node and transcritical bifurcations. The solid red line corresponds to the set of stable equilibrium points and the dashed blue line to the set of unstable equilibrium points.

in which a saddle point and a node coalesce and disappear, but the other dimension plays no essential role and this bifurcation is one-dimensional in nature.

For a first-order autonomous dynamical system, the normal form of a saddle-node bifurcation is

$$\dot{x} = F(x) = \mu - x^2. \quad (2.1.8)$$

The ODE (2.1.8) has two equilibria  $x_{eq} = \pm\sqrt{\mu}$ . The critical condition at which a bifurcation occurs in this system is given by  $\frac{dF(x)}{dx}\big|_{x=x_{eq}} = 0$ . Then,

$$\frac{dF(x)}{dx}\bigg|_{x_{eq}=\pm\sqrt{\mu}} = -2x\bigg|_{x_{eq}=\pm\sqrt{\mu}} = \pm 2\sqrt{\mu}. \quad (2.1.9)$$

Therefore, the bifurcation occurs when  $\mu = 0$ . Moreover, by plugging each equilibrium of (2.1.8) into (2.1.9), we know that one equilibrium point is stable and the other is unstable. We can summarise the results as follows [172]:

- For  $\mu < 0$ : both equilibria  $x_{eq} = \sqrt{\mu}$  and  $x_{eq} = -\sqrt{\mu}$  do not exist.
- For  $\mu > 0$ :  $x_{eq} = \sqrt{\mu}$  is stable and  $x_{eq} = -\sqrt{\mu}$  is unstable.

We refer to this bifurcation as a *supercritical* saddle-node bifurcation (Fig. 2.5a), since the equilibria appear at the bifurcation point  $(x, \mu) = (0, 0)$  as  $\mu$  increases through zero. With the opposite sign  $\dot{x} = \mu + x^2$ , the bifurcation is called *subcritical* saddle-node and the equilibria appear at the bifurcation point  $(x, \mu) = (0, 0)$  as  $\mu$  decreases through zero [106].

- Transcritical bifurcation.

This type of bifurcation occurs where one equilibrium point “passes through” another, changing their stabilities. This phenomenon is referred to as an *exchange of stability* [172]. The *transcritical* bifurcation arises in systems where there is some trivial solution branch, corresponding here to  $x = 0$  and that exists for all values of the parameter  $\mu$  (in saddle-node bifurcation, the solution branches exist locally on only one side of the bifurcation point). There is a second solution branch  $x = \mu$  that crosses the first one at the bifurcation point  $(x, \mu) = (0, 0)$ . The normal form of transcritical bifurcation is

$$\dot{x} = F(x) = \mu x - x^2. \quad (2.1.10)$$

This dynamical system always has the following two equilibria:  $x_{eq} = 0$  and  $x_{eq} = \mu$ .

$$\begin{aligned} \left. \frac{dF(x)}{dx} \right|_{x_{eq}} &= \mu - 2x, \\ \left. \frac{dF(x)}{dx} \right|_{x_{eq}=0} &= \mu, \\ \left. \frac{dF(x)}{dx} \right|_{x_{eq}=\mu} &= -\mu. \end{aligned} \quad (2.1.11)$$

The equilibrium  $x_{eq} = 0$  is stable for  $\mu < 0$  and unstable for  $\mu > 0$ , while the equilibrium  $x_{eq} = \mu$  is unstable for  $\mu < 0$  and stable for  $\mu > 0$  (Fig. 2.5b). Thus, the two branches have opposite stabilities and when cross one solution goes from stable to unstable while the other goes from unstable to stable [106].

- Pitchfork bifurcation.

In *pitchfork* bifurcation, an equilibrium point splits into three. The two outermost equilibria have the same stability as the original equilibrium point, while the one in between has opposite stability to the original [172]. There are two types of pitchfork bifurcations, the *supercritical* pitchfork if the nontrivial equilibrium points occur for parameter values greater than the bifurcation value. The normal form with the opposite sign of the nonlinearity is called *subcritical* pitchfork if the nontrivial equilibrium points occur for values of parameter lower than the bifurcation value [113]. The normal form of supercritical pitchfork, in which a stable equilibrium

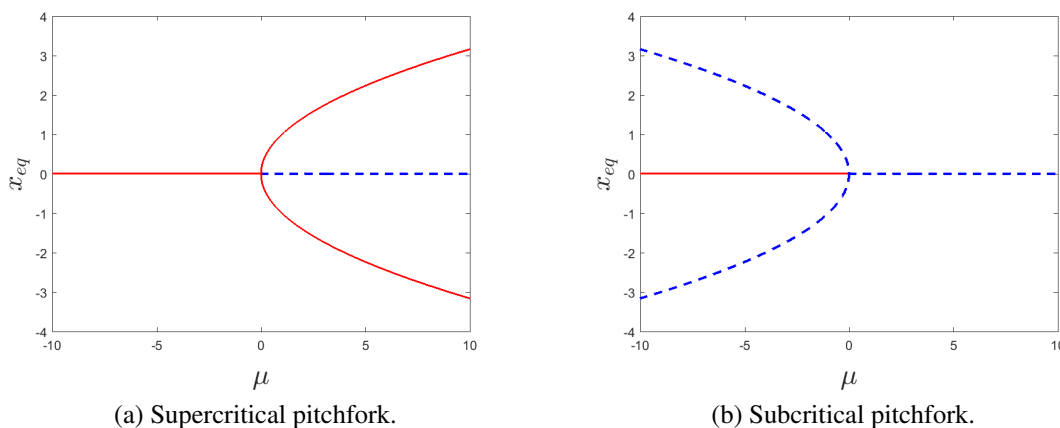


Figure 2.6: Supercritical and subcritical pitchfork bifurcations. The solid red line corresponds to the set of stable equilibrium points and the dashed blue line to the set of unstable equilibrium points.

point splits into three, two stable and one unstable is:

$$\dot{x} = \mu x - x^3. \quad (2.1.12)$$

This dynamical system has the following three equilibrium points:  $x_{eq} = (0, \pm\sqrt{\mu})$ . The two equilibrium points:  $x_{eq} = \pm\sqrt{\mu}$  exist only for  $\mu \geq 0$ . The equilibrium point  $x_{eq} = 0$  is stable for  $\mu < 0$  and unstable for  $\mu > 0$  while  $x_{eq} = \pm\sqrt{\mu}$  are always stable for  $\mu > 0$  (Fig. 2.6a). When the system crosses the bifurcation point coming from  $\mu < 0$ , it has to choose one of the two stable branches of the pitchfork and this choice is called a *symmetry breaking*.

The normal form of subcritical pitchfork which makes an unstable equilibrium point split into three, two unstable and one stable is:

$$\dot{x} = \mu x + x^3. \quad (2.1.13)$$

This dynamical system has the following three equilibrium points:  $x_{eq} = (0, \pm\sqrt{-\mu})$ , but the two equilibrium points  $x_{eq} = \pm\sqrt{-\mu}$  exist only for  $\mu \leq 0$  (Fig. 2.6b). Pitchfork bifurcations are generic to problems that have symmetry. Note that equation (2.1.12) is invariant under the change of variables  $x \rightarrow -x$  [106].

- Period doubling (flip) bifurcation.

A *period doubling* bifurcation corresponds to the creation or destruction of a periodic orbit with double the period of the original orbit. A period-doubling bifurca-

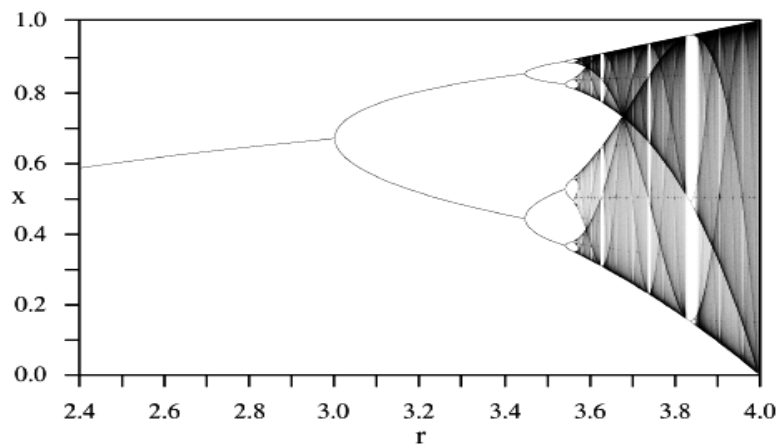


Figure 2.7: Period doubling bifurcation for the logistic map. The equilibrium  $x$  versus the parameter  $r$  [10].

tion occurs in both discrete and continuous dynamical systems. In a discrete system, a slight change in a parameter value in the system's equations leads to the system switching to a new behaviour with twice the period of the original system. In the following simplified version of the logistic map [18],

$$x_{n+1} = rx_n(1 - x_n), \quad (2.1.14)$$

where  $x_n$  is the value of  $x$  at time  $n$  and lies in the interval  $(0, 1]$ ,  $x_n$  changes over time and that depends on the values of the parameter  $r \in (0, 4]$ . For values of  $r$  between 1 and 3,  $x_n$  converges to a stable fixed point  $x^* = \frac{r-1}{r}$ . Then, it converges to a permanent oscillation between the fixed point  $x^*$  and the differential equation  $\dot{x}$  for values of  $r$  between 3 and 3.4494. Period doublings appears at  $r \approx 3.5699$  (see Fig. 2.7).

Period doubling bifurcations in continuous dynamical systems begin with a limit cycle behaviour. The limit cycle appears from a bifurcation involving a node or other fixed point and then it becomes unstable with the change of the control parameter. The main difference in case of period doubling bifurcation between a map and a differential equation is that for a map, at certain value of the control parameter, the fixed point first undergoes a period doubling bifurcation. This produces a period-2 solution which undergoes a second period doubling again at certain other values of the control parameter. However, for a system of differential equations, the first bifurcation is a Hopf bifurcation which produces a self-sustained oscillation,

and the second bifurcation is the first period doubling bifurcation of the periodic orbit. This indicates that the considered Hopf bifurcation is supercritical generating a stable limit cycle of the system [170].

A *period doubling cascade* is a sequence of doubling the repeating period, as the parameter is adjusted further and further. Cascades of period doubling bifurcations have been observed in many dynamical systems, both dissipative and conservative. Whereas, a *period halving* bifurcation is a bifurcation in which the system switches to a new behaviour with half the period of the original system. A series of period halving bifurcations can lead the system from chaos to order.

In general, the bifurcation phenomena that occur in one-dimensional nonlinear systems are usually referred to as *static* bifurcations. In higher dimensional systems, as the situation is more complicated, bifurcations in systems of dimension two or higher such as the Hopf bifurcation, are referred to as *dynamic* bifurcations [54].

- Hopf bifurcation.

A *Hopf* or *Poincare-Andronov-Hopf* bifurcation is a local bifurcation in which an equilibrium point of a dynamical system with two or more variables, loses stability as a pair of complex conjugate eigenvalues of the Jacobian matrix at the equilibrium point cross the imaginary axis of the complex plane (see Fig. 2.8) [113]. A Hopf bifurcation typically causes the appearance (or disappearance) of a limit cycle around the equilibrium point. A *limit cycle* is an isolated, closed trajectory in the phase space. When the pair of complex conjugate eigenvalues moves from the left-half plane to the right, crossing the imaginary axis, all the other eigenvalues remain stable. At the moment of crossing, the real parts of the two eigenvalues become zero, and the stability of the existing equilibrium changes from stable to unstable and a limit cycle appears at the moment of crossing [18, 54].

Consider the 2-dimensional system

$$\begin{aligned}\dot{x} &= y + \mu x, \\ \dot{y} &= -x + \mu y,\end{aligned}\tag{2.1.15}$$

where  $\mu$  is the bifurcation parameter. Then, the Jacobian matrix of the two dimen-

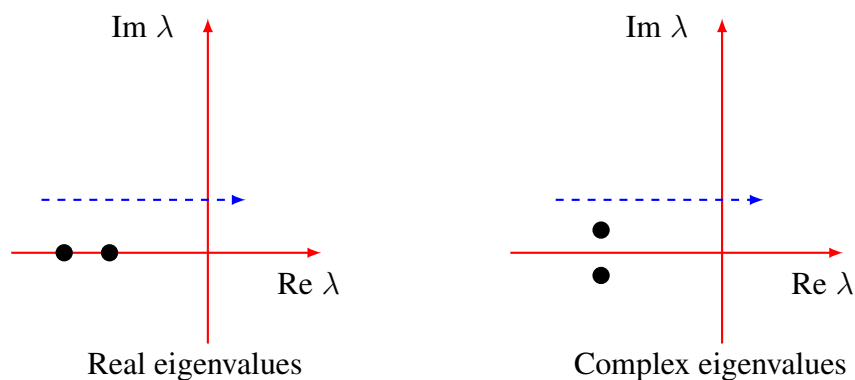


Figure 2.8: Real eigenvalues in supercritical saddle-node, transcritical and supercritical pitchfork bifurcations cross into the right half plane (in the direction of the blue dashed line). Complex conjugate eigenvalues in Hopf bifurcation simultaneously cross the imaginary axis into the right half plane (in the direction of the blue dashed line).

sional system is

$$J = \begin{pmatrix} \mu & 1 \\ -1 & \mu \end{pmatrix}, \quad (2.1.16)$$

for which the eigenvalues are  $\lambda_{1,2} = \mu \pm i$  where  $Re(\lambda_{1,2}) = \mu$  and  $Im(\lambda_{1,2}) = \pm i$ .

For  $\mu = 0$ , we have  $Re(\lambda_{1,2}) = 0$  and  $Im(\lambda_{1,2}) \neq 0$ . Hence, we can conclude that there exists a periodic solution for  $\mu = 0$  in every neighborhood of the origin [113].

### 2.1.3.2 Global bifurcations

A *global bifurcation* occurs when non-local features of the phase space, such as limit cycles collide with equilibria in a phase space. This type of bifurcation cannot be characterised by using only localised information around the equilibrium point. The changes in the topology of the trajectories in the phase space cannot be confined in a small neighbourhood, as is the case with local bifurcations. In fact, the changes in topology extend out to an arbitrarily large distance. Types of global bifurcations include Homoclinic and Heteroclinic bifurcations [87].

In a bifurcation, the number of parameters which must be varied for the bifurcation to occur is called the *codimension* of a bifurcation. Saddle-node bifurcations, where the equilibrium has a simple eigenvalue  $\lambda_1 = 0$  and no other eigenvalues with zero real part and Hopf bifurcations where the equilibrium has a simple pair of purely imaginary eigenvalues  $\lambda_{1,2} = iw_0, w_0 > 0$  and no other eigenvalues with zero real part, are the only generic local bifurcations which are really codimension-one. All others types of

bifurcations have higher codimension. However, transcritical and pitchfork bifurcations are often thought of as codimension-one, because the normal forms can be written with only one parameter.

## 2.2 Nonlinear chaotic systems

The science of nonlinear dynamics and chaos theory has sparked many researchers to develop mathematical models that simulate vector fields of nonlinear chaotic physical systems. In Mathematics and Physics, chaos theory is a mathematical sub-discipline that studies such systems and deals with the behaviour of certain nonlinear dynamical systems that under certain conditions exhibit an unpredictable behaviour known as chaos. Chaos explores the transitions between order and disorder, which often occur in surprising ways. Nonlinear phenomena arise in all fields of Engineering, Physics, Chemistry, Biology, Economics, and Sociology among others. Examples of nonlinear chaotic systems include climate prediction models, neural network models, data compression, information processing, turbulence, nonlinear dynamical economics. In general, for a nonlinear dynamical system to be classified as chaotic, it must have the following properties:

- An arbitrarily small change, or perturbation, of the current trajectory may lead to significantly different future behaviour. That means the chaotic system has positive *Maximal Lyapunov Exponent* (MLE) which is a quantity that characterises the rate of separation of infinitesimally close trajectories in the phase space [64]. The concept of nearby trajectories diverging away from each other plays an important role in chaotic systems. We can characterise the types of trajectory divergence as *linear* or *exponential* growth rates [136].
- It must be topologically mixing: this means that the system will evolve over time so that any given region or open set of its phase space will eventually overlap with any other given region in the phase space. This means any points initially far apart in the phase space have been brought close together, and vice versa.
- It must have dense periodic orbits which means that every point in the space is approached arbitrarily closely by periodic orbits.

### 2.2.1 Sensitivity to initial conditions

In chaotic dynamical system, a small change to the initial conditions may lead to significantly different future behaviour. Sensitivity to initial conditions (SDIC) is popularly known as the “butterfly effect” [129]. The name, coined by Edward Lorenz for the effect which had been known long before, is derived from the metaphorical example of the details of a hurricane (exact time of formation, exact path taken) being influenced by minor perturbations such as the flapping of the wings of a distant butterfly several weeks earlier. The flapping wing represents a small change in the initial condition of the meteorological system, which causes a chain of events leading to large-scale phenomena.

The concept of nearby trajectories diverge from each other which can be caused by a small perturbation to initial conditions plays an important role in chaotic systems. The two types of the trajectory divergence are the linear and the exponential growth rates. Linear growth can be represented by the simple expression  $y = ax + b$ , where  $a$  is an arbitrary positive constant (growth) and  $b$  an arbitrary constant. Exponential growth can be represented by the expression  $y = n_0 e^{ax}$ , where  $n_0$  is some initial quantity and  $a$  is an arbitrary positive constant [36]. Rapid divergence of trajectories, which are close together initially, when present in a dynamical system, makes long term predictions impossible and hence is regarded as one of the key features of “chaotic” behaviour [25].

### 2.2.2 Lyapunov exponents

*Lyapunov characteristic exponents* (LCEs) or *Lyapunov exponents* are quantities that characterise the rate of separation of trajectories which start infinitesimally close [18, 169]. They measure the sensitivity to initial conditions. Quantitatively, two trajectories in phase space with initial separation  $\delta Z_0$  diverge (provided that the divergence can be treated within the linearised approximation) at a rate given by

$$|\delta Z(t)| \approx e^{\lambda t} |\delta Z_0|, \quad (2.2.1)$$

where  $\lambda$  is the Lyapunov exponent [64, 88]. There is a *spectrum of Lyapunov exponents*  $\{\lambda_1, \lambda_2, \dots, \lambda_n\}$ , equal in number to the dimensionality of the phase space, because the rate of separation can be different for different orientations of initial separation vectors [88]. We refer to the largest one as the maximal Lyapunov exponent. It determines a notion

of unpredictability for a dynamical system. A positive (MLE) which is the exponential divergence rate is usually taken as an indication that the system is chaotic (provided that phase space compactness, dense periodic orbits and transitivity are met). The MLE can be defined as follows [18, 88]

$$\lambda = \lim_{t \rightarrow \infty} \lim_{\delta Z_0 \rightarrow 0} \frac{1}{t} \ln \frac{|\delta Z(t)|}{|\delta Z_0|}. \quad (2.2.2)$$

The *short time Lyapunov exponent* is a Lyapunov exponent defined over some finite time interval and the *local Lyapunov exponent* is a short time Lyapunov exponent in the limit where the time interval approaches zero. Both are dependent on initial conditions, and the short time Lyapunov exponent is also dependent on the magnitude of the time interval [137]. To compute the Lyapunov exponents for a continuous flow of a differential equation, consider the following system of  $n$  autonomous differential equations

$$\dot{v} = f(v), \quad (2.2.3)$$

where  $v = (v_1, v_2, \dots, v_n)$ . The flow  $F_T(v)$  is defined as the point at which the orbit with initial condition  $v$  arrives after  $T$  time units (time- $T$  map). We define the Lyapunov exponent of a flow as the Lyapunov exponent of its time- $T$  map for  $T = 1$ . If we fix  $T$  for the moment,  $DF_T(v)$  is the derivative of the time-1 map  $F_1(v)$  with respect to the initial value  $v$  and is a linear map on  $\mathbb{R}^n$  represented by an  $n \times n$  matrix. The matrix  $DF_T(v+w)$  is the small variation in the solution of (2.2.3) at time  $T$  caused by a small change in the initial value at  $t = 0$  from  $v$  to  $v + w$  [16]. Since  $\{F_t(v) : t \in \mathbb{R}\}$  is the solution of (2.2.3) with initial value  $v$ , by definition we have

$$\frac{d}{dt} F_t(v) = f(F_t(v)), \quad F_0(v) = v. \quad (2.2.4)$$

Equation (2.2.4) has two variables, time  $t$  and the initial value  $v$  in  $\mathbb{R}^n$ . Differentiating with respect to  $v$  yields

$$\frac{d}{dt} DF_t(v) = Df(F_t(v))DF_t(v), \quad (2.2.5)$$

which is known as the *variational equation* of the differential equation (2.2.3). Solving the equation for  $DF_t(v)$ , we would know the derivative matrix of  $F_t$ , and therefore know how  $F_t$  acts under small variations in the initial condition  $v$ .

Let's define

$$J(t) = DF_t(v),$$

and

$$A(t) = Df(F_t(v)),$$

to be the Jacobian matrix of the right-hand side of the differential equation (2.2.3) evaluated along the solution. Then, we can rewrite the variational equation (2.2.5) as

$$\dot{J}(t) = A(t)J(t). \quad (2.2.6)$$

In order to uniquely define  $J(t)$  from (2.2.6), we add an initial condition, which is  $J(0) = I$ , i.e. the identity matrix. The variational equation is a linear differential equation, even when the original differential equation is nonlinear and is non-autonomous since  $A(t)$  is in general time-dependent [16]. To compute the LCEs, we need the repeated application of the *Gram-Schmidt orthonormalisation process* (GS) to orthonormalise the deviation vectors of the variational equation (2.2.6) after computing the Lyapunov exponents which depend on the values of their deviation at each time-step.

Given a set  $\{J_1, J_2, \dots, J_n\}$  of  $n$  linearly independent vectors in  $\mathbb{R}^n$ , the Gram-Schmidt procedure generates an orthonormal set  $\{E_1, E_2, \dots, E_n\}$  of vectors that spans the same subspace spanned by  $\{J_1, J_2, \dots, J_n\}$  [169]. The vectors  $E_i$  are given by

$$\begin{aligned} U_1 &= J_1, & E_1 &= U_1/||U_1||, \\ U_2 &= J_2 - \frac{\langle J_2, U_1 \rangle}{\langle U_1, U_1 \rangle} U_1, & E_2 &= U_2/||U_2||, \\ & & & \vdots \\ U_n &= J_n - \sum_{j=1}^{n-1} \frac{\langle J_n, U_j \rangle}{\langle U_j, U_j \rangle} U_j, & E_n &= U_n/||U_n||, \end{aligned}$$

where  $E_i$  are the orthonormalised vectors of  $J_i$ . The volume of the space spanned by  $\{J_1, J_2, \dots, J_n\}$  is

$$Vol\{J_1, J_2, \dots, J_n\} = ||U_1|| \dots ||U_p||.$$

Then, for a short time interval  $T$  we can obtain the  $p$ -th LCE:

$$\lambda^p = \lim_{k \rightarrow \infty} \frac{1}{kT} \sum_{i=1}^k \ln(||U_1^i|| \dots ||U_p^i||),$$

where  $\|U_p\|$  is the length of deviation vectors  $J_p$  of the variational equation (2.2.6). For suitable value of  $T$ , we can compute the quantities [169]

$$\lambda_1 \approx \frac{1}{kT} \sum_{i=1}^k \ln \|U_1^i\|, \dots, \lambda_n \approx \frac{1}{kT} \sum_{i=1}^k \ln \|U_n^i\|. \quad (2.2.7)$$

It is worth it to mention that the classical Gram-Schmidt process is inherently numerically unstable, i.e. it is possible to create a basis that is no longer orthogonal. This loss of orthogonality comes from the accumulation of roundoff errors. To stabilize the approximation and guarantee that the numerical procedure will create an orthonormal basis with finite precision, one can use the *modified Gram-Schmidt process* which guarantees the vectors created will be numerically orthogonal than those from the classical Gram-Schmidt.

Other orthonormalisation methods use the *Householder transformation* or the *Givens method*. The Householder transformation [105] is usually preferred over the GS method since it is numerically more stable, i.e. rounding errors tend to have less serious effects. On the other hand, the GS method produces the  $j$ th orthonormalised vector after the  $j$ th iteration, while the Householder method produces all the vectors only at the end. Givens method (which is also called the *rotation method*) has one advantage over Householder transformations as it can be easily parallelised. It is often used for very sparse matrices which have a lower number of operations at each iteration. The three previous orthonormalisation methods are actually used in computing the *QR decomposition* (the decomposition of a matrix  $A$  into a product  $A = QR$  of an orthogonal matrix  $Q$  and an upper triangular matrix  $R$ ).

Two of the classical examples of chaotic systems are the *Lorenz system* which describes the motion of a fluid between two layers at different temperatures and the *Rössler system* that models chemical reactions [79]. Both models had been the focus of interest in a large number of studies and they continue to appear in literature [79, 170]. The main reason is that though these systems are well known, they are still not completely understood and have become test problems for almost all new analytical and numerical techniques in computational dynamics. They can display a rich diversity of periodic, multiple periodic and chaotic behaviours depending upon the specific values of one or more of their control parameters. Since the minimal dimension for chaos in case of autonomous

continuous systems is three, both models are systems of 3-dimensional nonlinear ordinary differential equations [170].

### 2.2.3 The Lorenz system

The *Lorenz system* arose from the work of meteorologist and mathematician Edward N. Lorenz. In 1963, Lorenz developed a simplified mathematical model for atmospheric convection (i.e. heat transfer by mass motion of a fluid) [18]:

$$\begin{aligned}\frac{dx}{dt} &= \sigma(y - x), \\ \frac{dy}{dt} &= x(\rho - z) - y, \\ \frac{dz}{dt} &= xy - \beta z,\end{aligned}\tag{2.2.8}$$

where  $x$ ,  $y$  and  $z$  are the system states,  $t$  the time and  $\sigma$ ,  $\rho$  and  $\beta$  the system's parameters ( $\sigma, \rho, \beta \geq 0$ ) [130, 131]. The Lorenz system is nonlinear, three-dimensional and deterministic system. Lorenz demonstrated that if one begins by choosing some values for  $x$ ,  $y$ , and  $z$  as initial conditions to plot the system trajectory, and then do it again with just slightly different values, one will quickly arrive at fundamentally different results when the two trajectories start to diverge from each other (Fig. 2.9). For certain parameter values and initial conditions, the MLE converges to a positive value which indicates that the system is chaotic (Fig. 2.10). In particular, the *Lorenz attractor* is a set of chaotic solutions which, when plotted, resemble a butterfly (Fig. 2.11). The Lorenz attractor is an example of a *strange attractor*. Strange attractors are unique from other phase-space attractors in that one does not know exactly where on the attractor the states of the system will reside. Two points on the attractor that are near each other at one time, will be far apart from each other at later times. The only restriction is that the states of the system remain on the attractor. Strange attractors are also unique in that they are not close on themselves as the motion of the system never repeats itself (aperiodic). The type of motion we are describing on strange attractors is what we mean by chaotic behaviour. The Lorenz attractor was one of the first strange attractor, but there are many systems that give rise to chaotic dynamics. Examples of other strange attractors include the *Rössler* [164, 165] and *Hénon* attractors [92].

Five of the terms on the right hand side of Lorenz equations are linear, while two are

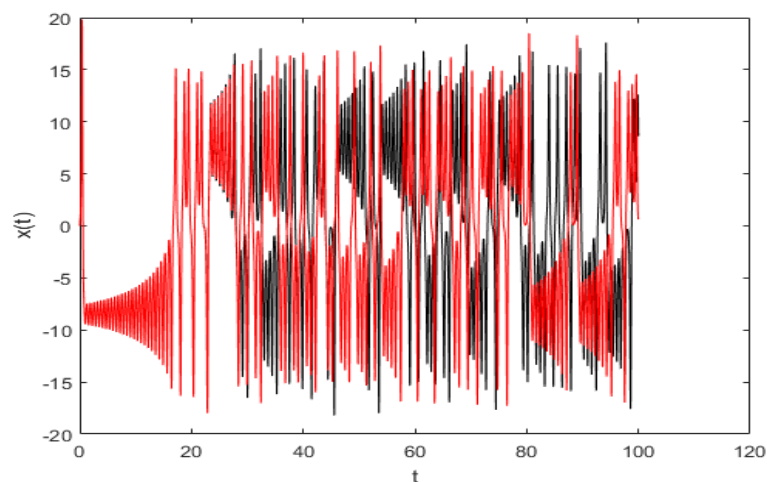


Figure 2.9: Two trajectories:  $(x_1, y_1, z_1)$  (red) and  $(x_2, y_2, z_2)$  (black) with slightly different initial conditions. After some time, the two trajectories start to diverge from each other.

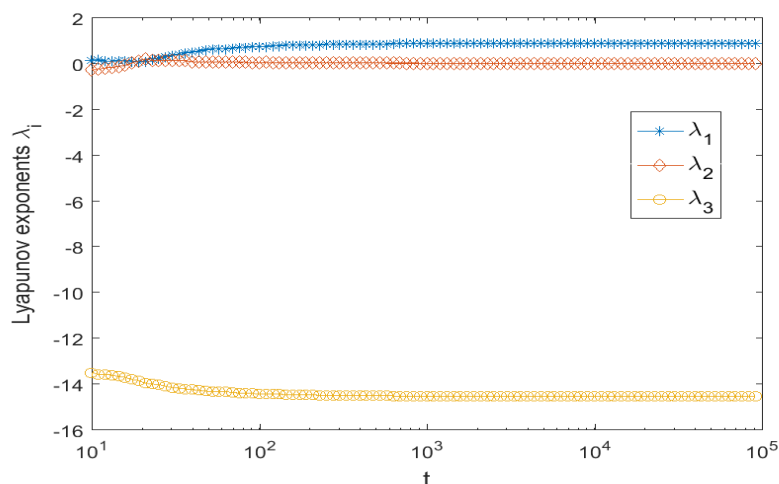


Figure 2.10: The Lyapunov exponents of the Lorenz attractor:  $\lambda_1$  (\*),  $\lambda_2$  ( $\diamond$ ) and  $\lambda_3$  ( $\circ$ ).  $\lambda_1$  represents the MLE which indicates that the system is chaotic as it converges to a positive value.

quadratic (see (2.2.8)). If one variable changes, the other two will change in response. Each of the parameters in these equations has a physical meaning. The parameter  $\sigma$  is the *Prandtl* number which describes the system physical characteristics. The two other parameters,  $\rho$  represents a control parameter and  $\beta$  is a value that describes the shape of the “box” which represents the boundaries that Lorenz attractor is contained within [99].

Originally, Lorenz used the parameter values  $\sigma = 10$ ,  $\rho = 28$  and  $\beta = 8/3$ , for which the system exhibits chaotic behaviour. To determine the overall stability of the equilibrium points, we need to linearise the system and find the eigenvalues of the Jacobian matrix

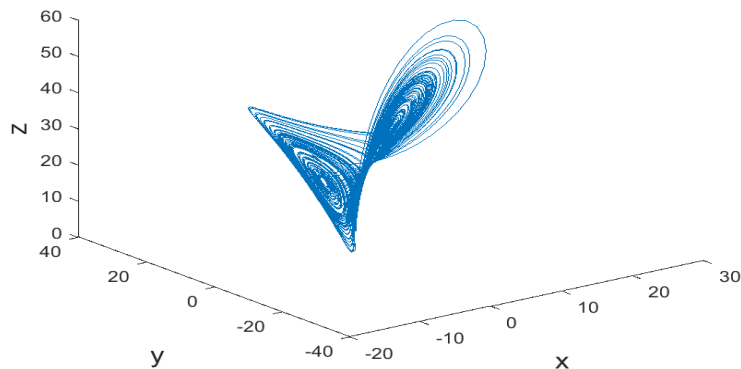


Figure 2.11: The Lorenz attractor for parameter values  $\sigma = 10$ ,  $\rho = 28$  and  $\beta = 8/3$ . Note its butterfly-like shape!

evaluated at the equilibrium points:

$$J = \begin{pmatrix} -\sigma & \sigma & 0 \\ \rho - z & -1 & -x \\ y & x & -\beta \end{pmatrix}. \quad (2.2.9)$$

Evaluating (2.2.9) at the origin (i.e. for  $(x,y,z) = (0,0,0)$ ),

$$J_0 = \begin{pmatrix} -\sigma & \sigma & 0 \\ \rho & -1 & 0 \\ 0 & 0 & -\beta \end{pmatrix}, \quad (2.2.10)$$

and the roots of the characteristic equation  $\det(J_0 - \lambda I) = 0$  are:

$$\begin{aligned} \lambda_1 &= -\beta, \\ \lambda_2 &= -\frac{\sigma + 1}{2} + \frac{\sqrt{(\sigma - 1)^2 + 4\sigma\rho}}{2}, \\ \lambda_3 &= -\frac{\sigma + 1}{2} - \frac{\sqrt{(\sigma - 1)^2 + 4\sigma\rho}}{2}. \end{aligned} \quad (2.2.11)$$

For  $\rho > 1$ , the origin is a saddle point (the eigenvalues have positive and negative real parts) and for  $\rho < 1$ ; the origin is a stable point (the eigenvalues have negative real parts). Thus, if  $\rho < 1$ , then there is only one fixed point located at the origin. This point corresponds to no convection (motionless state). All orbits converge to the origin, which is an attractor [16]. If  $\rho = 1$ , we have a pitchfork bifurcation as the origin loses its

stability, and for  $\rho > 1$ , two additional critical points appear [18]:

$$\begin{aligned} x_1^* &= (+\sqrt{\beta(\rho-1)}, +\sqrt{\beta(\rho-1)}, \rho-1), \\ x_2^* &= (-\sqrt{\beta(\rho-1)}, -\sqrt{\beta(\rho-1)}, \rho-1). \end{aligned} \quad (2.2.12)$$

The Jacobian matrix (2.2.9) at  $x_1^*$ :

$$J_{x_1^*} = \begin{pmatrix} -\sigma & \sigma & 0 \\ 1 & -1 & -\sqrt{\beta(\rho-1)} \\ \sqrt{\beta(\rho-1)} & \sqrt{\beta(\rho-1)} & -\beta \end{pmatrix}. \quad (2.2.13)$$

and at  $x_2^*$ :

$$J_{x_2^*} = \begin{pmatrix} -\sigma & \sigma & 0 \\ 1 & -1 & \sqrt{\beta(\rho-1)} \\ -\sqrt{\beta(\rho-1)} & -\sqrt{\beta(\rho-1)} & -\beta \end{pmatrix}. \quad (2.2.14)$$

The characteristic equation of (2.2.13) then becomes [99]:

$$\lambda^3 + (\sigma + \beta + 1)\lambda^2 + \beta(\sigma + \rho)\lambda + 2\beta\sigma(\rho - 1) = 0. \quad (2.2.15)$$

Let  $T = -(\sigma + \beta + 1)$ ,

$$K = \beta(\sigma + \rho),$$

$$D = -2\beta\sigma(\rho - 1),$$

where  $T, D$  indicate the trace and determinant of the Jacobian matrix. According to the *Routh-Hurwitz criterion* [170], a Hopf bifurcation occurs if

$$TK + D = 0 \quad \text{with } T, K, D < 0,$$

and all eigenvalues has negative real parts if

$$TK + D > 0 \quad \text{with } T, K, D < 0.$$

For  $\rho < \rho_H < \sigma \frac{\sigma+\beta+3}{\sigma-\beta-1}$ , we have  $TK + D > 0$ .

From the Routh-Hurwitz criterion, it follows that  $x_1^*$  is stable within the range

$$1 < \rho < \rho_H < \sigma \frac{\sigma+\beta+3}{\sigma-\beta-1} \quad \text{when } \sigma > \beta + 1.$$

At  $\rho = \rho_H = \sigma \frac{\sigma+\beta+3}{\sigma-\beta-1}$ , a change of stability occurs at which  $TK + D = 0$ . Complex eigenvalues cross the imaginary axis as subcritical Hopf bifurcation takes place [170].

To summarise: For  $0 < \rho < 1$ , the origin is a stable equilibrium point and all trajectories are attracted to it. At  $\rho = 1$ , a supercritical pitchfork bifurcation occurs. Two stable critical points are created and the origin loses its stability. For  $1 < \rho < \rho_H$ , both critical points are stable points and at  $\rho = \rho_H$ , a subcritical Hopf bifurcation occurs and both critical points  $x_1^*$  and  $x_2^*$  lose their stability. For  $\rho > \rho_H$ , there are no stable critical points anymore and trajectories are always bounded and can not escape to infinity.

For the choice of parameters  $\sigma = 10$ ,  $\beta = \frac{8}{3}$  and  $\rho = 28$ , the behaviour of the system after an initial transient period is chaotic. The solution settles into an irregular oscillation that persists as  $t$  tends to infinity but never repeats its path exactly. The motion is aperiodic and the solution is sensitive to changes in initial conditions. The plot of the solution in the  $(x, y, z)$  phase space resembles a butterfly structure, i.e., the Lorenz attractor [16].

### 2.2.4 The Rössler system

The *Rössler system* is a system of three nonlinear coupled ordinary differential equations originally studied by Otto Rössler in 1976 [164, 165]:

$$\begin{aligned}\frac{dx}{dt} &= -y - z, \\ \frac{dy}{dt} &= x + ay, \\ \frac{dz}{dt} &= b + z(x - c),\end{aligned}\tag{2.2.16}$$

where  $x$ ,  $y$  and  $z$  are the system states,  $t$  is the time and  $a$ ,  $b$  and  $c$  are the system's parameters. The system is a continuous-time dynamical system which for certain parameter values and initial conditions exhibits chaotic dynamics associated with the fractal properties of its attractor, the *Rössler attractor*. The Rössler attractor was initially intended to behave similarly to the Lorenz attractor, but also be easier to analyse qualitatively. An orbit within the attractor follows an outward spiral close to the  $x$ - $y$  plane around an unstable fixed point. Once the trajectory spirals out enough, a second fixed point influences the trajectory, causing a rise and twist in the  $z$ -dimension (see Fig. 2.12). In the time domain, it becomes apparent that although each variable is oscillating within a fixed range of values, the oscillations are chaotic such as for the parameter values  $a = 0.1$ ,  $b = 0.1$  and  $c = 14$ . This attractor has some similarities to the Lorenz attractor but is simpler.

The Rössler equations have one quadratic nonlinearity, and setting  $z = 0$  and  $b = 0$ ,

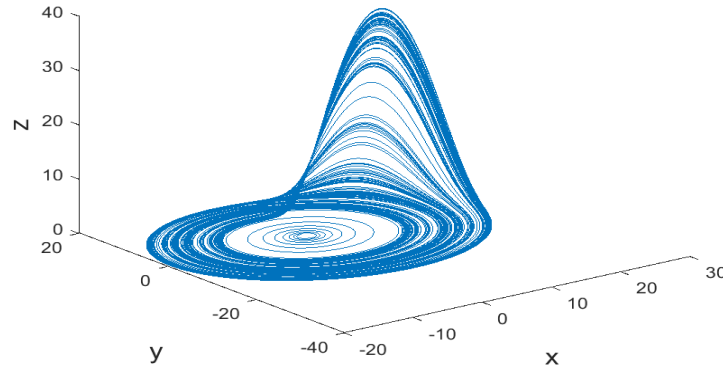


Figure 2.12: The Rössler attractor for the parameter values  $a = 0.1$ ,  $b = 0.1$  and  $c = 14$ .

can allow us to examine the behaviour of the system on the  $x$ - $y$  plane:

$$\begin{aligned}\frac{dx}{dt} &= -y, \\ \frac{dy}{dt} &= x + ay.\end{aligned}\tag{2.2.17}$$

The stability of the origin can be determined by finding the eigenvalues of the Jacobian matrix:

$$J = \begin{pmatrix} 0 & -1 \\ 1 & a \end{pmatrix},$$

which are  $\frac{a \pm \sqrt{a^2 - 4}}{2}$ . For  $0 < a < 2$ , the eigenvalues are complex and both have positive real parts, making the origin unstable with an outwards spiral on the  $x$ - $y$  plane. Rössler studied the chaotic attractor with the values  $a = 0.2$ ,  $b = 0.2$  and  $c = 5.7$ , though properties for  $a = 0.1$ ,  $b = 0.1$  and  $c = 14$  have been more commonly used since then. We can set Eq. (2.2.16) equal to zero and solve the resulting equations to find the equilibrium points of the system for a given set of parameter values. The coordinates of the equilibrium points are:

$$x = \frac{c \pm \sqrt{c^2 - 4ab}}{2}, y = -\left(\frac{c \pm \sqrt{c^2 - 4ab}}{2a}\right) \text{ and } z = \frac{c \pm \sqrt{c^2 - 4ab}}{2a}.$$

Two of these equilibrium points are:

$$\begin{aligned}x_1^* &= \left(\frac{c + \sqrt{c^2 - 4ab}}{2}, -\frac{c + \sqrt{c^2 - 4ab}}{2a}, \frac{c + \sqrt{c^2 - 4ab}}{2a}\right), \\ x_2^* &= \left(\frac{c - \sqrt{c^2 - 4ab}}{2}, -\frac{c - \sqrt{c^2 - 4ab}}{2a}, \frac{c - \sqrt{c^2 - 4ab}}{2a}\right).\end{aligned}\tag{2.2.18}$$

If  $c^2 = 4ab$ , both fixed points are equal. The Jacobian matrix of the linearised system is

$$J = \begin{pmatrix} 0 & -1 & -1 \\ 1 & a & 0 \\ z & 0 & x - c \end{pmatrix}, \quad (2.2.19)$$

The characteristic equation is

$$\lambda^3 + (c - a - x)\lambda^2 + (1 + ax + z - ac)\lambda + c - x - az = 0. \quad (2.2.20)$$

The three roots  $\lambda_1$ ,  $\lambda_2$  and  $\lambda_3$  of the characteristic equation are the eigenvalues of the Jacobian matrix of the linearised system.

## 2.3 Numerical integration methods

Many differential equations can be solved analytically for example, linear ODEs, i.e. obtain the solution in closed form, but in many cases, such as when the analytical solution of the mathematically defined problem is possible but time-consuming or even impossible to find, a numerical approximation to the solution is often sufficient. Numerical methods are used to find numerical approximations to the solutions of differential equations. For a differential equation that describes behaviour over time, the numerical method starts with the initial values of the variables, and then uses the equations to figure out the changes in these variables over a time interval. One of the most widely used method is the *Runge-Kutta method* [178]. The method is a family of implicit and explicit iterative methods, which includes the well-known *Euler method*, used in temporal discretisation for the approximate solutions of ODEs. These methods were developed around 1900 by two German mathematicians, C. Runge and M. Kutta [168]. In the following, we will discuss briefly two of these numerical methods.

### 2.3.1 The Euler method

The Euler method is a first-order numerical procedure for solving ordinary differential equations with a given initial value. It is the most basic explicit method for numerical integration of ODEs and is the simplest Runge-Kutta method. The method is named after Leonhard Euler who derived it in 1768 [71]. The order of numerical integration methods reflects how many terms of the Taylor series are accounted for in each method. The

Euler method is referred to as a first-order method which means that the *local truncation error* (LTE) is on the order of  $O(h^2)$ . LTE is an error that induced at every time-step due to the truncation of the Taylor series and a method with  $O(h^{k+1})$  is said to be of  $k$ th order. While LTE is the error caused by one iteration, the *global truncation error* is the accumulation of the local truncation error over all of the iterations. Higher order methods provide lower LTE for the same step-size. For *fourth-order Runge-Kutta method* (RK4), the local truncation error is of the order  $O(h^5)$  and the global truncation error is of the order  $O(h^4)$ .

From any point on a curve, one can find an approximation of a nearby point on the curve by moving a short distance along a line tangent to the curve. To find an approximate solution for the following first-order differential equation using Euler method,

$$\begin{aligned}y'(t) &= f(t, y(t)), \\y(t_0) &= y_0,\end{aligned}$$

we replace the derivative  $y'$  by the finite difference approximation,

$$y'(t) \approx \frac{y(t+h) - y(t)}{h},$$

which when we re-arrange it yields,

$$\begin{aligned}y(t+h) &\approx y(t) + hy'(t), \\y(t+h) &\approx y(t) + hf(t, y(t)).\end{aligned}$$

Then, we choose a step-size  $h$  and construct a time-sequence  $t_0, t_1 = t_0 + h, t_2 = t_0 + 2h, \dots$ . We denote the numerical estimate of the exact solution  $y(t_n)$  by  $y_n$  and compute these estimates by the following recursive scheme:

$$\begin{aligned}y_{n+1} &= y_n + hf(t_n, y_n), \\y(t_0) &= y_0.\end{aligned}\tag{2.3.1}$$

This is the *forward Euler method*. It is an *explicit* method which means the new value  $y_{n+1}$  is defined in terms of quantities already known, such as  $y_n$ . For the *backward Euler method*, we use the approximation,

$$y'(t) \approx \frac{y(t) - y(t-h)}{h},$$

which give us,

$$y_{n+1} = y_n + hf(t_{n+1}, y_{n+1}). \quad (2.3.2)$$

The backward Euler method is an *implicit* method, meaning that we have to solve an equation to find  $y_{n+1}$  such as using the fixed point iteration method [47].

### 2.3.2 The fourth-order Runge-Kutta method

The fourth order Runge-Kutta method (RK4) is a numerical technique used to solve systems of first order ordinary differential equation of the form [115]

$$\begin{aligned} y' &= f(x, y), \\ y(0) &= y_0, \quad y \in \mathbb{R}^n. \end{aligned}$$

Let us consider the following IVP problem:

$$\begin{aligned} y' &= f(t, y), \\ y(t_0) &= \alpha, \quad \alpha \in \mathbb{R}. \end{aligned}$$

Let  $h$  be the time-step and  $t_i = t_0 + ih$ . Then, the formula for the fourth order Runge-Kutta method (RK4) is:

$$\begin{aligned} y_0 &= \alpha, \\ k_1 &= hf(t_i, y_i), \\ k_2 &= hf(t_i + \frac{h}{2}, y_i + \frac{k_1}{2}), \\ k_3 &= hf(t_i + \frac{h}{2}, y_i + \frac{k_2}{2}), \\ k_4 &= hf(t_i + h, y_i + k_3), \\ y_{i+1} &= y_i + \frac{1}{6}(k_1 + 2k_2 + 2k_3 + k_4), \end{aligned}$$

which allows to compute the approximate solution, that is  $y_i \approx y(t_i)$ . Here,  $y_{i+1}$  is the RK4 approximation of  $y(t_{i+1})$ , and the next value is determined by the present value  $y_i$  plus the weighted average of four increments, where each increment is the product of time-step,  $h$ , and an estimated slope specified by  $f$  of the right-hand side of the differential equation.

In the fourth order Runge-Kutta method,

- $k_1$  is the increment based on the slope at the beginning of the interval, using  $y$  (Euler's method).

- $k_2$  is the increment based on the slope at the midpoint of the interval.
- $k_3$  is again the increment based on the slope at the midpoint of the interval.
- $k_4$  is the increment based on the slope at the end of the interval.

In averaging the four increments, greater weight is given to the increments at the midpoints, since we regard them to be a better estimate of the slope when going from  $y(t_0)$  to  $y(t_0 + h)$ . Both  $k_2$  and  $k_3$  proved to be more accurate than  $k_1$  for making new approximations for  $y(t_i)$ .

The difficulty in the Runge-Kutta methods is to find the appropriate time-step to be less than a predefined error  $\epsilon$ . We can use an adaptive time-step control during computations. To achieve this, we start with a moderate time-step and when we detect that the expected error is larger than  $\epsilon$ , we reduce the time-step and recalculate the current step. If we detect that the expected error is less than  $\epsilon$ , we keep the current step and slightly enlarge the time-step in the next step. This requires a good estimation of the “expected error”. An alternative time-step adjustment algorithm is based on the embedded Runge-Kutta formulae, originally invented by Erwin Fehlberg (1969) [72] and is known as the *Runge-Kutta-Fehlberg method* (RK45).

The purpose of this adaptive time-step control is to achieve some predetermined accuracy in the solution with minimum computational effort. An interesting fact about the Runge-Kutta formulae is that for orders  $M$  higher than four, more than  $M$  function evaluations are required. Fehlberg discovered a fifth-order method with six function evaluations where another combination of the six functions gives a fourth-order method. The difference between the two estimates of  $y(t + h)$  can then be used as an estimate of the truncation error to adjust the time-step. Several other embedded Runge-Kutta formulae have been found since Fehlberg’s original formula such as the *Bogacki-Shampine* [38] and *Cash-Karp* methods [51].

## 2.4 Complex systems

We are surrounded by many complicated and complex systems. For example, consider the society that requires cooperation between billions of individuals, or communications infrastructures that integrate billions of cell phones with computers and satellites. Our

biological existence is rooted in seamless interactions between thousands of genes within our cells. Our ability to understand and comprehend the world around us requires the coherent activity of billions of neurons in our brain. These systems are collectively called *complex systems*. Complex systems play an important role in our daily life and the society around us. Their understanding, mathematical description, prediction, and eventually control is one of the major scientific challenges of the 21st century [30].

Systems are entities composed of well-defined components which act together to form a functioning whole with dynamical behaviours and responses to the environment [37]. Complex systems are networks made of many components that interact with each other, typically in a nonlinear fashion. They may arise and evolve through the dynamical interaction of the components without an intervening regulatory body. Many complex systems generate spontaneously new and organised forms which are neither completely regular nor completely random. Real-world systems, e.g., the global climate, food webs, stock markets, social media, brains and other neural systems have these properties. The development of many conceptual, mathematical and computational tools in complex systems science enable us to properly describe systems that are made of interdependent components [172]. The science of complexity studies the relationships between these components that give rise to the cooperative behaviour of many interconnected components of the system and how it interrelates with its environment. The social systems formed (in part) out of people, the weather formed out of air flows, molecules formed out of atoms, the brain formed out of neurons are all examples of complex systems and their components.

Simple systems have few components and their behaviour is fully understandable and predictable [37]. The science of classical systems, as exemplified by Newtonian mechanics, reduces all complex phenomena to their simplest components, and then can describe these components in a complete, objective, and deterministic manner. In contrast, complex systems such as societies, organisms, stock markets or the Internet, have emergent properties that cannot be reduced to the mere properties of their parts and have intrinsically unpredictable behaviour [95]. The cooperative interactions of the individual components in complex systems determine their emergent functionalities. Small changes in one of these components can have far reaching consequences for the system as a whole but many complex system often show high level of robustness due to redundancy in their

components [37].

The field of complex systems connects all traditional disciplines of science, engineering, medicines, management, etc. [28]. Many cross-disciplinary applications are made available through the study of the structural and dynamical properties of various complex systems. Emergence and self-organisation are the two core concepts that go across almost all subareas of complex systems.

### 2.4.1 Emergence

*Emergence* refers to how collective properties of a complex system can arise from the properties of its components and how behaviour at a larger scale arises from the detailed structure, behaviour and relationships at a finer scale. However, many observed properties at the macroscopic scales cannot be reduced to microscopic physical rules which control the system's behaviour. Many macroscopic properties such as living and consciousness are emergent properties because it is hard to describe the neurophysiological processes that make them. As the whole system evolves over time, emergence produces novel and coherent interactions among the system's entities following basic principles.

Predictable patterns of emergent phenomena, such as anthills and traffic flows are examples of *weak emergence*. In contrast, disruptions that dramatically change a system's structure is called a *strong emergence* as in revolutions and renaissance. Rules or principles in weak emergence act as the authority and provide context for the system to function with no need for someone to be in charge. In strong emergence, the rules or assumptions that shape a system cease to be reliable. The system becomes chaotic, yet emergent systems increase order even in the absence of command and central control. Open systems extract information and order out of their environment and bring coherence to increasingly complex forms [102]. Scientists generally agree on these qualities of emergence:

- Radical novelty: At each level of complexity, entirely new properties appear.
- Coherence: A stable system of interactions.
- Wholeness: It is not just the sum of the system's parts, but also different and irreducible forms of its parts.
- Dynamic: The system is always in process, continuing to evolve.

- Downward causation: The system shapes the behaviour of its parts.

In any type of change in a complex system, emergence occurs when disruptions shape the interactions between its component and coherence breaks apart. Then, differences appear and reform in a novel system by one of the following dynamics:

- No one is in charge to orchestrate orderly activity (e.g., economic systems, ecosystems).
- complex behaviour emerges from simple rules which results in randomness becomes coherent as individuals interact with their neighbours, with each following a few basic principles or assumptions (e.g., traffic flows, birds flocks) [102].

The next subsection is devoted to self-organisation and its various aspects.

### 2.4.2 Self-organisation

*Self-organisation* can be defined as the spontaneous formation of global structures out of local interactions in a complex system. it represents the spontaneous emergence of order in natural and physical systems [61]. Emergence is about scale and self-organisation is about time in addition to scale. The global structures which involve the system as a whole, are the spatial, temporal, or functional structures. The self-organised system is the one that spontaneously organises itself and produce a nontrivial macroscopic structure and/or behaviour as time progresses. Many biological, physical and social systems show self-organising behaviour [172]. Great attention is being recently paid to the processes of self-organisation in various networks, including neuronal networks in the brain and of various swarms and flocks, where self-organisation is understood as the unexpected appearance of collective or coherent behaviour that is termed swarm intelligence.

A basic feature in all of these diverse systems is the means by which they acquire their order and structure. In self-organised systems, pattern formation occurs through interactions internal to the system, with no intervention by external directing influences. Moreover, the rules specifying interactions among the system's components are executed using only local information, without reference to the global pattern. Thus, pattern is an emergent property of the system, rather than a property imposed on the system by an external ordering influence. It represents an organised arrangement of objects in space

or time. A system of living cells or organisms builds a pattern and succeeds in doing so with no external directing influence. In systems lacking self-organisation, order can be imposed on them in many different ways, not only through instructions from a supervisory leader but also through various directives such as blueprints or recipes, or through pre-existing patterns in the environments [48].

The main challenge in self-organising systems is to understand how components interact to produce a complex pattern as processes in complex systems are often *nonlinear*, i.e., their effects are not proportional to their causes. The two basic modes of interactions among the components of self-organising systems are *positive* and *negative feedback*. Most self-organising systems use positive feedback which generally promotes changes in a system. Two familiar examples of the effects of positive feedback are the spread of a disease and the explosive growth of the human population (see Fig. 2.13). In the past centuries, the reproduction of each generation was much bigger than its original size, therefore more births occur with each successive generation. The snowballing effect of positive feedback takes an initial deviation in a system and reinforces that change in the same direction as the initial deviation. In negative feedback, effects are smaller than the causes and produce a damping effect. A small perturbation applied to the system triggers an opposing response that counteracts the perturbation. An individual acquires and processes information that causes a negative feedback. A decrease in body temperature can lead to shivering which counteracts the drop in body temperature [48].

Complex systems are distinguished by their capacity for self-organisation, i.e. rearranging and reforming their patterns of operation in mutual adaptation to changes in their environment and also the capacities of their components to the changing demands and opportunities from the environment. This process occurs as a result of communication, selection and adaptation processes within the system itself and between the evolving system and its environment and is not imposed externally. The result of this process is a new and more constructive order in dynamic response to a changing environment [61].

One feature of complex systems is *nonlinear dynamics*. In a complex system, nonlinear behaviour means it may respond in different ways to the same input. Inputs and outputs can be the current and next states of the system and if their relationship is not linear, the system is nonlinear. Nonlinearity means that the outputs of a system are given by a non-linear function of its inputs and then the change in the size of the input does not

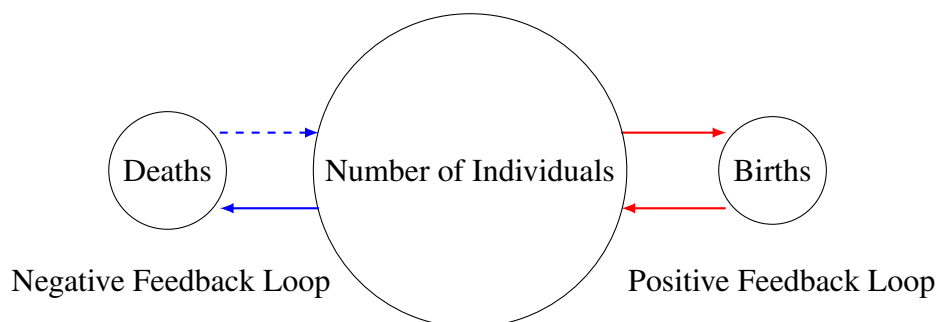


Figure 2.13: A simple model of population growth which involves a positive feedback loop of increased births and a negative feedback loop of increased deaths [48].

produce a proportional change in the size of the output. Nonlinearity is closely associated with chaos, even though not all nonlinear systems produce chaotic dynamics. *Systems theories* is another feature which contributed to the development of complex systems science. Systems theory is the interdisciplinary study of systems which developed during and after World War II in response to the huge demand for mathematical theories to formulate systems that could perform computation, control, and/or communication [172].

There is an intricate network behind each complex system. *Networks* represent the interactions between the system's components and there are extensive studies of complex system dynamics by means of complex network theory in recent years. The study of networks is known as graph theory in mathematics, which was started back in the 18th century. Many systems are composed of individual parts or components linked together in some way and their pattern of connections can be represented as a network. The scientific study of networks, such as computer networks, social networks, and biological networks is an interdisciplinary field that combines ideas from mathematics, physics, computer science, biology, the social sciences, and many other areas [147].

## 2.5 Complex networks

A *network* in its simplest form represents a collection of points joined together in pairs by lines. The points are referred to as *vertices* or *nodes* and the lines as *edges* or *links*. It can be viewed as a *graph* consisting of vertices connected by edges according to a certain rule or form. The network is a diagrammatical representation of some physical system or structure while the graph, on the other hand, is a mathematical notion that represents only the structure of a network without the physical meanings [55]. Each complex system com-

poses of an intricate network that encodes the interactions between the components of the system. The social network, sum of all family ties, friendship, and professional, is the fabric of the society that determines the spread of knowledge, behaviour and resources. The cellular network composes of genes, proteins, and metabolites integrates these components into live cells. The wiring diagram capturing the connections between neurons, called the neural network, holds the key to our understanding of the brain functions and consciousness [30].

Many aspects of these complex systems are worth studying. Some people study the nature of the individual components; how a human being feels or reacts, or how a computer works. Others study the nature of the connections or interactions; the dynamics of human friendships or the communication protocols used on the Internet. Another aspect which is always crucial to the behaviour of these interacting systems, is the pattern of connections between components. In a given system, the pattern of connections can be represented as a network, the components of the system being the network vertices and the connections the edges. Networks are the simplified representations of these complex systems. They reduce the systems to abstract structures capturing only the basics of connection patterns. Even vertices and edges in a network can be labeled with additional information, such as names or strengths to capture more details of the system, a lot of information is usually lost in the process of reducing a full system to a network representation [147].

We live in a connected world and its networks come in many shapes and sizes. We interact and communicate within vast social networks, the World Wide Web (WWW) contains nodes and links that connect branches across the Earth and the ecosystems contain countless species living in different environments. All these systems represent *dynamic networks* of interacting elements. They are dynamic networks, with nodes and links forming and disappearing over time. Network topology which defines how nodes of the network are connected determines how its properties evolve dynamically [151].

### **Definition 2**

*A network  $G$  is a pair  $(V, E)$ , where  $V$  is the vertex set of  $G$  and its elements are the vertices of  $G$ , while  $E$  is the set of edges.*

- *If  $E$  is symmetric, then  $G$  is an undirected network (Fig. 2.14a).*

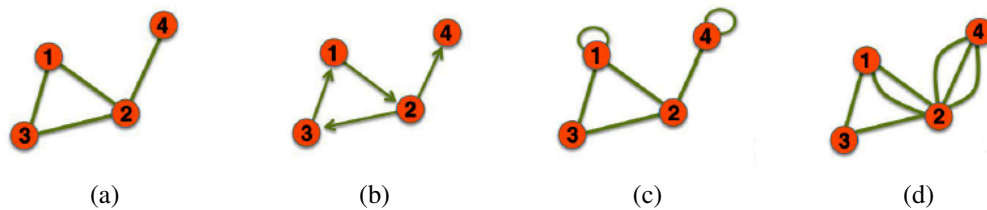


Figure 2.14: (a) An undirected network of 4 vertices and 4 edges (simple network). (b) A directed network of 4 vertices and 4 edges (simple network). (c) An undirected network of 4 vertices, both vertices 1 and 4 have selfedges. (d) An undirected network of 4 vertices has two vertices with multiedges. Vertices 1 and 2 connected to each other with 2 edges and vertices 2 and 4 with 3 edges [30].

- If  $E$  is nonsymmetric, then  $G$  is a directed network or (digraph) (Fig. 2.14b).
- If  $E$  is symmetric, anti-reflexive (no selfedges) (Fig. 2.14c) and contains no multiedges (duplicate links) (Fig. 2.14d) then  $G$  is a simple network [70].

### Definition 3

Let  $R \subseteq S \times S$  be a relation in  $S$ .  $R$  is anti-reflexive if and only if  $\forall x \in S : (x, x) \notin R$ .

The structure and evolution of networks behind each complex system is driven by a common set of fundamental laws and principles. Despite the differences in form, size, nature, age, and scope of real networks, most networks are driven by common organising principles. Networks are often defined in terms of statistics of nodes and links. There are many statistical measures of the topology of networks and the physical behaviour of dynamical networks may be distinguished depending on the different values of these measures [151].

The concept of degree is the most fundamental measure of a node in a network. The *degree* of the  $i$ th node is the number  $k_i$  of its existing edges. Thus, an isolated node has degree zero. The *out-degree* of a node is the number of outgoing edges and the *in-degree* the number of incoming edges. In a directed network, there is a distinction between in-degree and out-degree, describing the number of incoming edges and outgoing edges respectively. However, in an undirected network, there is no difference between in- and out-degrees.

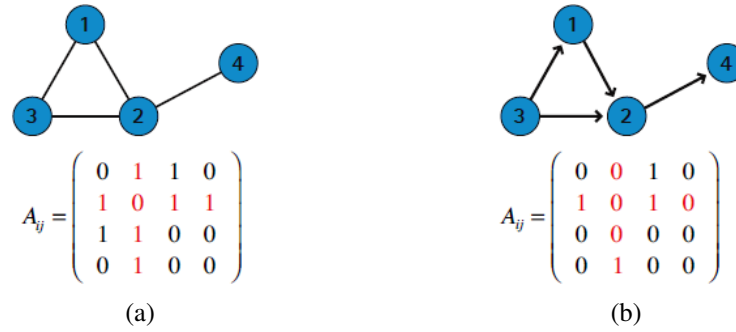


Figure 2.15: (a) The adjacency matrix of an undirected network of 4 nodes. The adjacency matrix is symmetric along the diagonal. (b) The adjacency matrix of a directed network of 4 nodes. The adjacency matrix is nonsymmetric along the diagonal [30].

#### Definition 4

Suppose  $G = (V, E)$  is a simple network where  $V = \{1, 2, \dots, N\}$  is the vertex set of  $G$ ,  $E$  the set of edges and  $N$  the number of vertices. For  $1 \leq i, j \leq N$ , define

$$a_{ij} = \begin{cases} 1, & (i,j) \in E, \\ 0, & (i,j) \notin E. \end{cases}$$

Then the square matrix  $A = (a_{ij})$  is called the adjacency matrix of  $G$  (Fig. 2.15) [70].

If the network is undirected, the adjacency matrix is symmetric along the diagonal as for every  $i$  and  $j$ ,  $a_{ij} = a_{ji}$  and  $a_{ii} = 0$  (Fig. 2.15a). The degree of the  $i$ th node is given by

$$k_i = \sum_j a_{ij}. \quad (2.5.1)$$

In an undirected network, the total number of links  $l$  can be expressed as the sum of the node degrees [30]:

$$l = \frac{1}{2} \sum_{i=1}^N k_i. \quad (2.5.2)$$

The average degree of an undirected network is

$$\langle k \rangle = \frac{1}{N} \sum_{i=1}^N k_i = \frac{2l}{N}. \quad (2.5.3)$$

In directed networks, we distinguish between incoming degree  $k_i^{in}$ , representing the number of edges that point to node  $i$ , and outgoing degree  $k_i^{out}$  representing the number of

edges that point from node  $i$  to other nodes. The total degree of node  $i$  is given by

$$k_i = k_i^{in} + k_i^{out}, \quad (2.5.4)$$

where  $k_i^{in}$  represents its incoming degree and  $k_i^{out}$  represents its outgoing degree. Then, the total number of links in a directed network is

$$l = \sum_{i=1}^N k_i^{in} + \sum_{i=1}^N k_i^{out}. \quad (2.5.5)$$

The average degree of a directed network is

$$\langle k \rangle = \frac{1}{N} \sum_{i=1}^N k_i^{in} + \frac{1}{N} \sum_{i=1}^N k_i^{out} = \frac{l}{N}. \quad (2.5.6)$$

In a network, each node has its degree value, some large and some small, the distribution of nodes in the network is an important concept. The *degree distribution* is defined by the probability function  $P(k)$  which represents the probability of a randomly picked node has degree  $k$ , where each node has an equal probability to be picked and

$$\sum_{k=1}^N P(k) = 1. \quad (2.5.7)$$

The degree distribution has assumed a central role in network theory [55]. Most calculations of network properties require us to know  $P(k)$ . For example, the average degree of a network can be written as

$$\langle k \rangle = \sum_{k=1}^N kP(k). \quad (2.5.8)$$

For directed networks, there are two different degree distributions, the in- and out-degree distributions depending on the number of incoming and outgoing edges at each vertex. Most of the large-size real-world networks have degree distributions with a tail representing the high-degree vertices (*hubs*) and they are called *right-skewed* degree distributions. Another concept which contains essentially the same-information as the degree distribution is the *degree sequence*, which is the set  $\{k_1, k_2, k_3, \dots\}$  of degrees for all vertices in the network [147]. The degree sequence is decreasing sequence of its vertices degrees for an undirected network and increasing sequence for a directed network.

### 2.5.1 Shortest path-length

In physical systems, the physical distance plays a key role in determining the interactions between the components. Distances between two atoms in a crystal or between two galaxies in the universe determine the forces that act between them. In networks, the physical distance is not relevant. Two individuals that live in the same building may not know each other while two webpages could be sitting on computers on the opposite sides of the globe have a link to each other. The physical distance in networks is replaced by the concept of *path-length* [30].

#### Definition 5

A **walk** in a network is an ordered subset of edges (not necessarily distinct)

$$(u_1, v_1), (u_2, v_2), \dots, (u_n, v_n),$$

for which node  $v_i = u_{i+1}$  ( $i = 1, 2, \dots, n-1$ ). If  $v_n = u_1$  then the walk is **closed**. A **path** is a walk in which all the nodes  $u_i$  are distinct. A closed path is called a **cycle** or **circuit**. A graph with no cycles is called **acyclic**. A cycle of length 3 is called a **triangle** [70].

Paths can be defined for both directed and undirected networks. In directed networks, each edge traversed by a path must be in the correct direction for that edge. While in undirected networks edges can be traversed in either direction as  $d_{ij} = d_{ji}$ , the distance (number of edges) between node  $i$  and  $j$  is the same as the distance between node  $j$  and  $i$ . Path can intersect itself, i.e. visiting again a vertex it has visited before, or even running along an edge or a set of edges more than once. Paths that do not intersect themselves are called *self-avoiding paths* and they are important in some areas of network theory.

An *Eulerian path* is a path that traverses each edge exactly once and a *Hamiltonian path* is a path that visits each vertex exactly once. A network can have one or many Eulerian or Hamiltonian paths, or none. By definition, a Hamiltonian path is self-avoiding, but an Eulerian need not be. In a network,

- The *path-length* is the number of links that a path contains (Fig. 2.16a),
- The *shortest path-length* (or *geodesic path*) is a path with the shortest distance  $d$  between two nodes (Fig. 2.16b),

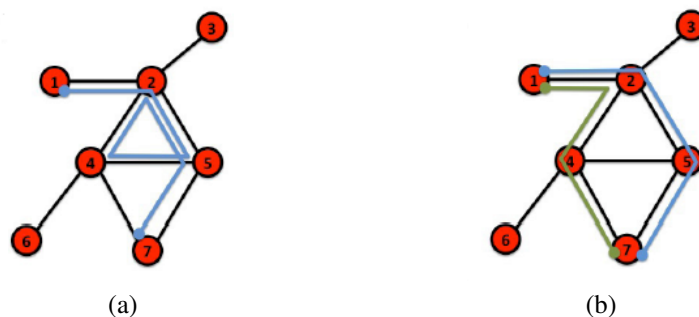


Figure 2.16: (a) A path between nodes 1 and 7 (blue line). The path-length = 6 links. (b) The shortest paths between nodes 1 and 7 (blue and grey lines). Both shortest path-length = 3 links. The graph diameter (the longest shortest path  $d_{max}$ ) = 3 links [30].

- The diameter ( $d_{max}$ ) is the longest shortest path in a graph, or the distance between the two furthest nodes (Fig. 2.16b) and
- The average path-length is the average of the shortest paths between all pairs of nodes.

For a directed network of  $N$  nodes, the average path-length  $L$  is

$$L = \frac{1}{N(N-1)} \sum_{i,j=1, i \neq j}^N d_{i,j}, \quad (2.5.9)$$

where  $d_{i,j}$  is the distance between nodes  $i$  and  $j$  [30].

It is possible that there is no geodesic path between two vertices in a network if these vertices are not connected together by a link, i.e., if they are in different components (subnetworks) of the network. In this case, one sometimes says that the geodesic distance between the vertices is infinite which really means that the vertices are not connected. Geodesic paths are not necessarily unique. It is possible to have two or more paths of equal length between a given pair of vertices. They are necessarily self-avoiding paths. If a path intersects itself, that means it contains a *loop*, also called a *self-loop* which is an edge  $(i, i)$  that connects a vertex  $i$  to itself. Then, it can be shortened by removing that loop while still connecting the same start and end points, and hence self-intersecting paths are never geodesic paths [147].

In a small-size network, finding the shortest path between two nodes is an easy task. For a network with millions of nodes, finding the shortest path between two nodes is a time consuming task. The length of the shortest path and the number of such paths can be

obtained from the adjacency matrix of the network. In practice, we use the *breadth first search* (BFS) algorithm [181] for this purpose. BFS is a traversing algorithm which works for both directed and undirected networks. We should start traversing from a selected node and traverse the network level by level exploring the neighbour nodes. A single run of the breadth-first search algorithm finds the shortest (geodesic) distance from a single node  $i$  to every other nodes in the network that contains the node  $i$ .

### 2.5.2 Clustering coefficient

The *clustering coefficient* measures the average probability that two neighbours of a node are themselves neighbours. In effect, it measures the density of triangles in a network. Many real-world networks are characterised by having relatively large number of triangles. The first definition for a clustering coefficient was introduced by Watts and Strogatz in 1998 [70].

$$C_i = \frac{\text{number of pairs of neighbours of } i \text{ that are connected}}{\text{total number of pairs of neighbours of } i}, \quad (2.5.10)$$

which is the fraction of pairs of neighbours of vertex  $i$  that are themselves neighbours. If  $l_i$  represents the number of triangles attached to node  $i$  of degree  $k_i$  then the local clustering coefficient for a node  $i$  is defined as

$$C_i = \frac{l_i}{\frac{k_i(k_i-1)}{2}} = \frac{2l_i}{k_i(k_i-1)}, \quad (2.5.11)$$

with  $C_i$  lying in  $[0, 1]$ .

- $C_i = 0$  if none of the neighbours of node  $i$  link to each other (e.g. a star-shaped graph and a set of isolated nodes).
- $C_i = 1$  if all neighbours of node  $i$  link to each other, i.e. they form a complete graph.
- $C_i = 0.5$  if there is 50% chance that two neighbours of a node link to each other.

The average clustering coefficient  $\langle C \rangle$  of the whole network which represents the probability that two neighbours of a randomly chosen node link to each other, is the

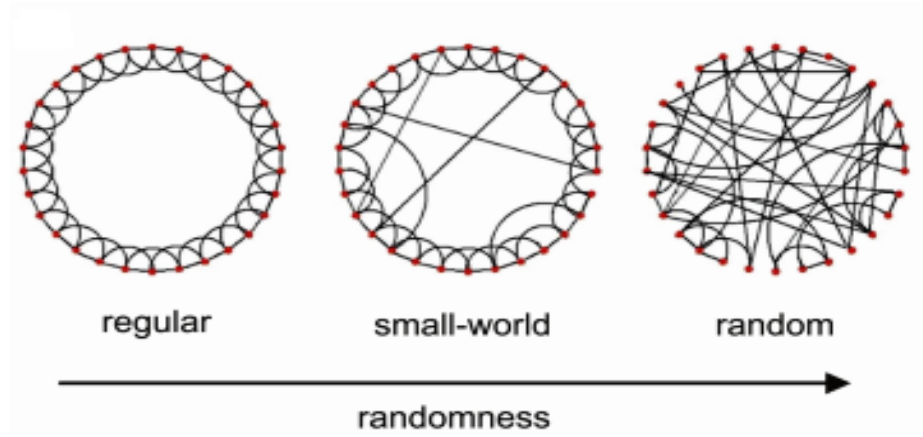


Figure 2.17: The increase in randomness; regular network with probability ( $\beta = 0$ ) and random network with probability ( $\beta = 1$ ) [12].

average of  $C_i$  over the total number of nodes  $N$ ,

$$\langle C \rangle = \frac{1}{N} \sum_{i=1}^N C_i. \quad (2.5.12)$$

The global clustering coefficient  $C$  for the entire network is given by

$$C = \frac{3 \times \text{number of triangles}}{\text{number of connected triples}}. \quad (2.5.13)$$

We defined the clustering coefficient as a measure of the density of triangles in a network. We can also look at the densities of other small groups of vertices, often called *motifs*. One can define similar clustering coefficient to measure the densities of different motifs in a network [147].

### 2.5.3 Random networks

If all nodes in a network have the same degree, we have a *regular network*. It is called *k-regular* or *regular of degree k* if the common degree is  $k$ . The *null graph* which is a network of  $N$  nodes but no edges is *0-regular* [70]. A *complete graph* is a fully-connected regular network, i.e. there exists an edge connecting every pair of nodes in the network. A fully-connected regular network with  $N$  nodes has number of edges equal to  $\frac{N(N-1)}{2}$ , average path-length  $L = 1$  and average clustering coefficient  $C = 1$  [55].

The extreme opposite to regular networks are completely *random networks* (see Fig. 2.17), where the typical model is the random graph introduced in 1959 by Paul Erdős and Alfréd Rényi [68].

The other model which is closely related to their random graph model was introduced in the same year by Edgar Gilbert [84], but it is closely associated with the names of Erdős and Rényi, who published a series of papers about the model. Most scientific papers refers to the model as Erdős-Rényi model (ER) or Erdős-Rényi random graph. The two variant models of random graph are

- The  $G(N, M)$  model: a graph is constructed taking  $N$  nodes and place  $M$  edges among them at random, provided that the network should not have self-edges (self-loop) or multiedges (i.e. a simple graph).

Another equivalent definition of the model defines the random network as a graph that is chosen uniformly at random from the set of all simple graphs with exactly  $N$  nodes and  $M$  edges. This random graph model is not defined in terms of a single randomly generated graph, but as an ensemble of graphs. The properties of random graphs generated by this model typically mean the average properties of the ensemble. Some properties of the random graph  $G(N, M)$  are easy to calculate: for instance, the average number of edges is  $M$  and the average degree is  $\langle k \rangle = \frac{2M}{N}$ . Other properties are not so easy to calculate, thus most mathematical works related to random graphs have actually been conducted on by the other variant of the model which is a slightly different model but much easier to handle [147].

- The  $G(N, \beta)$  model: a graph is constructed by connecting nodes randomly. Each edge is added to the graph with probability  $\beta$  independently from any other edge. The random network is generated as follows:

1- Start with  $N$  isolated nodes.

2- Choose all possible pairs of nodes, once and only once, from the  $N$  nodes, and connect each pair of nodes by an edge with probability  $\beta \in (0, 1)$ .

The larger  $\beta$  is, the denser the resultant network. For  $\beta = 0$ , we have isolated nodes and for  $\beta = 1$ , we obtain a fully-connected network [55].

The expected number of edges of such a network is  $\frac{\beta N(N-1)}{2}$ . The average node-degree is

$$\langle k \rangle_{ER} = \beta(N - 1) \approx \beta N, \quad (2.5.14)$$

where  $ER$  refers to the Erdős-Rényi model, the average path-length is

$$L_{ER} \sim \ln(N) / \ln(\langle k \rangle_{ER}), \quad (2.5.15)$$

and the clustering coefficient is

$$C \approx \langle k \rangle_{ER} / N = \beta. \quad (2.5.16)$$

The clustering coefficient of a random network represents one of several aspects in which random networks differ from most real-world networks as many of them have quite high clustering coefficients. In our Matlab code, we adopt the  $G(N, \beta)$  random graph model to generate a random graph because this model is more convenient to program. In the example in Fig. 2.18, we used this code to produce the range of probabilities, where we get small average path-length  $L$  and small clustering coefficient  $C$ . We compute the differences between  $L$  and  $C$  for all probability values  $\beta$  and the minimum difference happens for  $\beta \simeq 0.2595$ . The interval around the minimum difference is the range of  $\beta$  values that represents the random network property and is denoted by  $(\beta_1, \beta_2)$ .

The  $G(N, \beta)$  model has a binomial degree distribution. For a randomly chosen node in the network, its probability of being connected to  $k$  other nodes and not to any of the rest  $(N - 1 - k)$  nodes is given by the binomial distribution.

$$P_k = \binom{N-1}{k} \beta^k (1-\beta)^{N-1-k}. \quad (2.5.17)$$

In most cases, we are interested in properties of a large-size networks. For a large  $N$  limit, the  $G(N, \beta)$  model has Poisson degree distribution, called *Poisson random graph*,

$$P(k) = \frac{\mu^k}{k!} e^{-\mu}, \quad (2.5.18)$$

where  $\mu = \langle k \rangle_{ER}$  is a constant parameter. The two distributions have identical properties, but they depend on different parameters. While the Poisson distribution depends on only one parameter  $\langle k \rangle_{ER}$ , the binomial distribution has two parameters  $N$  and  $\beta$ . Both distributions have a peak around  $\langle k \rangle_{ER}$  but Poisson distribution has a simpler form and does not depend on the number of nodes  $N$  in the network. Therefore, networks of different sizes and same average degree  $\langle k \rangle_{ER}$  have indistinguishable Poisson degree distributions (see Fig. 2.19). This simplicity makes it the preferred form for the degree distribution of

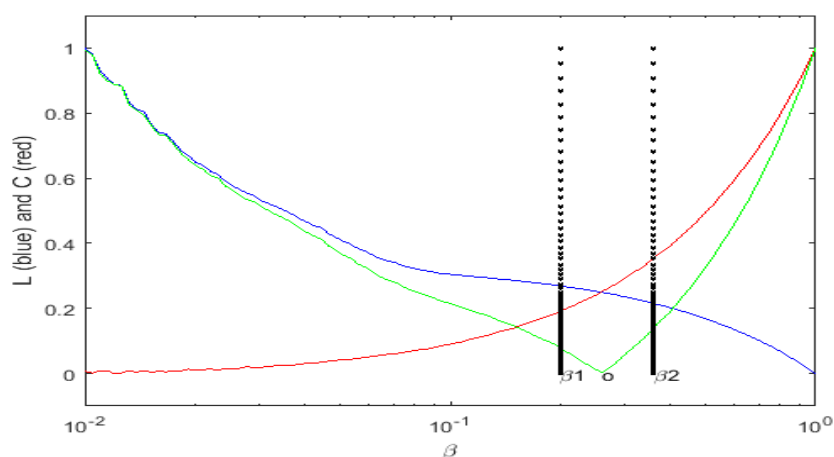


Figure 2.18: Plot of  $L$  in blue and  $C$  in red versus  $\beta$ . The green line represents the difference between  $C$  and  $L$  curves. In this figure, we have used  $N = 500$ . The minimum difference between  $C$  and  $L$  happens for  $\beta \simeq 0.2595$ , denoted by (o). The interval  $(\beta_1, \beta_2)$  represents the range of  $\beta$  values in which the resulting network becomes a random network with small average path-length and small clustering coefficient.

a random network [30].

For  $\beta = 0$ , there are no edges in the network and the size of the largest component (subnetwork) in the network is 1. When  $\beta = 1$ , every edge is connected to all others and the size of the largest component in the network is  $N$ . The size of the largest component in the first case is independent of the number of nodes  $N$  in the network while in the second case, it is proportional to  $N$  and is called a *giant component*. One of the interesting aspects of random graphs is that the increase of the size of the largest component doesn't occur gradually with the increase of  $\beta$ . It undergoes a sudden change from constant size to extensive size at one particular value of  $\beta$ .

The  $G(N, \beta)$  model is one of the best studied models of networks. It makes an useful source of insight into the structure of other networks. However, random graphs have some severe shortcomings as a network model. Its clustering coefficient tends to zero in the limit of large  $N$  and even for finite values of  $N$ , the typical clustering coefficient of random networks is very small. Also, real-world networks show grouping of nodes into communities but there is no similar structure in random networks. There are many other structures of real-world networks which are absent in random networks. The shape of the degree distribution of random graph is the most significant aspect in which the properties of random networks differ from those of real-world networks. While most real-world networks have right-skewed degree distribution which have small number of

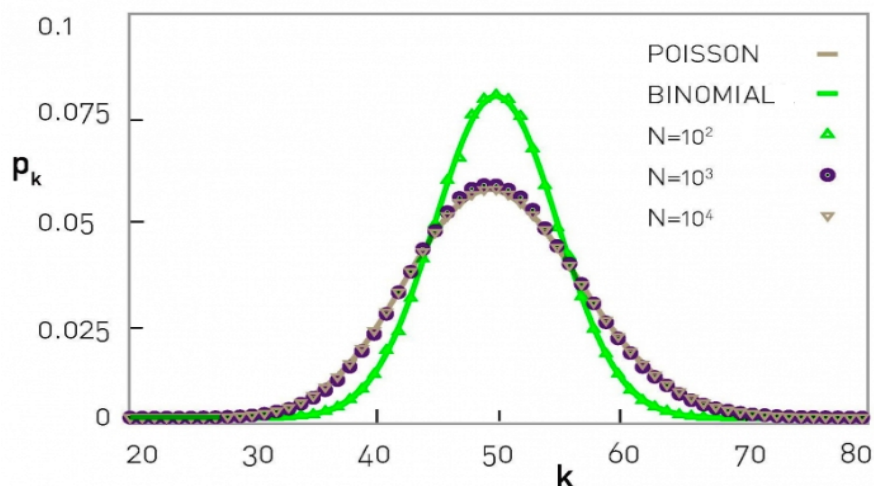


Figure 2.19: Binomial and Poisson distributions of a random network with  $N = 10^2, 10^3, 10^4$  and  $\langle k \rangle_{ER} = 50$ . The Poisson degree distribution is independent of the network size  $N$  [30].

nodes of high-degree “hubs” in the tail of the distribution, random networks have Poisson degree distribution. Poisson curve decays exponentially fast when  $k$  moves away from  $\langle k \rangle_{ER}$  which implies that nodes with too large or too small degree can hardly be found [55]. These properties of the Poisson random graph make it inadequate to explain many interesting aspects of networks [147].

The ER random graph has already been generalised to be more adequate in describing many of the real-world networks [55]. One can modify it so that it is no longer restricted in having a Poisson distribution. There are many ways to define random networks with general degree distributions. One of the most widely studied generalised random graphs is the *Configuration model*, developed by Bender and Canfield in 1978 [34]. The configuration model is specified in terms of a degree sequence but it allows to generate a random network with the same degree sequence or same degree distribution with a given network. We can construct a random graph using a given degree sequence by choosing a uniformly random matching on the degree “stubs” (half edges). This process generates all the possible matchings of stubs with equal probability (i.e. each stub is equally likely to be connected to any other). However, the number of stubs must be even to avoid no dangling stubs leftover. The configuration model does not construct simple networks as the random graph. Self-loops and multiedges are allowed in the configuration graph. The process of random permutation allows self-loops (created when picking two stubs from

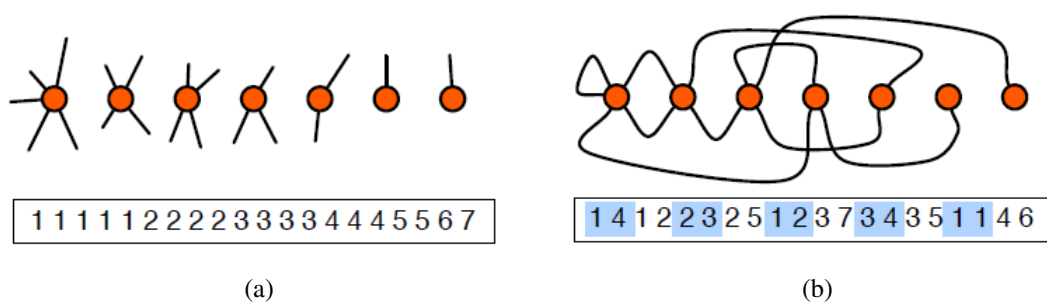


Figure 2.20: (a) Nodes of a network with their stubs (half the edges that are connected to each node). (b) The rewired pairs of the network: node 1 is reconnected to node 4 and also reconnected to node 2, node 2 is reconnected to node 3 and also reconnected to node 5, etc. Notice that node 1 is reconnected to node 2 which is a multiedge, and node 1 is reconnected to node 1 again, which is a self-loop [57].

the same node) and multiedges (created when picking pairs of stubs from the same pairs of nodes). Therefore, the generated graphs are not simple graphs but hypergraphs in which an edge can join any number of vertices. However, the self-loops and multiedges represent a tiny fraction of all edges. One can ignore their existence in configuration graphs as their average number is a constant and tends to zero when the number of nodes in a graph is very large that makes it closer to being simple graph. Avoiding the creation of self-loops and multiedges may result in a generated network which is no longer drawn uniformly [147]. One can remove such edges by rewiring them to another randomly chosen node. Such small change can preserve the degree sequence and also does not perturb too much the results of the mathematical analysis. However, rewiring does not guarantee that we obtain a simple graph.

Figure 2.20 shows an example of the “stub matching” construction of a configuration model for random graphs. Figure 2.20a shows both the nodes with their stubs which represent the initial contents of an array  $Y$  and Fig. 2.20b the wired up network defined by the in-order sequence of pairs given in the array, which has been replaced with a random permutation of  $Y$ .

### 2.5.4 Scale-free networks

The ER random networks model assumes the number of nodes  $N$  is fixed. In contrast, most real-world networks such as the World Wide Web (WWW) and citation networks grow very fast as a result of a growth process that continuously increases  $N$ . In real-world networks, nodes have the tendency to connect to nodes with higher degrees which

gradually turn into *hubs*. The presence of these few highly connected nodes (the hubs) represents the organising principle that we call the *scale-free property* [30].

In random networks, the degree distribution is described by the Poisson distribution which peaks at the average degree  $\langle k \rangle$  and decays as  $k \rightarrow 0, \infty$  (i.e. highly connected nodes, or hubs, don't exist) [55]. Real-world networks have *power-law* distributions. The relation between the logarithm of the degree distribution  $P_k$  and the node degree  $k$  is given by

$$\ln(P_k) = -\gamma \ln(k) + c, \quad (2.5.19)$$

where  $\gamma$  and  $c$  are constants. By taking the exponential of both sides of (2.5.19), we obtain

$$P_k = Ck^{-\gamma}, \quad (2.5.20)$$

where  $C$  is another constant. Equation (2.5.20) is called *power law distribution* and the exponent  $\gamma$  is its *degree exponent*. The range  $2 \leq \gamma \leq 3$  represents the typical values of the degree exponent although values outside this range are also observed occasionally. In general, degree distributions do not follow power law distribution over their entire range. Power law is obeyed in the tail of the distribution, for large values of  $k$ , but not for small  $k$  [147]. Networks whose degree distributions follow a power law distribution and are independent of the connectivity scale are called *scale-free networks*. In directed networks, each node is characterised by either its in- or out-degree. Therefore, we have two degree distributions,  $P_{k_{in}}$  and  $P_{k_{out}}$  as the scale-free property applies separately to the in- and out-degrees. Both can be approximated by a power law,

$$\begin{aligned} P_{k_{in}} &\sim k^{-\gamma_{in}}, \\ P_{k_{out}} &\sim k^{-\gamma_{out}}, \end{aligned} \quad (2.5.21)$$

where  $\gamma_{in}$  and  $\gamma_{out}$  are the degree exponents for in- and out-degrees [30].

The main difference between scale-free and random networks comes in the tail of the degree distribution which represents the region with high-degree node, or hubs (Fig. 2.21). The tendency of a forthcoming node to connect itself with nodes of high degree is referred to as *preferential attachment* which reflects the so-called ‘‘rich gets richer’’ phenomenon, or Matthew effect. The term preferential attachment was coined in 1999 by Albert-László Barabási and Réka Albert [29] who proposed a model of a growing

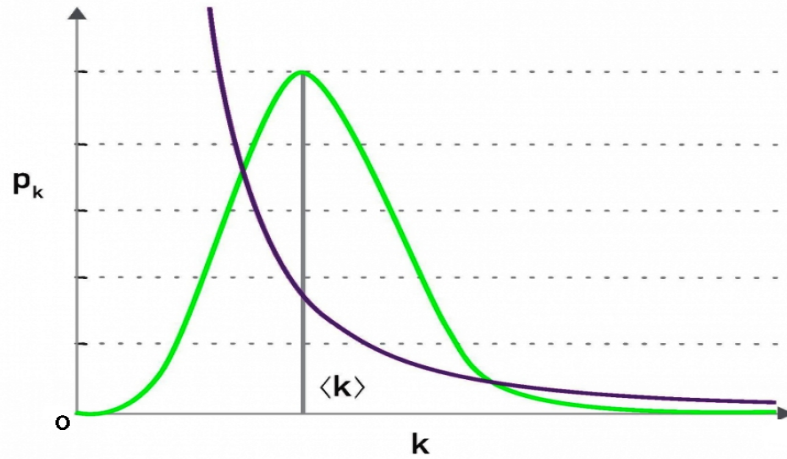


Figure 2.21: Poisson distribution (green line) of random networks and power law distribution (violet line) of scale-free networks. The vertical grey line represents the average node degree  $\langle k \rangle$  for both networks [30].

network; the *Barabási-Albert* (BA) model [15]. The BA model can generate undirected scale-free networks and shows that growth and preferential attachment are responsible for emergent phenomena in scale-free networks.

The BA algorithm is the following:

- Growth: Start from a connected network of small size  $m_o \geq 1$ , add one new node to the existing network each time. The new node is connected to  $m$  existing nodes in the network simultaneously, where  $1 \leq m \leq m_o$ .
- (Linear) Preferential attachment: The incoming new node is simultaneously connected to each of the  $m$  existing nodes, according to the probability

$$P_i = \frac{k_i}{\sum_{j=1}^N k_j},$$

where  $k_i$  is the degree of node  $i$  [55]. The average node-degree of the BA scale-free network is approximately equal to  $2m$ . The average path-length of the BA scale-free network is

$$L \sim \frac{\ln N}{\ln \ln N}. \quad (2.5.22)$$

The clustering coefficient of BA model follows

$$\langle C \rangle \sim \frac{(\ln N)^2}{N}, \quad (2.5.23)$$

and its degree distribution is approximately given by the power law

$$P(k) \sim 2m^2 k^{-\gamma}, \quad (2.5.24)$$

where  $2m$  represents the average node degree of the BA network and  $\gamma = 3$  characterises the network topology [55]. The degree distribution of BA model reveals the close relationship between topology and dynamics of the network. In BA model, many nodes are randomly connected by short paths and that means  $L$  is not very large in BA model. The term  $(\ln N)^2$  in (2.5.23) increases the clustering coefficient for large  $N$  and therefore, BA networks are locally more clustered than random networks [30].

### 2.5.5 Small-world networks

The *small-world effect*, also known as *six degrees of separation* is often associated with the psychologist Stanley Milgram's letter-passing experiment in the 1960s [190]. In Milgram's experiment, people were asked to send a letter from an initial recipient to a distant target person by passing it from one acquaintance to another through the social network. It states that if we choose any two individuals anywhere in the world, we will find a path of at most six acquaintances connecting them [147]. In mathematical terms, the small-world effect implies that the distance between any two randomly chosen nodes in a network is small. Hence, the small-world effect is defined by

$$L \propto \log(N), \quad (2.5.25)$$

where  $L$  is the typical distance between any two randomly chosen nodes (the number of steps required) and grows proportionally to the logarithm of the number of nodes  $N$  in the network.

The *Watts-Strogatz* (WS) model is a family of small-world networks formulated by Duncan Watts and Steve Strogatz in 1998 [197]. The WS model has small-world (SW) properties, i.e. high clustering coefficient and small average shortest path-length. WS network can be generated by the following algorithm (rewiring method):

- 1- It first creates a ring lattice with  $N$  nodes of mean degree  $2K$  as each node is connected to its  $K$  nearest neighbours on either side, where  $K$  is a small integer.
- 2- For every pair of connected nodes in the ring, rewire the edge in such a way that the beginning end of the edge is kept but the other end is disconnected with probability  $\beta$  and reconnected to a randomly chosen node from the ring.

The rewiring process is performed edge by edge, once only, and the rewired edge cannot be a duplicate or self-loop [55]. The randomly placed edges are commonly referred

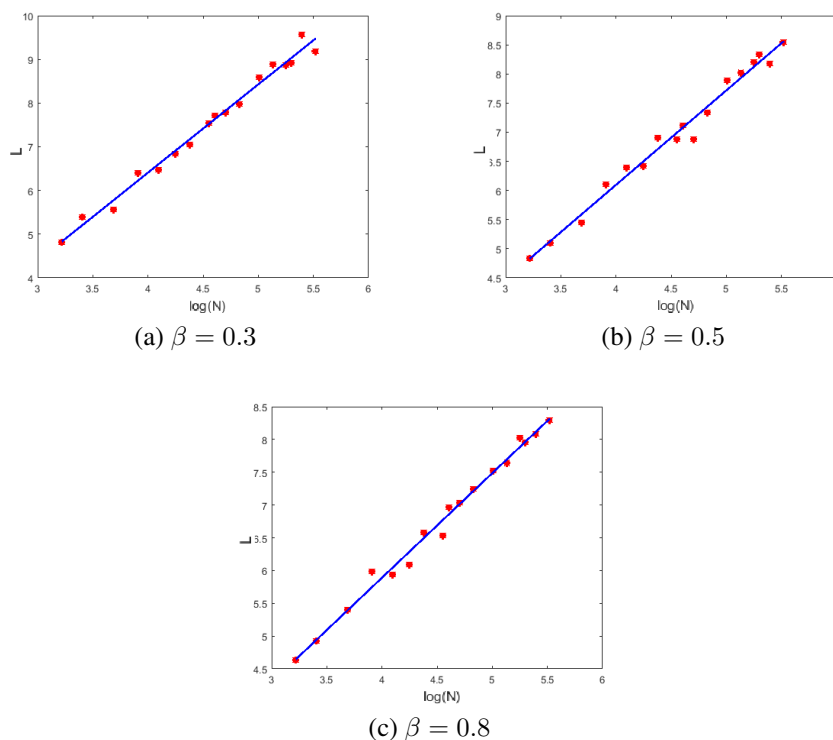


Figure 2.22: Plots of average shortest path-length  $L$  versus the logarithm of the number of nodes  $N$  for different size networks,  $\log(N)$  with  $K = 2$  and for different values of  $\beta$ , (a)  $\beta = 0.3$ , (b)  $\beta = 0.5$  and (c)  $\beta = 0.8$ . The red points represent  $L$  as a function of  $\log(N)$  for each network and the blue lines are fitting lines to the red points.

to as *shortcuts* because they create shortcuts from one part of the ring lattice to another. We implemented a Matlab code for the rewiring method for ring lattices. For increasing probability  $\beta$ , it computes the average shortest path-length  $L$  for each resulting graph and plots them versus the logarithm of the number of nodes  $N$  in each graph (Figs. 2.22).

The rewiring process in WS network can destroy the network connectivity by possibly creating some unconnected subnetworks. Later, a simplifying modification was made by *Newman and Watts* (NW) by replacing “random rewiring edges” with “random adding edges” (see Fig. 2.23). The NW algorithm is as follows:

- 1- Start from a ring with  $N$  nodes, in which each node is connected to its  $2K$  neighbours, where  $K > 0$  is an integer (usually small).
- 2- For every pair of originally unconnected nodes, with probability  $\beta$ , add a new edge to connect them.

In NW networks, one introduces new shortcut edges just as in the WS model, but without removing edges from the ring substrate. For each edge in the ring-shaped net-

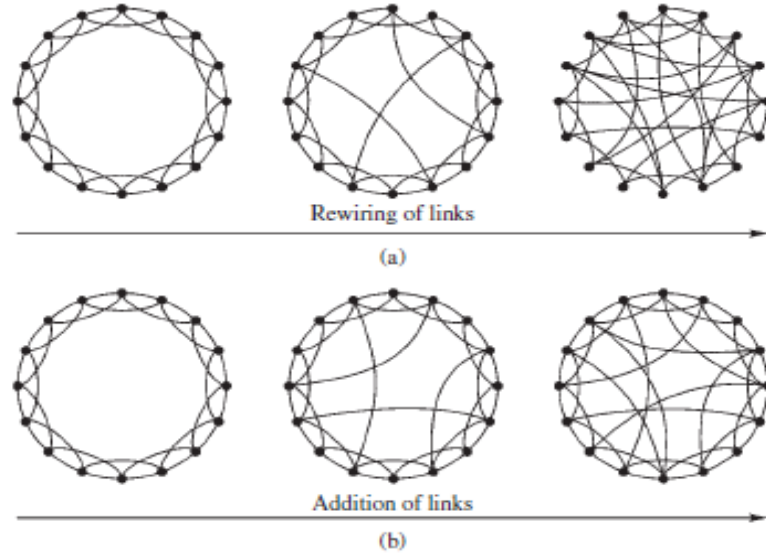


Figure 2.23: Two small-world network models: (a) Watts-Strogatz (WS) network model. (b) Newman-Watts (NW) network model [55].

work, there is an independent, uniform probability  $\beta$  of adding a shortcut between a pair of nodes that are chosen uniformly at random. Thus, no disconnected parts can appear in NW networks [203].

The average shortest path-length  $L$  of a WS small-world network is given by

$$L = \frac{2}{N(N-1)} \sum_{i=1}^N \sum_{j=1}^N d_{ij}, \quad (2.5.26)$$

where  $d_{ij}$  is the number of edges in the shortest path between nodes  $i$  and  $j$  and,  $N$  is the number of nodes in the network. The local clustering coefficient of node  $i$ ,  $C_i$  is the ratio of the actual number of edges between all neighbours of node  $i$  over the expected number of edges between all neighbours of node  $i$  and is represented by

$$C_i = \frac{2l_i}{k_i(k_i - 1)}, \quad (2.5.27)$$

where  $l_i$  represents the number of triangles attached to node  $i$  of degree  $k_i$ . The global clustering coefficient is

$$C = \frac{3 \times \text{Number of triangles}}{\text{Number of connected triples}}, \quad (2.5.28)$$

where a triangle consists of 3 nodes that are completely connected to each other and a connected triple consists of three nodes  $i, j, k$  such that node  $i$  is connected to node  $j$  and node  $j$  is connected to node  $k$ .

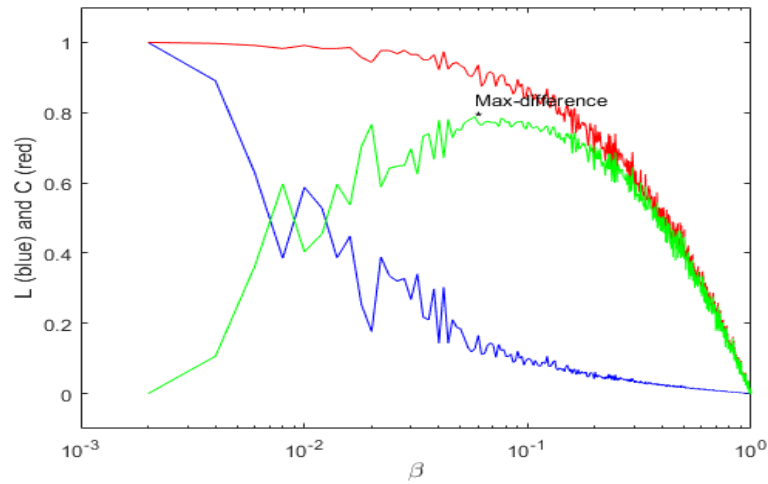


Figure 2.24: Plot of the average path-length  $L$  in blue and clustering coefficient  $C$  in red versus probability  $\beta$ . The green line represents the difference between  $C$  and  $L$  as a function of  $\beta$ .

The degree distribution of the WS small-world network is given by

$$P(k) = \sum_{i=0}^{\min(k-K, K)} \binom{K}{i} (1-\beta)^i \beta^{K-i} \frac{(K\beta)^{k-K-i}}{(k-K-i)!} e^{-K\beta} \quad (k \geq K), \quad (2.5.29)$$

with  $k$  represents the node-degree and  $K > 0$  is a small integer where  $2K$  is the initial connections for each node to its nearest neighbours [55].

The regular ring lattice for  $\beta = 0$  is a highly clustered network (large-world) where  $L$  grows linearly with  $N$  and the random graph for  $\beta = 1$  is a poorly clustered network (small-world) where  $L$  grows logarithmically with  $N$ . The small-world network results from the immediate drop in  $L$  caused by the introduction of a few shortcuts. For small  $\beta$ , each shortcut has a nonlinear effect on  $L$  and is reducing the distance not just between the pair of nodes but also in its immediate neighbourhood. By contrast, an edge rewired from a clustered neighbourhood to make a shortcut has, at most, a linear effect on  $C$  [197]. Figure 2.24 shows both the effects on the average path-length  $L$  and clustering coefficient  $C$  when  $\beta$  increases from 0 to 1. For a wide range of  $\beta$  values the resulting network becomes a small-world network with a small average path-length and a large clustering coefficient.

The class of small-world networks represents a middle ground between regular and random networks (Fig. 2.17), i.e, they have high clustering coefficient like regular networks, and small average path-lengths as random networks. The small-world networks

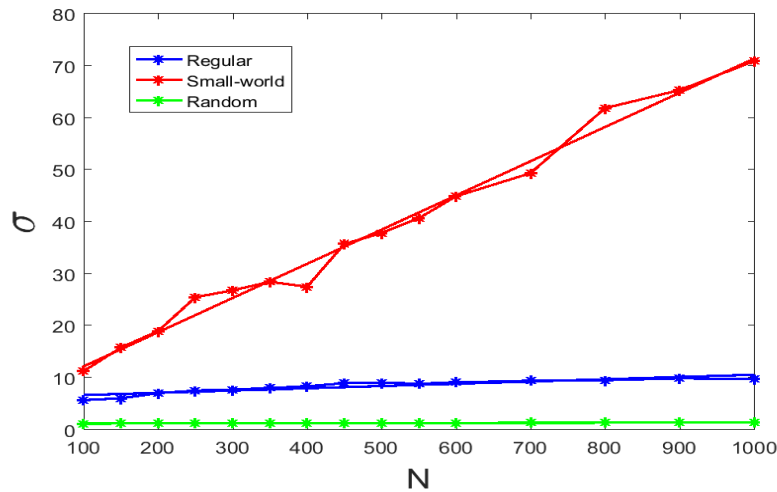


Figure 2.25: The values of  $\sigma$  for three types of networks: regular (blue), small-world (red) and random (based on the configuration model) (green) for different network sizes  $N$ . The lines are linear fittings to the data-points. The slope for the blue line (regular network) is 0.0043, the slope for the red line (small-world network) is 0.07 and the slope for the green line (random network) is 0.0002.

such as the Internet and neural networks also have other structural properties different from those of random or regular networks which resemble those of small-world networks.

### 2.5.6 Quantifying Watts-Strogatz small-world networks

The structural properties of small-worldness can be quantified by comparing the average shortest path-length  $L$  and clustering coefficient  $C$  of a given network to a random network with the same degree probability distribution function (pdf) and same network size  $N$  [33]. We first compute the average local clustering coefficient  $C$  of the studied network and the average of the local clustering coefficients of a large number  $n$  of random networks,  $\langle C_r \rangle_n$ , of the same degree pdf with the studied network and using the configuration model, the average shortest path-length  $L$  of the studied network and the average shortest path-length of the same  $n$  random graph networks,  $\langle L \rangle_n$  [20].

The small-world networks are in between the limits of regular networks with large  $L$  and  $C$  and random networks with small  $L$  and  $C$ . To quantify small-worldness we use the ratios [33],

$$\mu = \frac{L}{\langle L_r \rangle_n}, \quad \gamma = \frac{C}{\langle C_r \rangle_n}. \quad (2.5.30)$$

A simple measure of small-worldness can then be defined as

$$\sigma = \frac{\gamma}{\mu}. \quad (2.5.31)$$

The higher  $\sigma$  is from unity for a given network, the better it displays the small-world property. We implemented a Matlab code to quantify three types of networks; regular, small-world and random networks (based on the configuration model) for different sizes  $N$ . In Fig. 2.25, the slopes for the regular and random networks are closer to 0 and that indicates that both networks do not have small-world properties. However, in the case of the small-world network, the slope is about 0.07 which indicates that  $\sigma$  increases beyond 1 as the size of the network grows. This result shows that for large-size small-world networks,  $\sigma$  is higher than one. That shows that the network acquired the main two properties of a small-world network; namely, small average shortest path-length and high clustering coefficient.

# Chapter 3

## Biological neuron models

### Introduction

In this chapter, we will discuss properties of biological neuron models. First, we briefly review the anatomy of both the nerve cells (neurons) and the brain. Then, we will explain why we should think about the brain as a complex network and in particular, as a small-world network. Quantitative mathematical models have proved to be an indispensable tool in understanding neural dynamics and transmission of information. We discuss the Hindmarsh-Rose system which models the spike-bursting behaviour of the membrane potential of a single neuron and provides a mathematical description of neuronal activity.

### 3.1 The neuron

The *nervous system* is, in effect, a communication system transmitting electro-chemical impulses and the structural units of this communication system are the individual *nerve cells* or *neurons* [74]. Neurons are cells that receive, process, and transmit information to other nerve cells, muscle, or gland cells. Although neurons are highly diversified in both structure and function, a typical neuron has all the parts that any cell in the body would have, and also few specialised structures that set it apart. Its parts can be divided into: the *soma* or cell body, the *dendrites*, and the *axon* (Fig. 3.1a). The soma contains the *nucleus*, which in turn contains the genetic material in the form of *chromosomes*. Neurons have a large number of tree-like cellular extensions called dendrites. The dendrites are the primary sites for receiving and integrating information in the form of chemical messages from other neurons [188]. Dendrites typically branch and get thinner with each branching, and extend their farthest branches a few hundred micrometers from the soma. The dendritic branches are often crucial to the neuron's function. The axon is another ex-

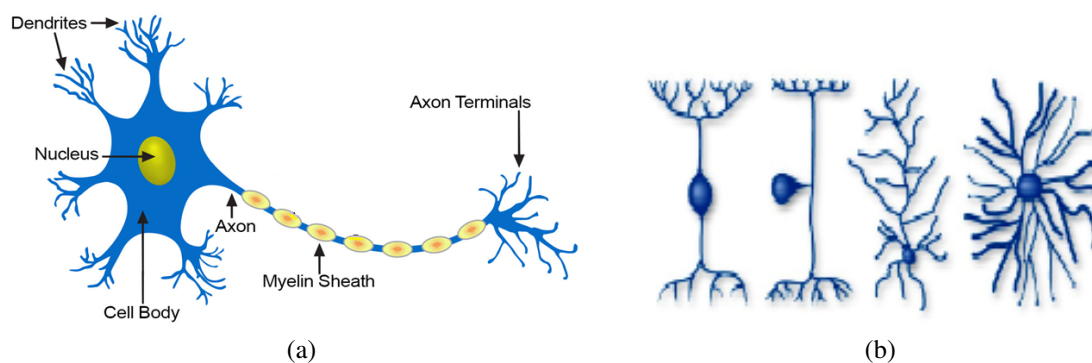


Figure 3.1: (a) The three basic parts of a neuron: the soma (cell body) containing the nucleus, the dendrites which are short branches off the cell body that receive incoming impulses and a single long axon that carries impulses away from the cell body and to the next neuron [7]. (b) Different types of branching in neurons [3].

tension from the cell body. It can extend for great distances and often gives rise to many smaller branches before ending at *axon terminals* (Fig. 3.1b). These axon branches enable the neurons to communicate with many target cells. But unlike dendrites, axons usually maintain the same diameter as they extend. The purpose of the axon is to transmit electrochemical signals to other neurons. Sometimes, that happens over a considerable distance, like in the neurons that make up the nerves running from the spinal cord to one's toes, the axons can be as long as three feet! Longer axons are usually covered with a *myelin sheath*, fatty cells which have wrapped around an axon many times. Myelin sheaths serve a similar function as the insulation around electrical wire.

The human brain has a large variety of shapes and sizes of neurons but most neurons can fit in one of two classes: *principle neurons* and *interneurons*. Principle neurons are the largest neurons in a given region of the brain and they control what kinds of messages will be sent out to the other regions through their myelinated axons. Whereas, interneurons come in a variety of shapes and sizes, they do not send their axons out to other regions. They connect neurons within specific regions of the central nervous system [188]. The structural classification of neurons depends on many aspects such as polarity, location and function. Most neurons can be anatomically characterised as *unipolar*, *bipolar*, *pseudounipolar* and *multipolar* (Fig. 3.2a). Other neuron types can be identified according to their location in the nervous system and their distinct shape such as the *pyramidal*, *granule*, *Purkinje* and *basket* nerve cells (Fig. 3.2b). There is a very tiny gap between the axon ending and the dendrite of the next neuron and is called the *synapse*. Synapses are spe-

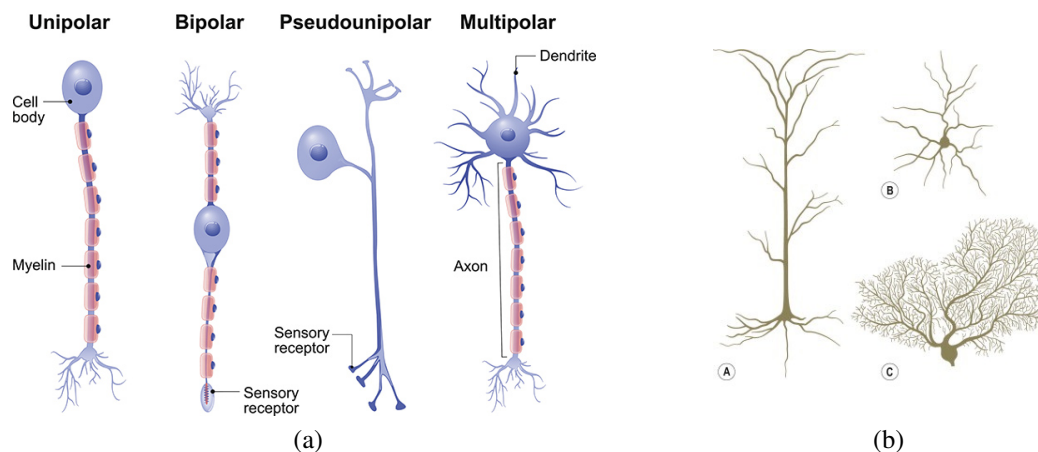


Figure 3.2: (a) Classification of neurons depends on their polarity: unipolar, bipolar, pseudounipolar and multipolar [4]. (b) Three neurons with distinct shapes: pyramidal (A), granule (B) and Purkinje (C) [13].

cialised structures where *neurotransmitter* chemicals are released to communicate with target neurons by chemically modifying the properties of the gap [147]. They compose of three main parts: the *presynaptic* endings which contain the neurotransmitters (inside the synaptic vesicles), the *postsynaptic* endings which contain the *receptors* and the *synaptic cleft* between them (Fig. 3.3). The most common types of synapses in the brain are the *chemical* synapses, in which the presynaptic neuron triggers the release of chemical messengers, the neurotransmitters through the *voltage-gated ion channels*. Neurotransmitters diffuse across the synaptic cleft and bind to specialised receptors of the postsynaptic cell. Most of these receptors are *ligand-gated ion channels* which open to allow ions to pass

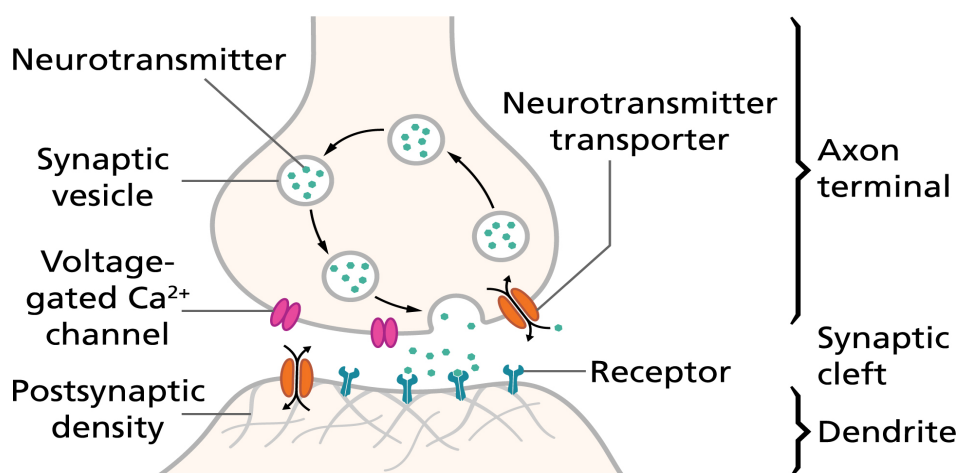


Figure 3.3: The typical structure of a synapse composes of presynaptic neuron, postsynaptic dendrite and the synaptic cleft. The neurotransmitters diffuse across the synaptic cleft and bind to the specialised receptors [14].

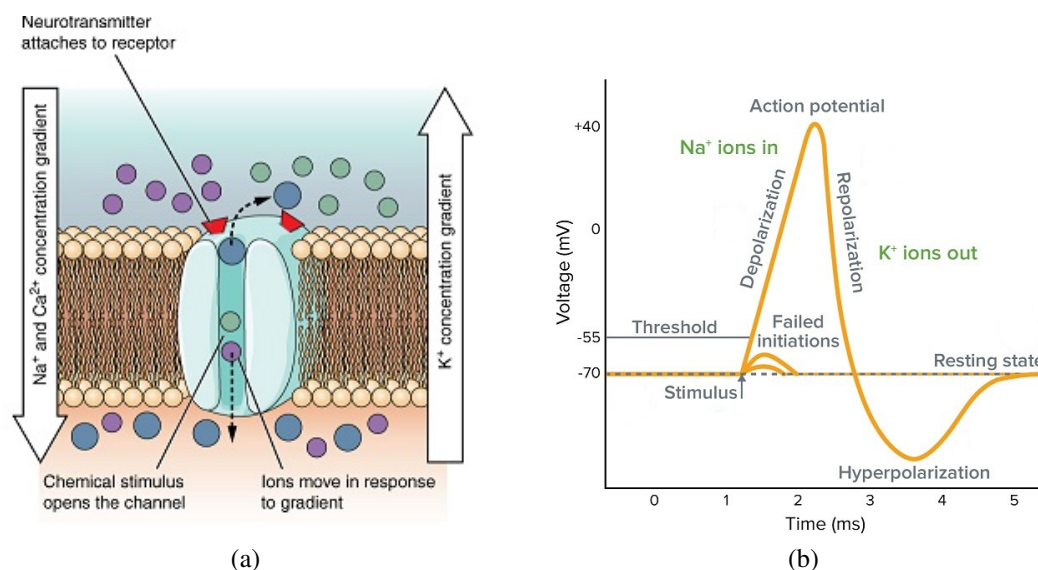


Figure 3.4: (a) The neurotransmitters bind to a specific location on the extracellular surface of the channel protein and the pore opens to allow selected ions to go through [8]. (b) The typical shape of an action potential that passes through a neuron, consists of four stages: depolarisation, repolarisation, hyperpolarisation and the resting potential [1].

through (Fig. 3.4a). The voltage-gated ion channels are proteins embedded in the plasma membrane. They are usually ion-specific; sodium  $Na^+$ , potassium  $K^+$ , calcium  $Ca^{2+}$ , and chloride  $Cl^-$  ions channels have been identified. Neurotransmitters, either excite or inhibit the postsynaptic neuron. *Glutamate* and *dopamine* are two types of neurotransmitters which have excitatory effects on the neuron. Whereas, inhibitory neurotransmitters such as *gamma-aminobutyric acid* (GABA) and *serotonin* keep the excitatory system from becoming overactive.

Apart from chemical synapses, neurons can also be coupled by *electrical* synapses which allow electrical signals to travel quickly from the presynaptic cell to the postsynaptic cell. Specialised membrane proteins make the direct electrical connections between the two neurons [82]. Chemical synapses can be excitatory or inhibitory while electrical synapses are excitatory only. The excitation leads to the firing of an *action potential* (also called *spike* or *impulse*) while inhibition prevents the propagation of the electrical signal.

In all types of cells, there is an electrical potential difference between the inside of the cell and the surrounding extracellular fluid and is termed the *membrane potential* of the cell. This phenomenon is especially important in nerve cells, because changes in their membrane potentials are used to code and transmit information. The action potential is the rapid rise and subsequent fall in voltage or membrane potential across the cellular

membrane of the neuron. Sufficient current must be administered to the neuron in order to raise the voltage above the *threshold voltage* (about -55 mV) to start membrane *depolarisation* which is caused by opening of sodium channels in the cellular membrane, resulting in a large influx of sodium ions. That is followed by rapid sodium channel inactivation as well as a large efflux of potassium ions resulting from activated potassium channels which causes the membrane *repolarisation*. *Hyperpolarisation* is a lowered membrane potential caused by the slow closure of the potassium channels. Then, the membrane potential returns to the resting voltage (*resting potential*, the value of which is in general about -70 mV) that occurred before the next stimulus (see Fig. 3.4b). While an action potential is in progress, another one cannot be initiated. This effect is referred to as the *refractory period*. It has two phases; the *absolute refractory period*, in which the neuron cannot spike no matter how the strength of the stimulus is and the *relative refractory period*, in which the neuron can spike given a sufficiently strong stimulus. In case that the membrane potential does not reach the threshold value, the neuron respects the *all or none principle* and no action potential is fired [63].

In addition to nerve cells, there are non-neuronal cells in the central nervous system called *glial cells* or *neuroglia*. They are quite different from nerve cells, glia do not participate directly in synaptic interactions and electrical signaling. They provide support and protection for neurons and their supportive role help define synaptic contacts and maintain the signaling abilities of neurons [160].

## 3.2 The brain

The *brain* is a jelly-like mass of tissue containing a staggering number of neurons. In the adult human brain, there exists approximately 86 billion neurons [23, 127] interacting through approximately 150 trillion synapses [127, 154]. It is divided into left and right cerebral hemispheres that are separated by a groove filled with cerebrospinal fluid (Fig. 3.5a). Each of these hemispheres has an outer layer of grey matter, the *cerebral cortex* which gives the brain its characteristic wrinkly appearance and supported by an inner layer of white matter. The grey matter consists of neuron cell bodies and subcortical nuclei is the site of neuronal interactions [188]. Each hemisphere has been divided into four lobes: *frontal*, *parietal*, *temporal* and *occipital* (see Fig. 3.5b). The frontal lobe is the biggest

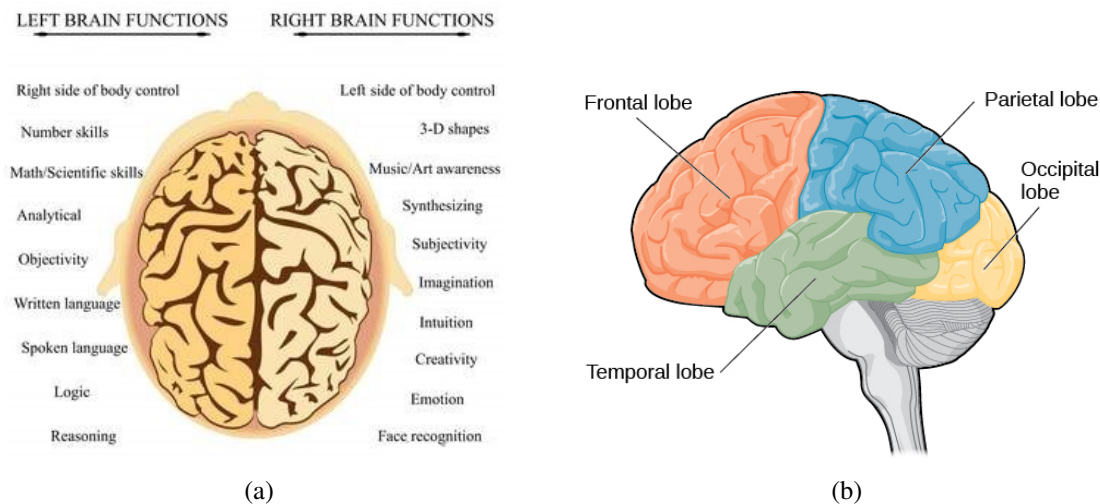


Figure 3.5: (a) The right hemisphere of the brain is responsible for the control of the left side of the body and the left hemisphere is responsible for the control of the right side of the body [2]. (b) Each hemisphere is divided into four lobes: frontal, parietal, temporal and occipital [6].

part of the brain and located at the front of each cerebral hemisphere. It looks after functions associated with attention, short-term memory tasks, planning, and the control of our behaviour and emotions. The parietal lobe is located above the occipital lobe and behind the frontal lobe. The parietal lobe is important in language processing and contains the primary sensory cortex which controls inputs from the skin (touch, temperature, and pain receptors). The temporal is the portion of the cerebral cortex laying roughly above the ears and includes the auditory areas, each receiving information primarily from the opposite ear. The occipital lobe is the visual processing centre of the brain. Several regions of the occipital lobe are specialised for different visual tasks, such as color differentiation, visuospatial processing and motion perception. In addition to the brain lobes, other important regions in the brain such as the *cerebrum*, *thalamus*, *hippocampus*, *cerebellum* and *brainstem* perform and coordinate many other functions of the brain and connect it to the spinal cord [188].

### 3.3 Brain plasticity

The capacity to change is a fundamental characteristic of nervous systems. *Brain plasticity*, also known as *neuroplasticity*, can be defined as the ability of the nervous system to change its activity in response to stimuli by reorganising its structure, functions or connections. Understanding brain plasticity is obviously of considerable interest because

it provides a window to understanding the development of the brain and behaviour and allows insight into the causes of normal and abnormal behaviour [41, 116, 135].

One of the main properties of neurons is their ability to modify the strength and efficiency of synaptic transmission through a diverse number of activity-dependent mechanisms which are typically referred to as *synaptic plasticity*. At the single cell level, it refers to changes in the connections between neurons, whereas *non-synaptic plasticity* refers to changes in their intrinsic excitability. Furthermore, synaptic plasticity can be classified as either *short-term* or *long-term* because it happens at different time scales, from tens of milliseconds to life-long changes in synaptic transmission [91]. Synaptic plasticity is essential to the development and function of the brain, especially for memory and learning processes [135]. *The Hebbian theory*, also called *Hebb's rule*, was a leading attempt to explain synaptic plasticity and the adaptation of brain neurons during the learning process. It was introduced by the Canadian psychologist Donald Hebb in his book "*The Organisation of Behaviour*" in 1949 [89]. It states that: "When an axon of cell *A* is near enough to excite cell *B* or repeatedly or persistently takes part in firing it, some growth process or metabolic change takes place in one or both cells such that *A*'s efficiency, as one of the cells firing *B*, is increased" [81, 89]. It claims that an increase in synaptic efficiency arises from a presynaptic neuron's repeated and persistent stimulation of a postsynaptic cell. Hebb's theory is often summarised by Siegrid Löwel's phrase: "Cells that fire together, wire together" [91, 132].

Brain plasticity is used in a broader context to indicate changes that occur throughout life either at the synapse or whole neurons or even at entire brain regions [91]. It allows an individual to adapt to a rapidly changing environment through strengthening, weakening, pruning, or adding of synaptic connections. Among the many factors that affect neuronal structure and behaviour are experiences, genetic factors, diseases, hormones and psychoactive drugs [116]. There are two types of neuroplasticity:

- **Functional plasticity:** The brain's ability to adapt to loss of or damage to tissue by transferring all or part of the functions previously performed by those damaged areas to other regions. The degree to which the brain is able to do this successfully has been called *functional reserve*, the ability of the brain to cope with increasing damage while still functioning adequately and that depends on several factors,

including age and health status of the brain.

- Structural plasticity: The brain's ability to actually change its physical structure by rewiring its connections as a result of learning and training.

Less is known about the possibility that plastic changes in neuronal circuits are likely to be the basis of pathological behaviour. Many drug addicts often show cognitive deficits and it seems reasonable to propose that at least some of these deficits could arise from abnormal neuronal circuitry [116]. The brain plasticity concept is not part of the research subject in the thesis and we did not deal with it. Still, it is an important concept related to the proper functioning of the brain and needs to be discussed.

### 3.4 Brain dynamical networks (BDNs)

Complex networks model the behaviour of systems that are composed of thousands or millions of interacting elements. They display diverse and organised patterns which are the outcome of highly structured and selective coupling between these elements through an intricate web of connectivity [183]. It is useful to approach the interactive nature of brain function from a complex network perspective. This approach can provide us with fundamental insights into the means by which thousands of simple elements can organise into complex and dynamic patterns. The collective actions of individual neurons linked together by a dense web of connectivity, shape our thoughts and behaviour, retrieve memories and create consciousness. To fully understand brain function, we need to approach the brain on multiple scales, by identifying the networks that bind the neurons. Brain networks compose of multiple spatial scales, from the *microscale* of individual cells and synapses to the *macroscale* of cognitive systems and embodied organisms [183].

Small-world networks lie in between regular and random networks but have the benefits of both configurations; short average path-length and high clustering coefficient. The small-world configuration represents an attractive model for the organisation of brain anatomical and functional networks. Its topology can support both segregated (specialised) and distributed (integrated) information processing in brain networks [22]. The high clustering in small-world network is compatible with segregated or modular processing and its short path-length is compatible with distributed or integrated processing of information [33].

The *network efficiency* of information transmission is an alternative metric that can be related to average path-length  $L$  and clustering coefficient  $C$ . The *global efficiency* can be represented as the inverse of the average path-length between all pairs of nodes in the network,  $E_{glob} \sim \frac{1}{L}$ . The shorter the average path-length, the more efficient the network. Global efficiency is preferable to average path-length as a metric of brain network topology. It is related to the efficiency of the system for information transmission between any two nodes via multiple parallel paths as we know the brain instantiates parallel processing [19]. Also, we can define the *local efficiency* of a network as proportional to the clustering coefficient  $C$ ,  $E_{loc} \sim C$  [33].

Another aspect related to the small-world brain network topology is the economic problem of cost-effective information processing. Many parts of brain structure are compatible with a selection to minimise wiring costs; the separation of visual cortical areas, the segregation of white and grey matters and the scaling of the number of areas/neuronal density with brain size. However, that can allow only local connections and not long-distance connections which could lead to delay in information transfer. By adding several long-distance connections, the brain minimises energy costs and creates a small-world network [33]. Watts and Strogatz (1998) indicate that with the increasing of random connections in a regular network by only 4%, the network efficiency can be increased by a staggering 40%! Thus, the small-world model is of special interest when describing human brain networks. It is well suited for complex brain dynamics (e.g. a high rate of information transmission) because it supports efficient information segregation and integration with low energy and wiring costs [197].

The graphical analyses of cortical networks preceded the mathematical development of the small-world model. Later, many aspects of the anatomical connectivity had been identified to be compatible with the structure of the small-world networks. The neural network of the *Caenorhabditis elegans* worm was the first to be formally quantified as a small-world network. The brain of *C. elegans* is simple and almost every specimen of the worm has the same wiring pattern which has been exactly described in terms of the 2462 synaptic connections between each of 282 constituent neurons. The characteristics of its network were found neither random nor regular but a small-world network, with an average path-length of  $L = 2.65$  and an average clustering coefficient of  $C = 0.28$  [197].

The primary information processing element in the brain is the neuron which com-

bines several inputs to generate a single output. The output signal of the presynaptic neuron must be conveyed through synapse to reach the postsynaptic neuron. If inputs to neurons are excitatory, they increase the chance of firing. Otherwise, inhibitory inputs make the receiving neuron less likely to fire. The combination of excitatory and inhibitory inputs allows neurons to perform quite complex information processing tasks, while brain regions which each consists of large number of neurons can perform tasks of extraordinary complexity. In the thesis, we use simplified models of brain networks by reducing the amount of detailed information. In network terms, nodes can represent the functional units, information sources or brain regions and edges can represent the connections between them [147].

### 3.5 Biologically inspired neuron models

The fundamental building block of every nervous system is the neuron. Neurons have remarkable numbers of shapes, sizes and functions, and therefore exhibit many different types of dynamics [119]. Understanding the dynamics and computations of single neurons and their role within brain dynamical networks is therefore at the core of neuroscience [94, 185].

Neuronal modelling is the process that produces a mathematical structure which incorporates the biophysical and geometrical characteristics of a biological neuron. This structure is referred to as a model of the neuron which serves a number of purposes such as; it can be used as the basis for estimating the biophysical parameters of real neurons or it may be used to define the computational and information processing properties of a neuron [128]. Quantitative models have been designed to address the question: how do single-cell properties contribute to information processing and, ultimately, behaviour? Later, experiments with single-cell models led to the development of data analysis tools for efficient parameter estimation and assessment of model performance. A delicate balance is required between incorporating sufficient details to account for complex neuron dynamics and reducing this complexity to the essential characteristics to make a model tractable. Incorporating every biological detail of the investigated neurons is likely to obscure the focus on the essential dynamics whereas highly abstract processing schemes casts doubt on the biological relevance of specific findings. It remains unclear which level

of neuron modelling is appropriate to understand the dynamics and computations carried out by the brain network. However, by understanding how neurons operate as part of a network can help us assess the appropriate level of detail required for modelling as that depends on the particular goal of the model. Deriving model parameters from experimental data has its own problems: how should we deal with the cell-to-cell variability of parameters values? In general, the dynamical behaviour of single-cell models is not a monotone function of their parameters [94].

Neuron biological models can be divided into two categories according to the physical units of the interface of the model. Each category could be further divided according to the abstraction/detail level:

- Electrical input-output membrane voltage models: models in this category describe the relationship between neuronal membrane currents at the input stage, and membrane voltage at the output stage. The types of models in this category include:
  - Integrate-and-fire [46].
  - Leaky integrate-and-fire [186].
  - Fractional-Order Leaky integrate-and-fire [187].
  - Exponential integrate-and-fire [32, 44].
  - Compartmental models [124].
- Natural input stimulus neuron models: models in this category were derived following experiments involving natural stimuli such as sound, light, touch or odour. The average response of several different spike patterns often converges to a clear pattern. The types of models in this category include:
  - Non-homogeneous Poisson process model [90, 161].
  - Two-state Markov model [152].

The *integrate and fire* neuron model is probably the best-known and the most widely used model for analysing the behaviour of neural systems. The signals received by a neuron via its synaptic contacts rise its membrane potential as the result of the stimulation and an action potential (spike) is generated when the membrane potential reaches a threshold. These signals are labelled as excitatory or inhibitory depending upon whether

the membrane potential is depolarised or hyperpolarised. The spike provides a stimulus to neighboring neurons. At the beginning of the spike time, currents of appropriate shapes are injected into neighboring neurons [46, 119]. This complicated process is described by the *Hodgkin-Huxley* (HH) model which is a neuronal model developed by Alan Hodgkin and Andrew Huxley in 1952 [101]. The model consists of three coupled first order nonlinear ordinary differential equations, known as the Hodgkin-Huxley equations which describe the ionic mechanisms underlying the initiation and propagation of action potentials in the squid giant axon:

$$\begin{aligned}
 I_{ion} &= \bar{g}_{Na}m^3h(V_m - E_{Na}) + \bar{g}_kn^4(V_m - E_k) + \bar{g}_L(V_m - E_L), \\
 \dot{m} &= \alpha_m(V)(1 - m) - \beta_m(V)m, \\
 \dot{h} &= \alpha_h(V)(1 - h) - \beta_h(V)h, \\
 \dot{n} &= \alpha_n(V)(1 - n) - \beta_n(V)n,
 \end{aligned} \tag{3.5.1}$$

where  $V_m$  is the membrane potential,  $E_k$  the equilibrium potential and  $I_{ion}$  the total ionic current. The sodium conductance is modelled with gates of types  $m$ ,  $h$  and the potassium conductance is modelled with gates of type  $n$ .  $\bar{g}_{Na}$ ,  $\bar{g}_k$  are voltage-dependent quantities and the leakage current  $g_L$  is a constant [101, 146]. The Hodgkin-Huxley model will continue to play an active role in our understanding of neural information processing but because of its complexity and limitations, several simplified neuronal models have also been developed such as the *Fitzhugh-Nagumo* model [75]. There are many forms of the equations in the Fitzhugh-Nagumo model. In general, it is a 2-dimensional model given by:

$$\begin{aligned}
 \dot{V} &= f(V) - W + I, \\
 \dot{W} &= a(bV - cW),
 \end{aligned} \tag{3.5.2}$$

where  $V$  is the membrane potential,  $W$  a recovery variable,  $I$  the magnitude of the stimulus current and  $a$ ,  $b$  and  $c$  are constant parameters. The function  $f(V) = V - \frac{V^3}{3}$  is a third order polynomial that provides the positive feedback, while the slower recovery variable  $W$  provides the negative feedback [192].

### 3.6 The Hindmarsh-Rose model

The *Hindmarsh-Rose* (HR) model developed by Jim Hindmarsh and Malcolm Rose (1982-1984), is a system for neuronal activity which studies the spike-bursting behaviour of the membrane potential of a single neuron. It can be seen either as a simplification of the Hodgkin-Huxley model or a generalisation of the Fitzhugh-Nagumo model. The HR model not only simplifies the HH model but it also mimics almost all the behaviours of real, biological neurons [110, 185]. The HR 1984 model comprises three nonlinear ordinary differential equations and thus, has three dynamical variables, namely  $x(t)$ ,  $y(t)$ , and  $z(t)$  written in dimensionless units. The relevant variable  $x(t)$  is the *membrane potential*. The two other variables are  $y(t)$  and  $z(t)$ , which represent the transport of ions across the membrane potential through the ion channels. The rate of transport of ions through the fast ion channels is measured by  $y(t)$ , which is called the *spiking variable* (also known as the *recovery current*). The transport of other ions is made through the slow channels, and its rate is measured by  $z(t)$ , which is called the *bursting variable* (also known as the *adaptation current*). The system is given by

$$\begin{aligned}\frac{dx}{dt} &= y - ax^3 + bx^2 - z + I_{ext}, \\ \frac{dy}{dt} &= c - dx^2 - y, \\ \frac{dz}{dt} &= r[s(x - x_o) - z],\end{aligned}\tag{3.6.1}$$

where  $a, b, c, d, s, r, x_o$  and  $I_{ext}$  are the system's eight parameters. It is common to fix the values of some of them and let the others be control parameters.  $I_{ext}$  mimics the membrane input current for biological neurons. It is usually taken as a control parameter and its value ranges between  $-10$  and  $10$ . The other control parameters are  $a, b, c, d$  and when fixed, they take the values  $a = 1, b = 3, c = 1, d = 5$ .  $r$  modulates the slow dynamics of the system by controlling the speed of variation of the slow variable  $z(t)$  and takes value of the order of  $10^{-3}$ . The parameters that are kept fixed are  $s = 4$  and the resting potential  $x_o = -1.6$  [20, 21, 98, 185]. It is worth mentioning that as the parameter  $r$  is set to a very small value, it divides the model into a *fast subsystem* (i.e. the first two equations) and a *slow subsystem*, the third equation [108].

The original HR system is the 2-dimensional HR 1982 model. It is a two-variable model of the action potential which is a modification of the Fitzhugh 1961 model [97, 98].

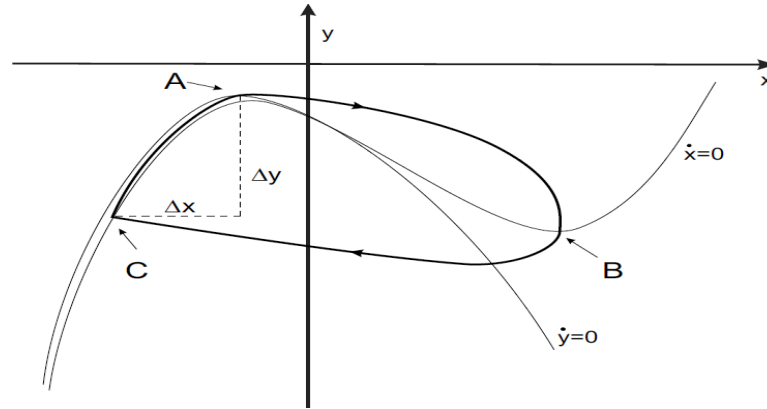


Figure 3.6: The changes in  $x$  and  $y$  as the state changes up the narrow channel between the  $x$ - and  $y$ -nullclines (thin lines) from  $C$  to  $A$  are  $\Delta x$  and  $\Delta y$  which cause the long interspike interval. The closed curve  $A, B, C, A$  represents the firing limit cycle (thick line) in HR 1982 model [97, 184].

$$\begin{aligned}\frac{dx}{dt} &= a(y - f(x) + I(t)), \\ \frac{dy}{dt} &= b(g(x) - y),\end{aligned}\tag{3.6.2}$$

where  $x$  is the membrane potential,  $y$  the recovery variable,  $I(t)$  the applied current as function of  $t$  and  $a, b$  are time constants.  $f$  is a cubic and  $g$  a linear function. However, the model does not provide a very realistic description of the rapid firing of the neuron. In an attempt to achieve a more realistic description of firing, Hindmarsh and Rose did replace the linear function  $g(x)$  in the Fitzhugh 1961 model with a quadratic function [184]. This slight modification provides the HR 1982 model with the property that each action potential is separated by a long interspike interval (i.e. a long interval between rapid firing) typical of real neurons. This property results from the close proximity of the  $x$ - and  $y$ -nullclines (curves in the phase plane where  $\dot{x} = 0$  and  $\dot{y} = 0$ ), in the nullcline diagram which Hindmarsh and Rose called the *narrow channel* property [97, 98]. When the state is in this channel, it changes slowly because it is close to both nullclines and that means both  $\dot{x}$  and  $\dot{y}$  are small. This slow change causes the long interspike interval (see Fig. 3.6) [97, 184, 185]. The value of the membrane potential  $x$  rises steadily during the application of the current pulse and the model discharges repetitively after the termination of the current as in a real neuron.

*Spiking* is represented by a generation of action potentials while *bursting* refers to a patterns of neural activity in which the neuron fires bursts of spikes. Each burst is followed by a period of inactivity (*quiescence*) until the next burst occurs. The 2-dimensional

model is not able to reproduce some interesting phenomena such as terminating a triggered state of firing [108]. Later, Hindmarsh and Rose realized that the model required more than the one equilibrium point of the 1982 model, one point for the subthreshold stable resting state and another one inside the firing limit cycle (an isolated closed orbit). Therefore, some modifications were done on the nullclines intersection and thus create the additional two equilibrium points [97, 184]. The equations were chosen to be

$$\begin{aligned}\frac{dx}{dt} &= y - ax^3 + bx^2 + I, \\ \frac{dy}{dt} &= c - dx^2 - y.\end{aligned}\tag{3.6.3}$$

In order to terminate firing of the neuron in the model, an adaptation variable  $z$  was added which represents the slowly varying current (changing the applied current  $I$  to an effective applied current  $I - z$ ). Since the additional variable  $z$  is needed for the sole purpose of terminating the firing, a third first order differential equation was added to the system to obtain the 3-dimensional HR 1984 model (3.6.1) [98, 148],

$$\frac{dz}{dt} = r[s(x - x_o) - z].$$

The third equation raises the value of  $z$  when the model is firing and so lower the effective applied current leading to the termination of firing. The additional variable  $z$  is designed to act on a longer time scale and that divides the model into a fast and a slow subsystem. Several phenomena of the system can be accurately described only by studying the fast subsystem, eventually with some interactions with the slow component but only with the 3-dimensional model one can explain the complete variety of the behaviours exhibited by the HR model [108].

The HR 1984 model has three equilibrium points representing the stable resting state, the threshold potential and the equilibrium point inside the limit cycle, respectively. The basic equations of the HR 1984 model are given by

$$\begin{aligned}\frac{dx}{dt} &= y - ax^3 + bx^2, \\ \frac{dy}{dt} &= c - dx^2 - y.\end{aligned}\tag{3.6.4}$$

The three equilibrium points (e.p.s) are given by the intersection of the  $x$ - and  $y$ -nullclines:

$$x^3 + px^2 = q,\tag{3.6.5}$$

where  $p = (d - b)/a$  and  $q = c/a$ . Denoting  $h(x) = x^3 + px^2$ , the function  $h$  has a local maximum at  $(\frac{-2p}{3}, \frac{4p^3}{27})$ . Therefore, the condition for three equilibrium points is  $27q < 4p^3$  which requires that  $b < d$ . The roots of (3.6.5) are the  $x$ -coordinates of the intersection points  $A$ ,  $B$  and  $C$  with the horizontal line  $q$ ;  $-1.6$ ,  $-1$  and  $0.6$  (Fig. 3.7).

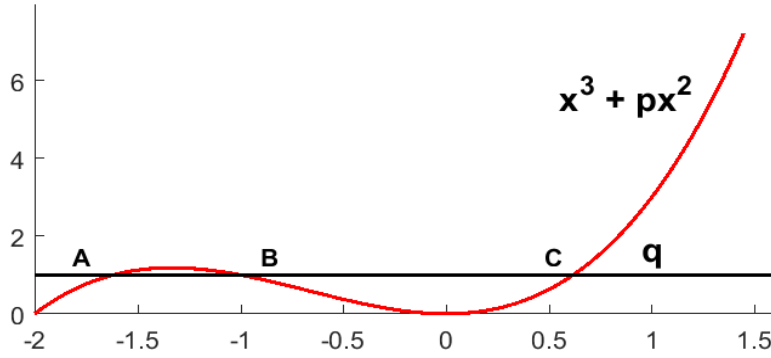


Figure 3.7: The locations of roots of the equation  $x^3 + px^2 = q$  equal to the  $x$ -coordinates of the points of intersection  $A$ ,  $B$  and  $C$ . The parameter values are:  $a = 1$ ,  $b = 3$ ,  $c = 1$ ,  $d = 5$ .

We use linear stability analysis to determine the stability of the equilibrium points. The Jacobian matrix of the linearised system evaluated at an equilibrium point  $x_{eq}$  is given by

$$J(x_{eq}) = \begin{pmatrix} -3ax_{eq}^2 + 2bx_{eq} & 1 \\ -2dx_{eq} & -1 \end{pmatrix}. \quad (3.6.6)$$

The type of the equilibrium points can be determined using the signs of the trace and determinant of  $J$  [98, 114]

$$\begin{aligned} Tr(J(x_{eq})) &= -3ax_{eq}^2 + 2bx_{eq} - 1, \\ Det(J(x_{eq})) &= 3ax_{eq}^2 + 2(d - b)x_{eq}. \end{aligned}$$

For  $b^2 \geq 3a$ ,  $Tr(J(x_{eq})) = -3ax_{eq}^2 + 2bx_{eq} - 1$  has two positive real roots;  $\gamma_1 = \frac{b - \sqrt{b^2 - 3a}}{3a}$  and  $\gamma_2 = \frac{b + \sqrt{b^2 - 3a}}{3a}$ .  $Tr(J(x_{eq}))$  will be positive for  $x_{eq} \in (\gamma_1, \gamma_2)$  and negative otherwise.  $Det(J(x_{eq}))$  is positive for all  $x_{eq} \notin (\frac{-2(d-b)}{3a}, 0)$ . Thus, the  $x$ -axis can be divided into five regions of stability depending on the signs of  $Tr(J(x_{eq}))$  and  $Det(J(x_{eq}))$  [98, 114].

For  $b^2 < 3a$ ,  $Tr(J(x_{eq}))$  does not have real roots and therefore  $Tr(J(x_{eq})) < 0$  for any  $x_{eq} \in \mathbb{R}$ . In this case, the only possible types of equilibrium points are saddle points or

stable spiral focuses. This could block the possibility of having an unstable spiral focus whose phase paths approach a stable limit cycle. Therefore, for a model of a repetitive firing, the condition  $b^2 > 3a$  must be imposed [98, 114].

To find the three equilibrium points of the 3-dimensional HR 1984 model (3.6.1), we can solve the system's equations directly or by using the new approach in Cardano's method [149]:

$$x^3 + \frac{(d-b)}{a}x^2 + \frac{s}{a}x + \frac{(-c-I-sx_0)}{a} = 0. \quad (3.6.7)$$

The roots are given by:

$$X_1 = xN + 2\sqrt{\delta} \cos(\theta),$$

$$X_2 = xN + 2\sqrt{\delta} \cos(\theta + \frac{2\pi}{3}),$$

$$X_3 = xN + 2\sqrt{\delta} \cos(\theta + \frac{4\pi}{3}),$$

where  $xN = \frac{-(d-b)}{3a}$ ,

$$\delta = \frac{1}{9} \left( \frac{(d-b)^2}{a^2} - \frac{3s}{a} \right), \quad y = \frac{2}{27} \frac{(d-b)^3}{a^3} - \frac{1}{3} \frac{s(d-b)}{a^2} + \frac{(-c-I-sx_0)}{a},$$

$$h = 2(\sqrt{\delta})^3, \quad \cos 3\theta = \frac{-y}{h}, \quad \theta = \frac{\arccos(\cos 3\theta)}{3}.$$

By substituting the parameter values [20, 35]:  $a = 1, b = 3, c = 1, d = 5, r = 0.005, s = 4, x_0 = -1.6$  and  $I_{ext} = 3.25$ , the three equilibrium points ( $eq_{1,2,3}$ ) are:

$$eq_1 = -0.6951302412, -1.416030261, 3.619479035$$

$$eq_2 = -0.6524348794 + 1.633179200I, 12.20801514 + 10.65543074I, 3.790260482 + 6.532716800I$$

$$eq_3 = -0.6524348794 - 1.633179200I, 12.20801514 - 10.65543074I, 3.790260482 - 6.532716800I, \text{ where } I \text{ is the imaginary unit.}$$

We need to do linearisation to the nonlinear system and solve the characteristic equation of the linearised system. The overall stability of the equilibrium points is determined by the eigenvalues of the Jacobian matrix of the linearised system evaluated at each equilibrium point. The Jacobian matrix of the linearised system is given by

$$A(x_{eq}) = \begin{pmatrix} -3ax_{eq}^2 + 2bx_{eq} & 1 & -1 \\ -2dx_{eq} & -1 & 0 \\ rs & 0 & -r \end{pmatrix}. \quad (3.6.8)$$

The eigenvalues for  $eq_1$  are:  $\lambda_1 = -6.813233982, \lambda_2 = 0.176752442, \lambda_3 = 0.0110819368$ , and for  $eq_2$ :  $\lambda_1 = 1.872078132 + 15.60278796I, \lambda_2 = -0.064015272 + 0.589503045I,$

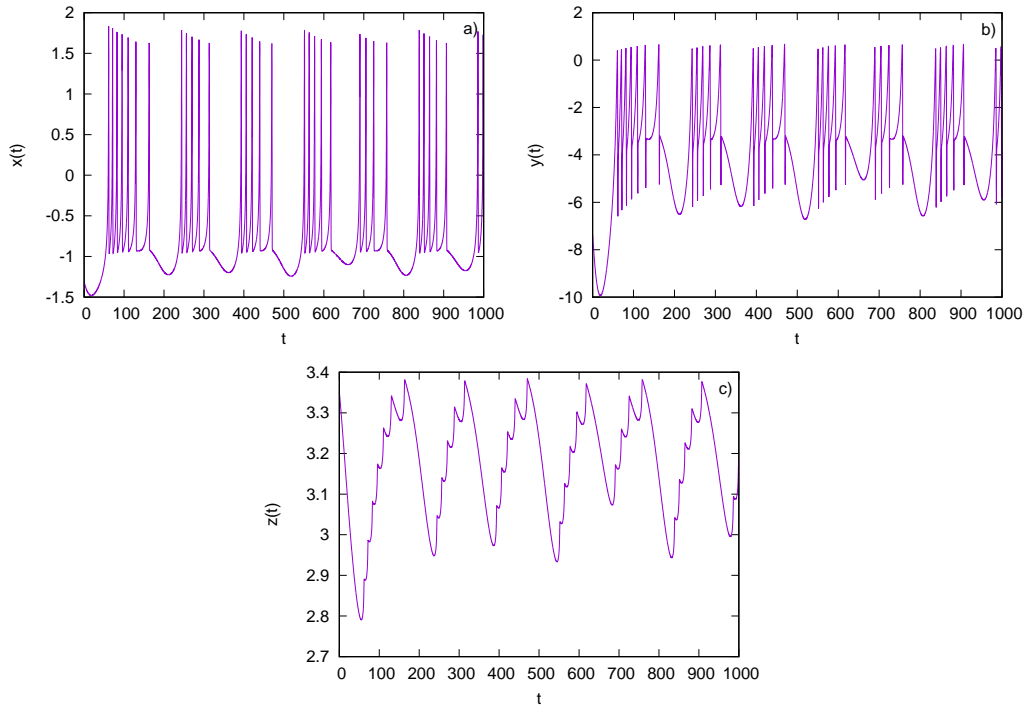


Figure 3.8: Spike-bursting behaviour in the HR system: Panel a) shows the membrane potential  $x(t)$  vs time, panel b) shows the transport of ions across the membrane through the fast ion channels (sodium and potassium ions)  $y(t)$  (spiking variable) vs time and panel c) the transport of other ions through slow channels (bursting variable)  $z(t)$  vs time. The parameter values are:  $a = 1$ ,  $b = 3$ ,  $c = 1$ ,  $d = 5$ ,  $r = 0.005$ ,  $s = 4$ ,  $x_o = -1.6$  and  $I_{ext} = 3.25$ .

$$\lambda_3 = -0.002863058 + 0.000042639I.$$

Finally, for  $eq_3$ , the eigenvalues are:  $\lambda_1 = 1.872078132 - 15.60278796I$ ,  $\lambda_2 = -0.064015272 - 0.589503045I$ ,  $\lambda_3 = -0.002863058 - 0.000042639I$ .

### 3.6.1 Lyapunov exponents of the Hindmarsh-Rose system

The HR 1984 model has three Lyapunov exponents equal to the dimensionality of the system. The system exhibits a multi-scale chaotic behaviour characterised as spike-bursting for the specific parameter values mentioned in section 3.6. We used Matlab codes to compute the Lyapunov exponents (LEs) of the HR model. For these parameters, the HR system enables the spike-bursting behaviour of the membrane potential (see Figs. 3.8, 3.9) [20]. In calculating LEs, we use two different time-integration schemes, namely the Runge-Kutta (RK4) and Euler's forward method. To compute LEs, we adopted in our Matlab codes the steps covered in more detail in subsection 2.2.2. After computing the LEs with the use of the variational equations, the deviation vectors enter the loop for the

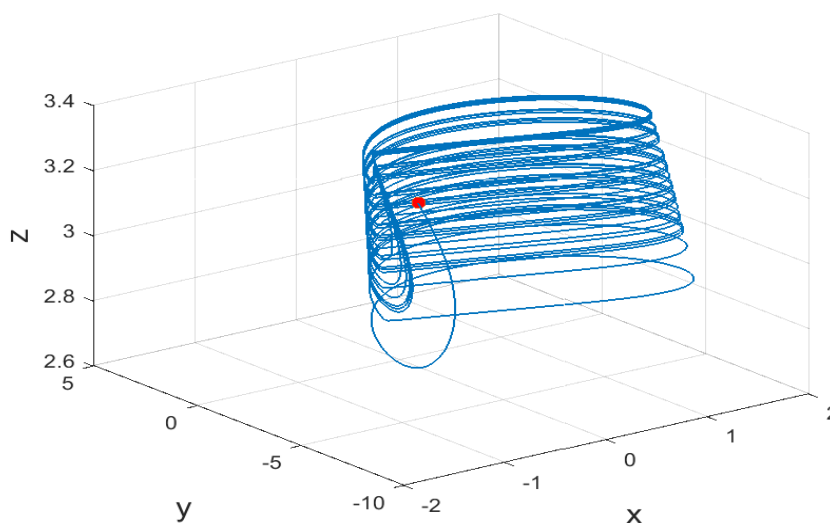


Figure 3.9: The Hindmarsh-Rose (3.6.1) attractor for parameter values  $a = 1$ ,  $b = 3$ ,  $c = 1$ ,  $d = 5$ ,  $r = 0.005$ ,  $s = 4$ ,  $x_o = -1.6$  and  $I_{ext} = 3.25$ .

application of the Gram-Schmidt orthonormalisation process to orthonormalise them.

The Matlab code computes the Lyapunov exponents using the Runge-Kutta (RK4) method. The parameter values used are:  $a = 1$ ,  $b = 3$ ,  $c = 1$ ,  $d = 5$ ,  $r = 0.005$ ,  $s = 4$ ,  $x_o = -1.6$  and  $I_{ext} = 3.25$ . We used the initial condition  $(x_0, y_0, z_0) = (-1.30784489, -7.32183132, 3.35299859)$  with time interval:  $[0, 10^4]$  and time-step  $h = 0.001$ . The symbol  $zz$  in the Matlab code represents the number of deviation vectors which equals the number of Lyapunov exponents.

In Fig. 3.10a), we used  $zz = 1$  and the execution time is 1189 sec. For small times, the maximal Lyapunov exponent (MLE) is positive and then changes to negative values. As time increases, the MLE starts to converge to positive values which indicate that the HR system behaves chaotically for the current parameters and initial condition.

Then, we used  $zz = 2$  and the execution time is 2189 sec. Initially, in Fig. 3.10b), the first and second Lyapunov exponents (i.e. the two largest) alternate between positive and negative values. However, after a transient period (i.e.  $[0, 1000]$ ), the MLE starts to converge to positive values indicating that the HR system is again chaotic.

For  $zz = 3$ , the execution time is 3620 sec. The first and second Lyapunov exponents alternate in time between positive and negative values. The third Lyapunov exponent is not shown in the figure because it is negative and we are using logarithmic scale in both axes which makes the figure for  $zz = 3$  similar to Fig. 3.10b). However, as time increases

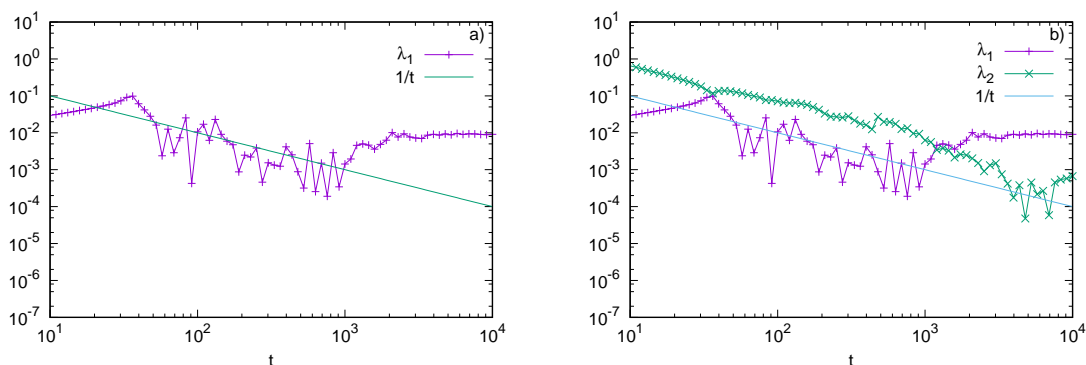


Figure 3.10: The Lyapunov exponents of the HR system using the RK4 method for the time interval  $[0, 10^4]$  and time-step 0.001:  $\lambda_1$  (+) and  $\lambda_2$  ( $\times$ ). In panel a),  $\lambda_1$  represents the MLE which indicates that the system is chaotic. In panel b), we run the same code for two deviation vectors and after a transient period (i.e.  $[0, 1000]$ ), the MLE starts to converge to positive values indicating that the system is chaotic. We also plot  $1/t$  to guide the eye. Note that both axes are logarithmic.

the maximal Lyapunov exponent starts to converge to a positive value indicating that the HR system with the current parameters is chaotic. The execution time for  $zz = 1$  is 1189 sec, for  $zz = 2$  is 2189 sec and for  $zz = 3$  is 3620 sec. It takes about 1000 to 1400 seconds to compute each additional deviation vector and its associated LE. For example, the CPU time for the computation of the three LEs is three times the CPU time for the computation of the maximum, as expected.

The second Matlab code computes the Lyapunov exponents using the Euler's 1<sup>st</sup> order method. We used the same parameter values, initial condition, time interval and time-step to compare the execution time and accuracy for both the RK4 and Euler's methods.

For one LE, the execution time for the code using the Euler's method is 162 sec and for the code using the RK4 method is 249 sec.

In Fig. 3.10a) and Fig. 3.11a), the values for maximal LE for HR system are almost the same for both codes with same time-step because the first deviation vector does not enter into the loops in the Gram-Schmidt orthonormalisation process. The code with the Euler method is thus much faster.

For two LEs, the execution time using the Euler's method is 331 sec and for the RK4 method is 488 sec.

In Fig. 3.10b) and Fig. 3.11b) the values for both the first and second LEs for the HR system are almost the same for both codes with slight differences. Still, the code that uses the Euler method in Fig. 3.11b) is faster. However, in both panels, after a transient period

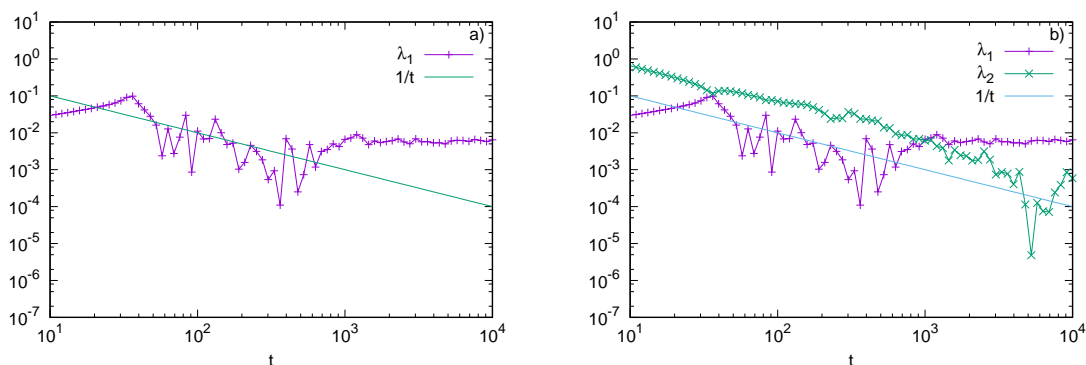


Figure 3.11: The Lyapunov exponents of the HR system using the Euler's method for the time interval  $[0, 10^4]$  and time-step 0.001:  $\lambda_1$  (+) and  $\lambda_2$  (×). In panel a),  $\lambda_1$  represents the MLE which indicates that the system is chaotic. In panel b), we run the same code for two deviation vectors and after a transient period (i.e.  $[0, 1000]$ ), the MLE starts to converge to positive values indicating that the system is chaotic. We also plot  $1/t$  to guide the eye. Note that both axes are logarithmic.

(i.e.  $[0, 1000]$ ), the maximum LE starts to converge to a positive value indicating that the HR system is chaotic.

For three LEs, the execution time for the code that uses the Euler's method is 582 sec and the RK4 method is 776 sec. The values for both the first and second LEs for the HR system are almost the same for both codes and the third Lyapunov exponent is not shown in both figures because it is negative and we use logarithmic scale in both axes, which makes the figures for  $zz = 3$  look almost the same as for  $zz = 2$ . The code for the Euler's 1<sup>st</sup> order method is much faster than the one using the RK4 method for the same time-step.

In both Matlab codes for the RK4 and Euler's methods, we used the same parameter values, initial condition, time interval:  $[0, 10^4]$  and time-step: 0.001 to compute the Lyapunov exponents of the HR system. Then, we compare the accuracy and the CPU time for both the RK4 and Euler's method codes. There is not much differences in accuracy as the LEs look almost the same in all figures for both methods. However, Euler's method is much faster in computing all LEs and therefore it is more preferable than the RK4, especially when shorter integration times are required.

### 3.6.2 Bifurcations in biological neuron models

Bifurcations are among the most important dynamical properties in dynamical systems in general, and in particular, in chaotic neural systems. It corresponds to the dynamical

systems, in which different initial conditions can converge to different solutions while all parameters are held constant. A difference in convergence or a change in the behaviour of a system can be observed but no bifurcation might have occurred. To quantify as a bifurcation, the change in the behaviour of the system must be associated with a change in a parameter value [42]. A dynamical system can exhibit local and/or global bifurcations. Local ones are more common in neuroscience and also much easier to recognise and understand. It can also provide us with a better understanding of the properties of equilibria in neuronal systems [194]. The simplest local bifurcation involves assessing the existence and stability of equilibrium points. Both the existence and stability of equilibrium points depend on the values of a parameter, in which case the possibility of a local bifurcation exists. To determine if a bifurcation occurs, we need to linearise the system about each equilibrium point and analyse the eigenvalues of the Jacobian matrices. The eigenvalues also depend on the parameter values. Bifurcation analysis can be used to simplify the identification of different kinds of stable and unstable solutions. In many dynamical systems, the conditions for identifying the existence of a bifurcation are often easier to satisfy than proving the existence of an actual solution [42].

Bifurcations play an essential role in describing mode transitions between a quiescence state and different kinds of oscillatory motion such as spiking and bursting in neuronal activities [63, 194]. Bifurcations in neuroscience are not only important at the single-cell level but also in understanding the dynamics of the whole network. A bifurcation mechanism that has been identified at the single-cell level often suggests how dynamical changes occur at the network level. The most widely studied bifurcations which arise in single neuronal models are saddle node and Hopf bifurcations [42].

The most important neuronal activities such as quiescence, spiking, bursting, irregular spiking and irregular bursting depend on the neuron biophysical parameter values. The HR system is able to reproduce all these dynamical activities and has been analysed with respect to one or two bifurcation parameters [185]. We chose two parameters  $I$  and  $b$ :  $I$  mimics the membrane input current for biological neurons and  $b$  allows one to switch between bursting and spiking behaviours and to control the spiking frequency. They cause several types of bifurcations in the system: saddle-node, Hopf (either supercritical or subcritical), period doubling and homoclinic [185]. In the parameter space plots in Fig. 3.12, we used  $(b, I) \in [0, 5] \times [1, 6]$  for 100 x 100 points to plot the three Lyapunov

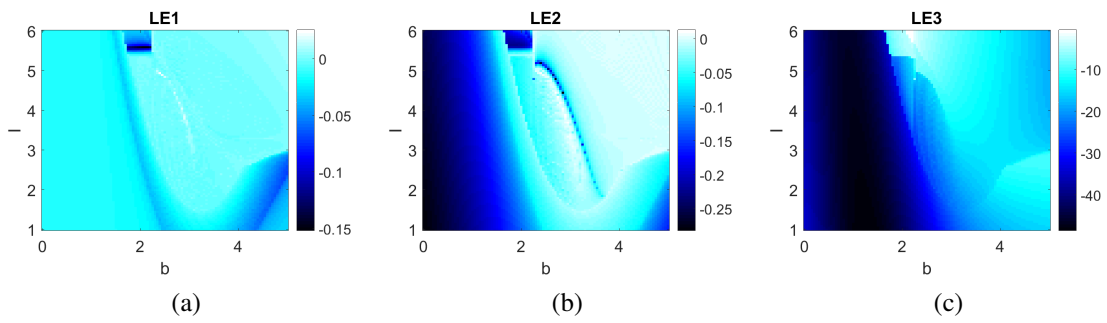


Figure 3.12: Plots of the parameter spaces of the three Lyapunov exponents of the HR system for: a) LE1, b) LE2 and c) LE3 on the  $(b, I)$  plane.

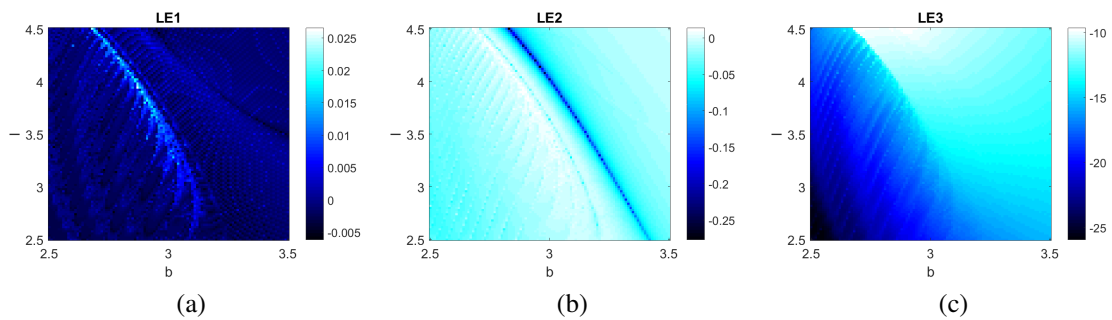


Figure 3.13: Plots of the parameter spaces of the three Lyapunov exponents of the HR system for: a) LE1, b) LE2 and c) LE3 on the  $(b, I)$  plane. The white spots reflect the chaotic behaviour of the system.

exponents to examine the changes in the dynamics of the system through the changes of values of the two HR parameters  $I$  and  $b$ . In the parameter space plots in Fig. 3.13, we used  $(b, I) \in [2.5, 3.5] \times [2.5, 4.5]$  for  $100 \times 100$  points to further examine the dynamics in the central chaotic region. In these plots, the HR model exhibits most of the dynamical behaviours mentioned above [185]. The parameter values used are:  $a = 1$ ,  $c = 1$ ,  $d = 5$ ,  $r = 0.01$ ,  $s = 4$  and  $x_0 = -1.6$ .

In spite of the fact that the HR system can produce several modes of spike-bursting behaviours seen in biological neurons, its parameter space for chaotic activity is much more limited than the one observed in real neurons [148]. That is why in the last few years, a wide variety of modified versions of the HR neuron model such as extended or nonlinear feedback coupled HR models [148, 189], time-delayed HR models [122, 195], fractional-order HR models [111] have been proposed. These models are further studied by bifurcation analysis methods to understand better the dynamics of electrical activity among neurons [26].

# Chapter 4

## Dynamics in networks of coupled HR systems

### Introduction

In this chapter, we will present a detailed study on the characteristics and dynamics of neurons that are connected by electrical and chemical synaptic couplings. We examine the dynamics of coupled HR neurons through elementary examples of 2, 3 and 4 neurons connected simultaneously by undirected chemical and electrical links (i.e. link  $(i, j) = (j, i)$ ). We review neural synchronisation which plays an important role in information processing in neuronal systems. Then, we discuss the two important concepts in information theory; the mutual information and the mutual information rate (MIR). The upper bound for MIR can be derived by the two largest Lyapunov exponents of the dynamics of the full system. Finally, we study the upper bound of MIR and the effect of synchronisation on the dynamics of three interacting bursting neurons depending on the values of the coupling strengths.

### 4.1 Electrical and chemical couplings

The functions of the brain rely on the ability of neurons to communicate with each other. Interneuronal communication takes place primarily at synapses, where information from one neuron is rapidly conveyed to another. Synapses mediate the functional interaction between two neurons or between a neuron and another cell type. The two main types of synaptic transmission are chemical and electrical. The electrical and chemical synapses can operate independently or through the interaction with each other [156]. These interactions that occur via chemical and electrical synaptic transmissions are re-

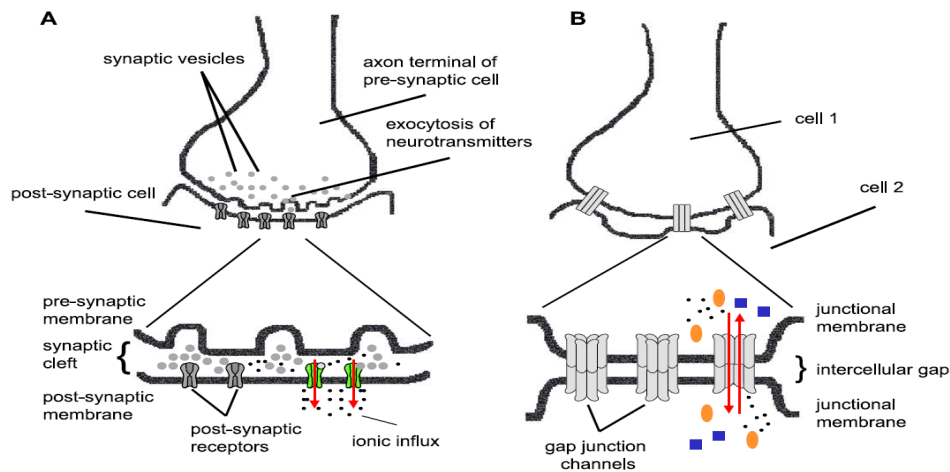


Figure 4.1: The principal features of the two types of synapses. A) In chemical synapses, an action potential arriving at the presynaptic terminal triggers the release of neurotransmitters (grey) which diffuse in the synaptic cleft and bind to specific receptors on the postsynaptic cell. B) In electrical synapses, gap junction channels allow a direct communication between the two coupled cells. While chemical transmission is unidirectional, electrical synapses usually pass signals equally well in both directions [104].

quired for normal brain development and function [104, 156]. Electrical and chemical synapses differ in their molecular mechanisms of information transfer and also in their structural organisation. In chemical synapses, the information is transferred via the release of neurotransmitters from presynaptic to postsynaptic neurons. Their synaptic cleft distance is of the order of 20-40 nm. Chemical transmission is unidirectional and requires sophisticated presynaptic molecular machinery that regulates neurotransmitter release in a probabilistic manner when an action potential enters the synaptic terminal. In electrical synapses, the action potential in the presynaptic neuron induces a passive current flow into the postsynaptic cell. The electrical transmission is bidirectional and not probabilistic in nature. The synaptic cleft distance in electrical synapses is in the order of 2-4 nm and their gap junction channels have relatively large pores that allow ions as well as small molecules to pass from one cell to another (see Fig. 4.1) [104, 156].

The electrical and chemical coupling strengths play a crucial role in the information transmission and synchronous activities in neural systems. Many studies of neuronal networks dealt with fixed coupling strength values. However, neuronal coupling is always changing due to the dynamics of synapses and ion channels [201] and often coupling strengths are used as bifurcation parameters [53].

## 4.2 Coupled Hindmarsh-Rose systems

One can couple the HR system to create an undirected brain dynamical network of  $N_n$  neurons connected simultaneously by electrical (linear coupling) and chemical (nonlinear coupling) synapses [20, 21, 100], i.e.,

$$\begin{aligned}
 \frac{dx_i}{dt} &= y_i - ax_i^3 + bx_i^2 - z_i + I_{ext} - g_n(x_i - V_{syn}) \sum_{j=1}^{N_n} B_{ij}S(x_j) \\
 &\quad - g_l \sum_{j=1}^{N_n} G_{ij}H(x_j), \\
 \frac{dy_i}{dt} &= c - dx_i^2 - y_i, \\
 \frac{dz_i}{dt} &= r[s(x_i - x_o) - z_i], \\
 \frac{d\phi_i}{dt} &= \frac{\dot{y}_i x_i - \dot{x}_i y_i}{x_i^2 + y_i^2}, \quad i = 1, \dots, N_n,
 \end{aligned} \tag{4.2.1}$$

where  $\phi_i$  is the phase variable defined by the fast variables  $(x_i, y_i)$  of the  $i$ -th neuron,  $H(x_j) = x_j$  and  $S(x_j)$  is the synaptic coupling modelled by a sigmoidal function with a threshold

$$S(x_j) = \frac{1}{1 + e^{-\lambda(x_j - \theta_{syn})}},$$

with  $\theta_{syn} = -0.25$ ,  $\lambda = 10$  and the reversal potential  $V_{syn} = 2$  to create excitatory BDNs.  $g_n$  is the coupling strength associated to the chemical synapses and  $g_l$  to the electrical synapses [20, 100]. The Laplacian matrix  $G_{ij}$  accounts for the way neurons are electrically coupled ( $G_{ij} = K_{ij} - A_{ij}$ , where  $A$  is the binary adjacency matrix of the electrical connections and  $K$  is the degree matrix based on  $A$ ).  $B_{ij}$  is the binary adjacency matrix of the chemical connections. In both matrices  $A$  and  $B$ , diagonal elements are equal to zero and any connection between neuron  $i$  and neuron  $j$  is represented by a positive off-diagonal value (i.e. 1). The binary adjacency matrices  $C$  of the BDNs are given by [20]

$$C = A + B.$$

Any change in the electrical or chemical connections in the network will be reflected by a similar change in the structure of their adjacency matrices  $A$  and  $B$ . Their sum  $C$  represents the adjacency matrix for the whole network at any time-step.



Figure 4.2: An elementary example of 2 neurons  $N_1$  and  $N_2$  connected simultaneously by undirected electrical ( $EL$ ) and chemical ( $CL$ ) links.

### 4.2.1 Expanding the coupling terms in two coupled Hindmarsh-Rose neurons

The two coupling terms in the HR system (4.2.1) enable us to use the system for any number of neurons. The variational equations of the coupled HR system are

$$\dot{J}_t = M(t)J_t, \quad (4.2.2)$$

where  $J_t$  is the matrix of deviation vectors and  $M(t)$  the Jacobian of (4.2.1).

In the case of the coupled HR system, we need to expand and derive the two coupling terms in Eq. (4.2.1) to include them in the Jacobian  $M(t)$  in Eq. (4.2.2). We expand and derive the electrical and chemical terms for an elementary example of two neurons ( $N_n = 2$ ) connected simultaneously by undirected electrical and chemical links (Fig. 4.2):

$$A = \begin{pmatrix} 0 & 1 \\ 1 & 0 \end{pmatrix}, \quad B = \begin{pmatrix} 0 & 1 \\ 1 & 0 \end{pmatrix}, \quad K = \begin{pmatrix} 1 & 0 \\ 0 & 1 \end{pmatrix}, \quad G = \begin{pmatrix} 1 & -1 \\ -1 & 1 \end{pmatrix},$$

where  $A$  is the binary adjacency matrix of the electrical connections,  $K$  is the degree matrix based on  $A$ ,  $G$  is the Laplacian matrix of the electrical connections and  $B$  is the binary adjacency matrix of the chemical connections.

Expanding the electrical coupling term  $G_l(i) = -g_l \sum_{j=1}^{N_n} G_{ij}H(x_j)$ , we get:

For  $i = 1$ :

$$G_l(1) = g_l(x_2 - x_1).$$

For  $i = 2$ :

$$G_l(2) = g_l(x_1 - x_2).$$

The derivative of the  $G_l(i)$  terms with respect to  $x_i$  are:  $\frac{dG_l(i)}{dx_1} = -g_l$  and  $\frac{dG_l(i)}{dx_2} = -g_l$ .

Expanding the chemical coupling term  $G_n(i) = [-g_n(x_i - V_{syn}) \sum_{j=1}^{N_n} B_{ij}S(x_j)]$ , we get:

$$G_n(i) = -g_n(x_i - V_{syn}) \sum_{j=1}^2 B_{ij}S(x_j) \Leftrightarrow$$

$$G_n(i) = -g_n(x_i - V_{syn})[B_{i1}S(x_1) + B_{i2}S(x_2)] \Leftrightarrow$$

$$G_n(i) = -g_n[x_i B_{i1} S(x_1) + x_i B_{i2} S(x_2) - V_{syn} B_{i1} S(x_1) - V_{syn} B_{i2} S(x_2)].$$

The derivative of the four terms with respect to  $x_i$  is:

$$\frac{dG_n(i)}{dx_i} = -g_n[x_i B_{i1} \dot{S}(x_1) + \dot{x}_i B_{i1} S(x_1) + x_i B_{i2} \dot{S}(x_2) + \dot{x}_i B_{i2} S(x_2) - V_{syn} B_{i1} \dot{S}(x_1) - V_{syn} B_{i2} \dot{S}(x_2)],$$

where  $\dot{S}(x_j)$  is the derivative of  $S(x_j)$  with respect to  $x_j$ .

For  $i = 1$ :

$$\begin{aligned} \frac{dG_n(i)}{dx_1} &= -g_n[x_1 B_{11} \dot{S}(x_1) + \dot{x}_1 B_{11} S(x_1) + x_1 B_{12} \dot{S}(x_2) + \dot{x}_1 B_{12} S(x_2) - V_{syn} B_{11} \dot{S}(x_1) - \\ &V_{syn} B_{12} \dot{S}(x_2)] \Leftrightarrow \\ \frac{dG_n(i)}{dx_1} &= -g_n[x_1 B_{11} \dot{S}(x_1) + B_{11} S(x_1) + B_{12} S(x_2) - V_{syn} B_{11} \dot{S}(x_1)]. \end{aligned}$$

For  $i = 2$ :

$$\begin{aligned} \frac{dG_n(i)}{dx_2} &= -g_n[x_2 B_{21} \dot{S}(x_1) + \dot{x}_2 B_{21} S(x_1) + x_2 B_{22} \dot{S}(x_2) + \dot{x}_2 B_{22} S(x_2) - V_{syn} B_{21} \dot{S}(x_1) - \\ &V_{syn} B_{22} \dot{S}(x_2)] \Leftrightarrow \\ \frac{dG_n(i)}{dx_2} &= -g_n[x_2 B_{22} \dot{S}(x_2) + B_{22} S(x_2) + B_{21} S(x_1) - V_{syn} B_{22} \dot{S}(x_2)]. \end{aligned}$$

After we have obtained the variational equations for two HR neurons, we compute the lengths of the eight deviation vectors of the variational equations. Then, we use equation (2.2.7) in section 2.2.2 to compute the eight LEs of the system. We apply the Gram-Schmidt orthonormalisation process to orthonormalise these deviation vectors for the computation of LEs for the next time-step.

## 4.2.2 Lyapunov exponents of three and four coupled Hindmarsh-Rose neurons

For one neuron, the HR system has three Lyapunov exponents equal to the dimensionality of the system. The system exhibits a multi-scale chaotic behaviour characterised as spike-bursting for the following parameter values as described in the previous chapter (see Fig. 3.8) [35, 100]:  $a = 1$ ,  $b = 3$ ,  $c = 1$ ,  $d = 5$ ,  $r = 0.005$ ,  $s = 4$ ,  $x_o = -1.6$ ,  $I_{ext} = 3.25$ .

We ran the Matlab code of the coupled HR system with same parameter values and slightly different initial conditions, studying the dynamics of elementary examples of three and four neurons (Fig. 4.3). The initial conditions used are:  $(-1.30784489 + x_1 + \text{rand}(x_2 - x_1) - 7.32183132 + x_1 + \text{rand}(x_2 - x_1) \ 3.35299859 + x_1 + \text{rand}(x_2 - x_1) \ 0)$ , where the term  $\text{rand}(x_2 - x_1)$  is a perturbation to the initial conditions. These initial conditions place faster the trajectory in the attractor of the dynamics, so there is less need



Figure 4.3: Two elementary examples of 3 and 4 neurons connected simultaneously by undirected chemical ( $CL$ ) and electrical ( $EL$ ) links. In a), 3 neurons connected by one chemical and two electrical links. In b), 4 neurons connected by two chemical and two electrical links as shown.

to consider longer transient periods [20]. We used Euler forward integration method with time interval  $[0, 10^4]$  and a time-step = 0.001. The values we chose for the chemical and electrical coupling parameters are  $g_n = 0.2$  and  $g_l = 0.25, 0.35$ . These values for the time interval, time-step and coupling parameters provide us with best runtime to get the convergence of LEs to positive constant values in the long run with less time for the transient period.

In Fig. 4.4a), we plot nine of the twelve Lyapunov exponents of the coupled HR system for three neurons in the time interval  $[0, 10^4]$  with time-step = 0.001,  $g_n = 0.2$  and  $g_l = 0.25$ . The other three LEs are equal to zero because we set the deviation vector equations for the fourth variable  $\phi$  to zero to reduce the CPU time. We used the Euler integration method and the identity matrix as initial deviation vectors in Eq. (4.2.2). The vectors of the identity matrix are linearly independent and form a basis of  $\mathbb{R}^3$  (i.e. they are orthogonal and unit vectors). After the transient period (i.e.  $[0, 400]$ ), in which the dynamics of the system is unsettled,  $\lambda_1$  starts to converge to a positive value and represents the maximal Lyapunov exponent (MLE). Due to the dynamics of the system, three of the LEs are equal to zero. In Fig. 4.4b), we used a random matrix for  $A(t = 0)$  as initial deviation vectors in Eq. (4.2.2). The vectors of the random matrix are not orthogonal but that does not effect the computation of the LEs as we use them only for the first time-step. In the transient period (i.e.  $[0, 400]$ ), all nine LEs converge to 0 as  $1/t$  trend. Then, the MLE starts to converge to a positive value indicating that the system is chaotic and three of the LEs decrease to 0 like  $1/t$  as we use the logarithmic scale. Due to the dynamics of the system, at least three LEs must equal to zero.

Finally, in Fig. 4.5a), we plot the twelve of the sixteen Lyapunov exponents of the coupled

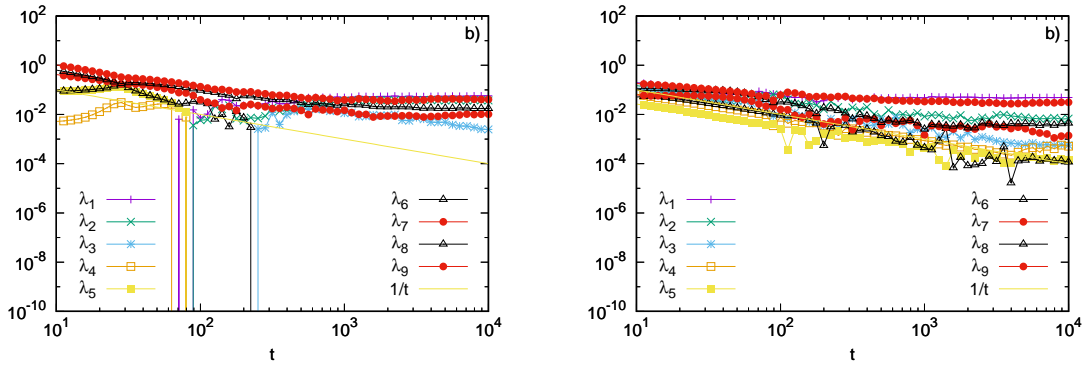


Figure 4.4: The nine of the twelve Lyapunov exponents for 3 coupled HR neurons in the time interval  $[0, 10^4]$  with time-step = 0.001,  $g_n = 0.2$  and  $g_l = 0.25$ . In panel a), we used an identity matrix as initial deviation vectors in Eq. (4.2.2). After the transient period (i.e.  $[0, 400]$ ),  $\lambda_1$  starts to converge to a positive value and represents the MLE. Three of the LEs are equal to zero. In panel b), we used a random matrix for  $A(t = 0)$  as initial deviation vectors in Eq. (4.2.2). In the transient period (i.e.  $[0, 400]$ ), all nine LEs follow a  $1/t$  trend. Then, MLE starts to converge to a positive value indicating that the system is chaotic and three of the LEs decrease to 0 like  $1/t$  trend. We used the Euler integration method in both panels and we plot  $1/t$  to guide the eye. Note that all axes are logarithmic.

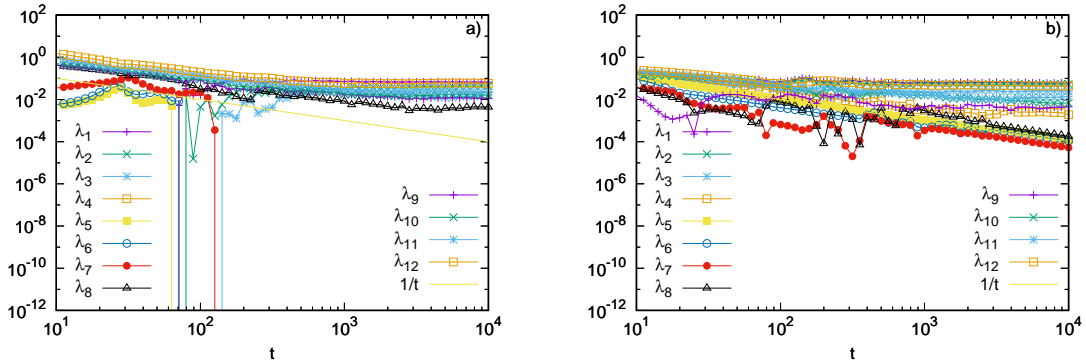


Figure 4.5: The twelve of the sixteen Lyapunov exponents for 4 coupled HR neurons in the time interval  $[0, 10^4]$  with time-step = 0.001,  $g_n = 0.2$  and  $g_l = 0.35$ . In panel a), we used an identity matrix as initial deviation vectors in Eq. (4.2.2). After the transient period (i.e.  $[0, 400]$ ),  $\lambda_1$  starts to converge to a positive value and represents the MLE. Four of the LEs are equal to zero. In panel b), we used a random matrix for  $A(t = 0)$  as initial deviation vectors in Eq. (4.2.2). In the transient period (i.e.  $[0, 400]$ ), all twelve LEs follow a  $1/t$  trend. Then, MLE starts to converge to a positive value indicating that the system is chaotic and four of the LEs decrease to 0 like  $1/t$  trend. We used the Euler integration method in both panels and we plot  $1/t$  to guide the eye. Note that all axes are logarithmic.

HR system for four neurons in the time interval  $[0, 10^4]$  with time-step = 0.001,  $g_n = 0.2$  and  $g_l = 0.35$ . The other four LEs are equal to zero because we set the deviation vector

equations for the fourth variable  $\phi$  to zero to reduce the CPU time. We used the Euler integration method and the identity matrix as initial deviation vectors in Eq. (4.2.2). The dynamics of the system is unsettled in the transient period (i.e.  $[0, 400]$ ), however after that,  $\lambda_1$  starts to converge to a positive value. Due to the dynamics of the system, four of the LEs are equal to zero. In Fig. 4.5b), we used a random matrix for  $A(t = 0)$  as initial deviation vectors in Eq. (4.2.2). In the transient period (i.e.  $[0, 400]$ ), all twelve LEs converge to 0 as  $1/t$ . Then, the MLE starts to converge to a positive value indicating that the system is chaotic and four of the LEs decrease to 0 like  $1/t$  as we use the logarithmic scale. Due to the dynamics of the system, at least four LEs must equal to zero.

### 4.3 Synchronisation measures in brain dynamical networks

*Synchronisation* plays an important role in information processing in neuronal systems. The word “synchronisation” has a Greek root, *syn* = *common* and *chronos* = *time*, which means to occur at the same time [62]. Synchronisation, as a collective behaviour in coupled systems, seems to be the central mechanism for neuronal information processing and transmission, communication between different brain areas and neurological diseases such as epilepsy or Parkinson’s disease [41, 53, 193]. Synchronisation in chaotic systems has attracted considerable interest and attention because of its potential applications in many scientific disciplines such as biology, physics, chemistry, communication theory and others [103]. At first sight, synchronisation in chaotic systems seems to be rather surprising. One may expect the sensitive dependence on initial conditions would lead to an immediate breakdown of any synchronisation of coupled chaotic systems. Over the past decade, research showed that two chaotic systems could be synchronised by coupling them as one system and that could decrease or increase the number of positive Lyapunov exponents [62]. In neuronal networks, the interactions between bursting neurons may exhibit different forms of synchrony depending on the coupling strengths and coupling configurations [73].

Many nonlinear measures of neuronal signal synchrony have been developed to quantify the degree of synchronisation in signals, such as transfer entropy [45, 173], mutual information [200], nonlinear interdependence [43] and phase synchronisation. *Phase synchronisation* of chaotic systems is defined as the appearance of a certain relation between

the phases of interacting systems while the amplitudes may remain uncorrelated [163]. It is widely used in neurophysiology since the analysis can be restricted to certain frequency bands which reflect specific brain rhythms and allows relating the results to cognitive processes.

To compute the synchronisation level of neural activity, we use the *order parameter*  $\rho$  which is originated from the theory of dynamical coherence measures with a population of  $N_n$  *Kuramoto* type oscillators [120]. It can be computed by taking the modulus  $\rho$  of the complex number  $z(t)$ :

$$z(t) = \rho(t)e^{i\Phi(t)} = \frac{1}{N_n} \sum_{j=1}^{N_n} e^{i\phi_j(t)}, \quad (4.3.1)$$

where  $\phi_j(t)$  is the phase variable of the  $j$ -th neuron of the HR system Eq (4.2.1) given by its fourth equation and  $\Phi(t)$  is the average phase of the population of oscillators. We obtain the order parameter by averaging  $\rho$  over time:

$$\rho = \langle \rho(t) \rangle_t,$$

which represent the tendency of  $\rho$  in time. The value of  $\rho = 1$  corresponds to complete synchronisation and  $\rho = 0$  to complete desynchronisation [20, 100]. For Newman-Watts (NW) small-world network model with  $N_n$  neurons, the synchronisability of the network increases as more edges are being added to the network (i.e. as the probability  $\beta$  is increased from 0 to 1). This is the case for any fixed coupling strength  $g > 0$ . A network with a large enough number of nodes so that  $N_n > \frac{d}{g}$ ,  $d > 0$  is a constant and the probability becomes larger than a threshold  $\bar{\beta}$ ,  $\bar{\beta} \leq \beta \leq 1$  then the network will synchronise. In general, different small-world models generated by different coupling strengths have different phase synchronisation characteristics. For weak coupling strength  $g \rightarrow 0$ , all nodes are uniformly distributed for which no synchronous group exists. As  $g$  increases, a synchronous group is formed and then grows in size. The whole group of nodes synchronise in phase at  $\rho = 1$  regardless of the network topology [55].

## 4.4 Upper bound for Mutual Information Rate

Claude Shannon's entropy quantifies information [175]. It defines as a measure of the amount of uncertainty an observer has about an event being produced by a random

system. The *mutual information* (MI) is another important concept in Shannon's theory of information which measures how much uncertainty one has about a state variable after observing another state variable. MI is an important quantity because it not only quantifies linear and nonlinear interdependencies between two systems but also measures how much information exchanged between them. It is used as a measure to quantify the information capacity of a communication system. MI became a fundamental quantity to understand the development and function of the brain and also to characterise and model complex and chaotic systems [27, 35].

### Definition 6

Given two discrete random variables  $X$  and  $Y$  whose joint probability distribution is  $P_{XY}(x, y)$ , the mutual information between them, denoted  $I(X; Y)$ , is given by

$$I(X; Y) = \sum_{x,y} P_{XY}(x, y) \log \frac{P_{XY}(x,y)}{P_X(x)P_Y(y)},$$

where  $P_X(x) = \sum_y P_{XY}(x, y)$  and  $P_Y(y) = \sum_x P_{XY}(x, y)$  are the marginal probability distribution functions of  $X$  and  $Y$  respectively. In case of  $X$  and  $Y$  are two continuous random variables, the mutual information between them is given by

$$I(X; Y) = \int_Y \int_X P_{XY}(x, y) \log \frac{P_{XY}(x,y)}{P_X(x)P_Y(y)} dx dy,$$

where  $P_{XY}(x, y)$  is the joint probability density function of  $X$  and  $Y$ .  $P_X(x) = \int_Y P_{XY}(x, y) dy$  and  $P_Y(y) = \int_X P_{XY}(x, y) dx$  are the marginal probability density functions of  $X$  and  $Y$  respectively [35, 198].

The units of information depend on the base of the logarithm. When base 2 is used, the unit is called the *shannon* (SH), also known as the *bit*, and one shannon is equal to the information content of one bit. It can be in one of two states 0 or 1.

The amount of information exchanged per unit of time between two nodes in a dynamical network is a powerful concept for analysing complex systems. This quantity, known as the *mutual information rate* (MIR), is obtained from the mutual information and measures the time rate of information exchanged between two non-random and correlated variables. MIR is an appropriate quantity to access the amount of information exchanged in complex systems, since variables in complex systems are not purely random [27, 35]. An upper bound  $I_c$  for the MIR between two nodes or two groups of nodes of a complex



Figure 4.6: Two elementary examples of 3 neurons connected simultaneously by undirected chemical ( $CL$ ) and electrical ( $EL$ ) links. In a), 3 neurons connected by one chemical and two electrical links. In b), 3 neurons connected by one electrical and two chemical links.

dynamical network can be derived depending on the two largest Lyapunov exponents [20]

$$\text{MIR} \leq I_c = L_1 - L_2, \quad L_1 \geq L_2, \quad (4.4.1)$$

where  $L_1, L_2$  are the two finite time and size Lyapunov exponents which typically should approach the two largest Lyapunov exponents  $\lambda_1, \lambda_2$  of the dynamical network if it is connected and the time used to compute  $L_1, L_2$  is sufficiently small [20]. Therefore,  $I_c = \lambda_1 - \lambda_2$ , (i.e.  $\lambda_1 = L_1$  and  $\lambda_2 = L_2$ ). In non-excitatory networks, the formula  $\rho \propto \frac{1}{\lambda_2}$  where  $\lambda_2$  is the second largest Lyapunov exponent of the BDN, represents the relation between the order parameter  $\rho$  and the upper bound  $I_c$ . The non-excitatory factor is expected to be prominent when the electrical coupling has the largest contribution to the behaviour of the network comparing to the chemical. This situation raises the level of global neural synchronisation [20, 27].

In Fig. 4.7, we plot the upper bound  $I_c$ , order parameter  $\rho$  and the two largest Lyapunov exponents  $\lambda_1$  and  $\lambda_2$  versus the chemical coupling  $g_n$  and electrical coupling  $g_l$  for an elementary example of 3 neurons connected simultaneously by undirected one chemical and two electrical links (see Fig. 4.6a).

$$A = \begin{pmatrix} 0 & 1 & 1 \\ 1 & 0 & 0 \\ 1 & 0 & 0 \end{pmatrix}, \quad B = \begin{pmatrix} 0 & 0 & 0 \\ 0 & 0 & 1 \\ 0 & 1 & 0 \end{pmatrix}, \quad K = \begin{pmatrix} 2 & 0 & 0 \\ 0 & 1 & 0 \\ 0 & 0 & 1 \end{pmatrix}, \quad G = \begin{pmatrix} 2 & -1 & -1 \\ -1 & 1 & 0 \\ -1 & 0 & 1 \end{pmatrix},$$

where  $A$  is the binary adjacency matrix of the electrical connections,  $K$  is the degree identity matrix based on  $A$ ,  $G$  is the Laplacian matrix and  $B$  is the binary adjacency matrix of the chemical connections.

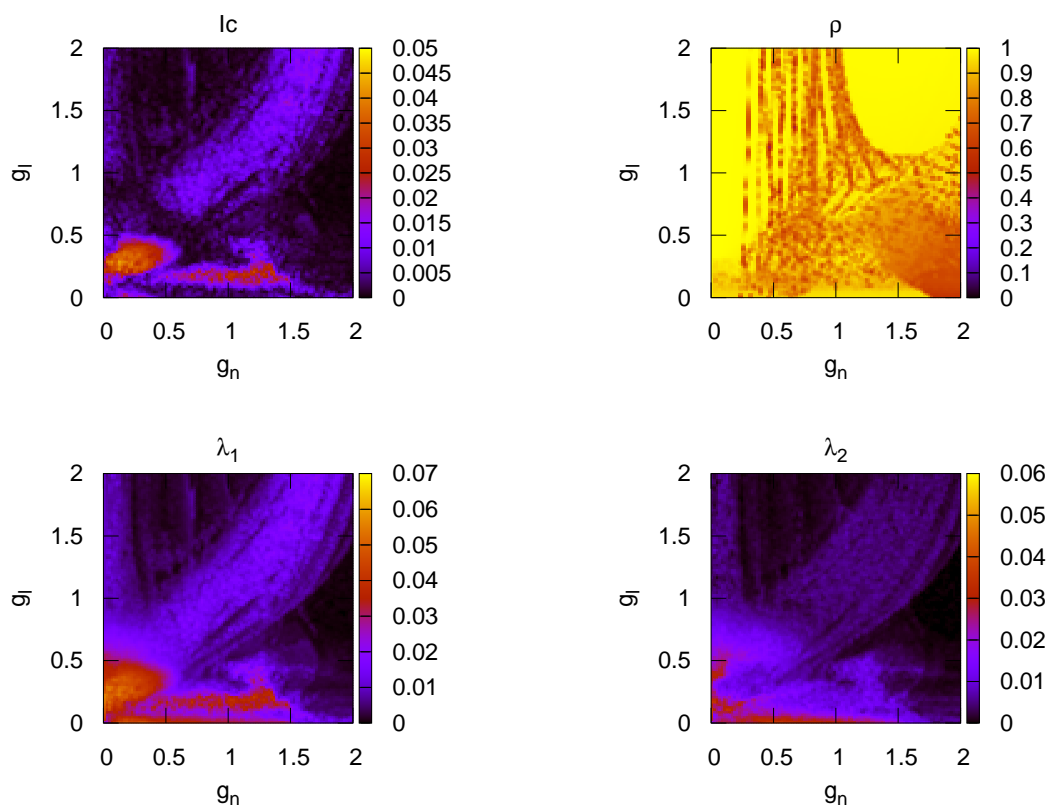


Figure 4.7: Plots of the upper bound  $I_c$ , the order parameter  $\rho$  and the two largest Lyapunov exponents  $\lambda_1$  and  $\lambda_2$  versus the chemical coupling  $g_n$  and electrical coupling  $g_l$  for an elementary example of 3 neurons connected simultaneously by one undirected chemical and two undirected electrical links (see Fig. 4.6a).

For the parameter spaces in Fig. 4.7, we used  $(g_n, g_l) \in [0, 2] \times [0, 2]$  for 100 x 100 points. The plot for the upper bound  $I_c$  versus  $g_n$  and  $g_l$  shows that the highest value for  $I_c$  is at the lower left corner. The dynamics of neurons in many spots in this area of the plot is chaotic but at the lower right and upper left corners, the motion is completely periodic. In the plot for the order parameter, the values of  $\rho$  increase with the increase of  $g_l$  (almost equal to 1) and that indicates the behaviour of the neurons is chaotically synchronised but on the other regions is periodically synchronised. The two other plots represent the two largest Lyapunov exponents  $\lambda_1$  and  $\lambda_2$  versus  $g_n$  and  $g_l$ . The upper bound  $I_c = \lambda_1 - \lambda_2$  and with both values of  $\lambda_1$  and  $\lambda_2$  being positive, the plot for  $\lambda_1$  is different to the  $I_c$  plot.

To further examine the dynamics of the system, we select three different values for  $g_n$  and  $g_l$  from regions with different dynamics and plot the trajectories for all neurons at each of these values to analyse the behaviour of the system in these regions.

In Fig. 4.8,  $g_n = 0.2$  and  $g_l = 1.9$ . Plots of panels a) to d) represent the behaviour of

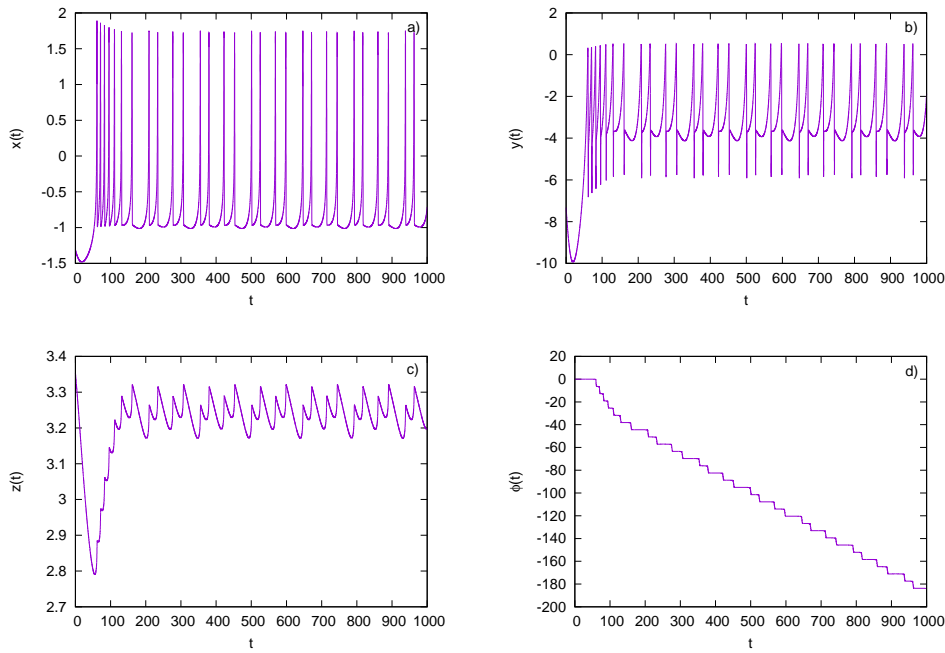


Figure 4.8: Spiking behaviour of neuron 1 in the coupled Hindmarsh-Rose system for  $g_n = 0.2$  and  $g_l = 1.9$ . Panels a) to d): plots of the behaviours of variables  $x$ ,  $y$ ,  $z$  and  $\phi$  of neuron 1 show the spiking dynamics and resembles the behaviour of neuron 2 and 3. The dynamics of the three neurons is periodic.

variables  $x$ ,  $y$ ,  $z$  and  $\phi$  of neuron 1 with a spiking behaviour which indicates that the dynamics of neuron 1 is periodic and resembles the dynamics of the other two neurons 2 and 3. In Fig. 4.9,  $g_n = 1.4$  and  $g_l = 1.1$ . Plots of the panels a) to d) represent the behaviour of variables  $x$ ,  $y$ ,  $z$  and  $\phi$  of neuron 1 with a spike-bursting dynamics and resembles the dynamics of neuron 2 and 3 and that indicates the behaviours of the three neurons are chaotic.

Finally, in Fig. 4.10,  $g_n = 1.9$  and  $g_l = 1.3$ . Plots of the panels a) to d) represent the behaviour of the variables  $x$ ,  $y$ ,  $z$  and  $\phi$  of neuron 1. The plots of  $x$  and  $y$  show the intense spiking for a short period of time, then the trajectory converges to one of the fixed points and resembles the behaviour of neuron 2 and 3.

For the second elementary example of 3 neurons connected simultaneously by undirected one electrical and two chemical links (see Fig. 4.6b), we take

$$A = \begin{pmatrix} 0 & 1 & 0 \\ 1 & 0 & 0 \\ 0 & 0 & 0 \end{pmatrix}, B = \begin{pmatrix} 0 & 0 & 1 \\ 0 & 0 & 1 \\ 1 & 1 & 0 \end{pmatrix}, K = \begin{pmatrix} 1 & 0 & 0 \\ 0 & 1 & 0 \\ 0 & 0 & 0 \end{pmatrix}, G = \begin{pmatrix} 1 & -1 & 0 \\ -1 & 1 & 0 \\ 0 & 0 & 0 \end{pmatrix}.$$

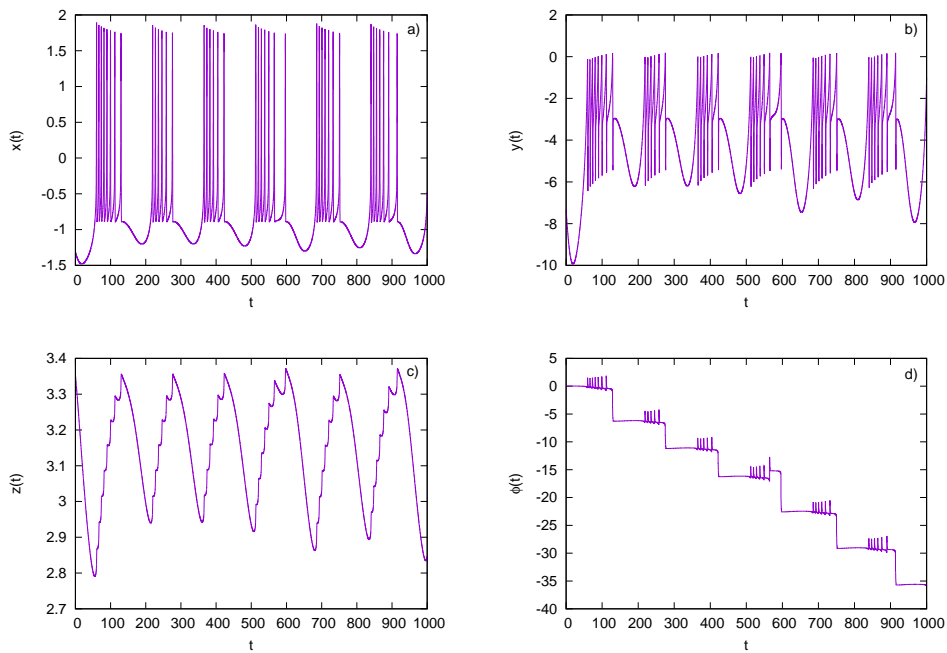


Figure 4.9: Spike-bursting behaviour of neuron 1 in the coupled Hindmarsh-Rose system for  $g_n = 1.4$  and  $g_l = 1.1$ . Panels a) to d): plots of variables  $x$ ,  $y$ ,  $z$  and  $\phi$  of neuron 1 show the spike-bursting behaviour and resembles the behaviour of neuron 2 and 3.

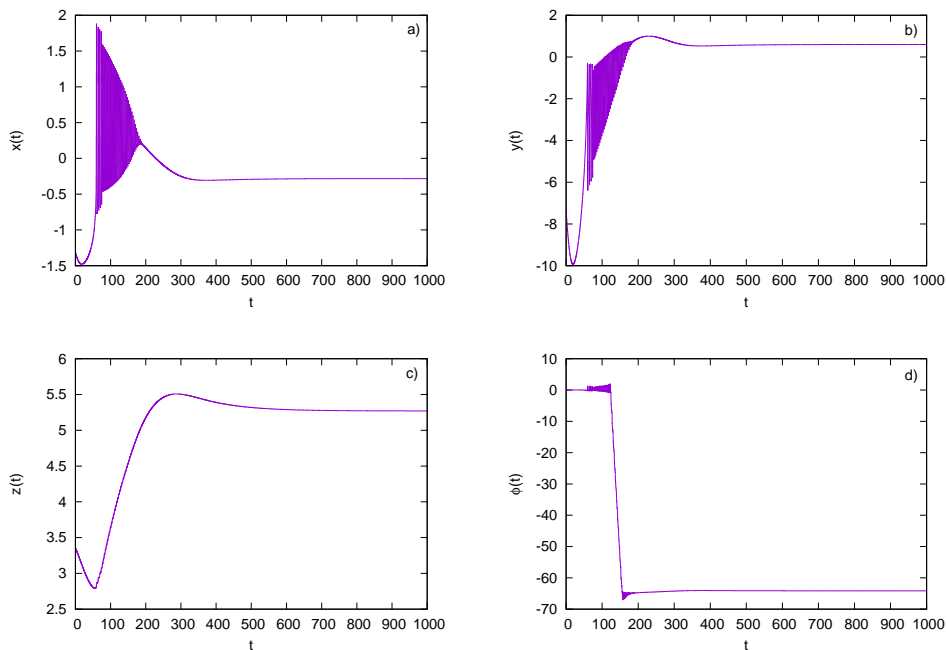


Figure 4.10: The behaviour of neuron 1 in the coupled Hindmarsh-Rose system for  $g_n = 1.9$  and  $g_l = 1.3$ . Panels a) to d): plots of the behaviour of the variables  $x$ ,  $y$ ,  $z$  and  $\phi$  of the neuron 1. The plots of  $x$  and  $y$  show the intense spiking for a short period of time then the trajectory converges to one of the fixed points and resembles the behaviour of neuron 2 and 3.

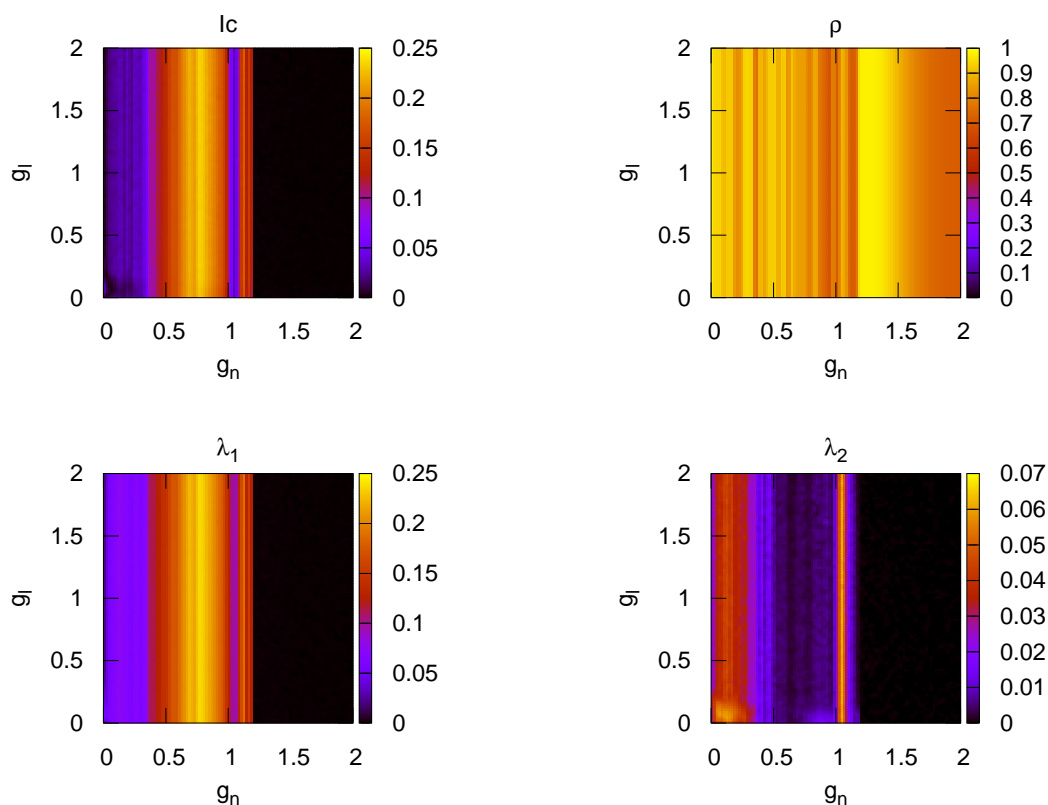


Figure 4.11: Plots of the upper bound  $I_c$ , the order parameter  $\rho$  and the two largest Lyapunov exponents  $\lambda_1$  and  $\lambda_2$  versus the chemical coupling  $g_n$  and electrical coupling  $g_l$  for an elementary example of 3 neurons connected simultaneously by one undirected electrical and two undirected chemical links (see Fig. 4.6b).

We also used the density plots to plot the upper bound  $I_c$  and the order parameter  $\rho$  and the two largest Lyapunov exponents  $\lambda_1$  and  $\lambda_2$  versus  $g_n$  and  $g_l$  to analyse the dynamics of the system with different coupling connections between the same number of neurons. In Fig. 4.11, we used  $(g_n, g_l) \in [0, 2] \times [0, 2]$  for 100 x 100 points. The plot for the upper bound  $I_c$  versus  $g_n$  and  $g_l$  shows that the highest value for  $I_c$  is between  $g_n = 0.7$  and  $0.8$  and for all the values of  $g_l$ . The dynamics of neurons in this area of the plot is chaotic. For  $g_n \geq 1.2$ , the motion is completely periodic. In the order parameter plot, the highest value of  $\rho$  is between  $g_n = 1.2$  and  $1.4$  and for all the values of  $g_l$  (almost equal to 1) and that indicates the behaviour of the neurons is periodically synchronised. The two other plots represent the two largest Lyapunov exponents  $\lambda_1$  and  $\lambda_2$  versus  $g_n$  and  $g_l$ . The upper bound  $I_c = \lambda_1 - \lambda_2$  and, the value of  $\lambda_1$  is positive and  $\lambda_2$  is either negative or equal to 0, the plot for  $\lambda_1$  is more similar to the  $I_c$  plot. Then, we plotted the trajectories for the 3 neurons at two different values for  $g_n$  and  $g_l$ . We select the values for  $g_n$  and  $g_l$  from

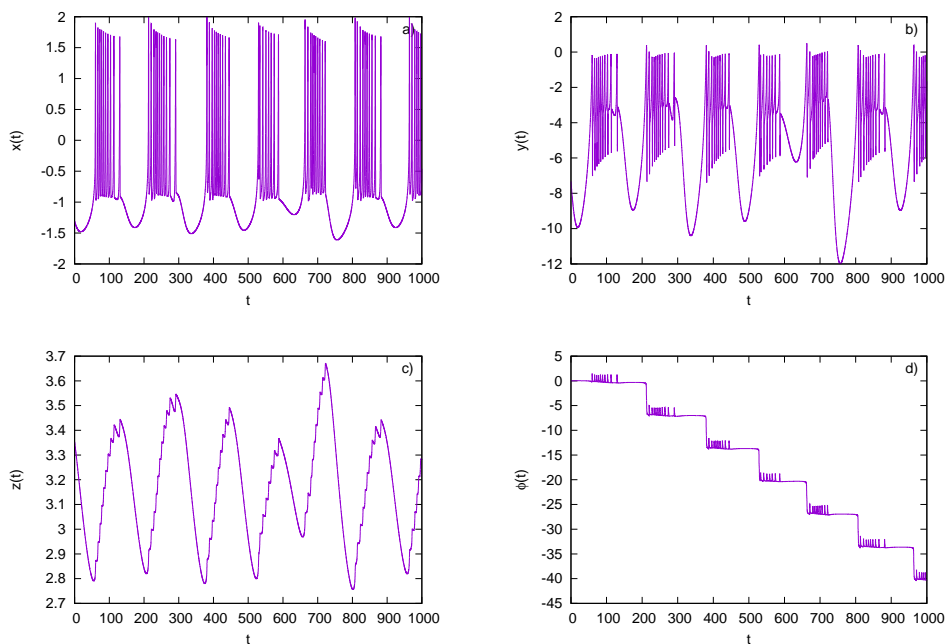


Figure 4.12: Spike-bursting behaviour of neuron 1 in the coupled Hindmarsh-Rose system for  $g_n = 0.75$  and  $g_l = 1$ . Panels a) to d): plots of the behaviours of variables  $x$ ,  $y$ ,  $z$  and  $\phi$  of the neuron 1 show the chaotic dynamics and resembles the behaviour of neuron 2 and 3. The dynamics of the three neurons is chaotic.

regions with different dynamics and plot the trajectories for all neurons at each of these values to analyse the behaviour of the system in these regions.

In Fig. 4.12,  $g_n = 0.75$  and  $g_l = 1$ . Plots of panels a) to d) represent the behaviour of variables  $x$ ,  $y$ ,  $z$  and  $\phi$  of neuron 1 with a spike-bursting behaviour which indicates that the dynamics of neuron 1 is chaotic and resembles the dynamics of the other two neurons 2 and 3.

In Fig. 4.13,  $g_n = 1.3$  and  $g_l = 1$ . Plots of panels a) to d) represent the behaviour of variables  $x$ ,  $y$ ,  $z$  and  $\phi$  of neuron 1. The plots of  $x$  and  $y$  show the intense spiking for a short period of time, then the trajectory converges to one of the fixed points of the dynamics and resembles the behaviour of neuron 2 and 3.

## 4.5 Conclusions

In this chapter, we used two elementary examples with different types of coupling to examine the effect of chemical and electrical couplings on the dynamics of three coupled neurons. To compare the resulting dynamics, we use the parameter space plots in Figs. 4.7 and 4.11.

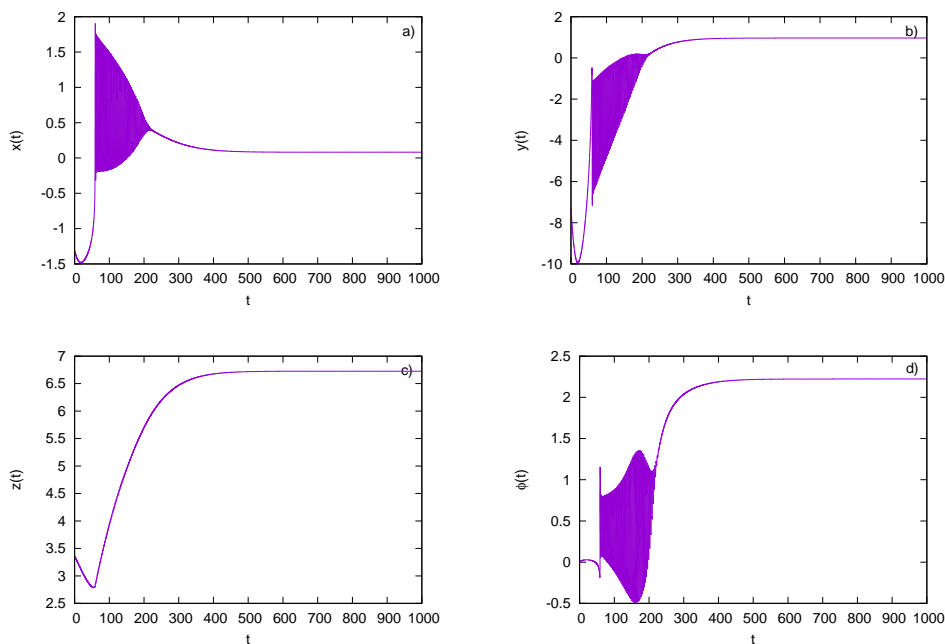


Figure 4.13: The behaviour of neuron 1 in the coupled Hindmarsh-Rose system for  $g_n = 1.3$  and  $g_l = 1$ . Plots of panels a) to d) represent the behaviour of variables  $x$ ,  $y$ ,  $z$  and  $\phi$  of neuron 1. The plots of  $x$  and  $y$  show the intense spiking for a short period of time, then the trajectory converges to one of the fixed points of the dynamics and resembles the behaviour of neuron 2 and 3.

In 4.7, the range of  $g_l$  for spike-bursting behaviour for the three neurons is between 0 and 0.6 and for values of  $g_n$  between 0 and 1.5. For any value of  $g_l$  greater than 0.6 the dynamics of the three neurons is either spiking or completely periodic, for all values of  $g_n$ . The electrical coupling has more effect on the dynamics of the coupled neurons but its range is smaller than the chemical coupling in the second example. The plot of the order parameter shows that we have chaotically synchronised neurons for all values of  $g_l$  and that depends on the values of  $g_n$ .

In 4.11, the range for  $g_n$  for spike-bursting behaviour for the three neurons is between 0.4 and 1.2, for all values of  $g_l$ . For any value of  $g_n$  greater than 1.2 the dynamics is periodic regardless of the value of  $g_l$ . This indicates that the chemical coupling dictates the dynamics of the coupled neurons but increasing it beyond a specific value (i.e. 1.2), the dynamics converges to one of the fixed points of the dynamics. In the order parameter plot, the highest values for  $\rho$  is for  $g_n$  between 1.2 and 1.4, for all values of  $g_l$ . This indicates the neurons are periodically synchronised. Both examples do not have desynchronised neurons.

---

The resulting dynamics indicate that the two types of coupling produce different patterns of dynamics. The dynamics depends on the number of neurons and the type of coupling strength between them. Even for small numbers of neurons, increasing the number of chemical links can produce chaotic dynamics for the whole range of electrical coupling values. However, the increase of chemical coupling beyond a specific value can result in periodic motion for wide range of chemical coupling values. Whereas, in the first example which has more electrical links, the periodic motion appears in various regions for different values of the couplings.

# Chapter 5

## Evolution of networks of Hindmarsh-Rose neurons (by increasing the KS entropy)

### Introduction

In this chapter, we review the development of the concept of entropy. We first describe the work of the physicist Rudolf Clausius (2 January 1822 - 24 August 1888). He used the concept of entropy in his work to tackle the problem of finding a mathematical expression to describe all transformations of a body through heat exchange between that body and another one or the environment. His work stated the second law of thermodynamics. In statistical mechanics, Ludwig Boltzmann developed a statistical mechanical evaluation of the concept of entropy. Then, we review with some detail the metric entropy also known as the Kolmogorov-Sinai entropy which is based on the notion of entropy introduced earlier by Claude Shannon. The Pesin identity formula relates Kolmogorov-Sinai entropy to positive Lyapunov exponents of the dynamics of a chaotic system. Later, we briefly review the concept of brain entropy which can provide an informative tool to assess brain states and brain functions. Finally, we discuss the topic of the evolution of brain dynamical networks. In evolving dynamical networks; topology, dynamics and evolution are all affecting one another. We used the Kolmogorov-Sinai entropy  $H_{KS}$  which equals the sum of positive Lyapunov exponents (Pesin identity) as the evolutionary rule for a coupled Hindmarsh-Rose system to evolve a network of 6 clusters composed of 10 neurons each with different values for both the chemical and electrical coupling parameters.

## 5.1 Entropy

The term “entropy” was coined by the German physicist Rudolf Clausius in 1850 from the Greek words “εν” and “τροπη” which mean “in a turning” or internal change [58]. The word reveals analogy to “energy” and was designed to mean a form of energy that eventually “turns into” useless heat. Entropy has multiple definitions related to distinct entropic functions that belong to different disciplinary domains such as Clausius’ physical entropy which is proportional to the quantity of energy no longer available to do physical work. In 1877, Ludwig Boltzmann put entropy into the probabilistic setup of statistical mechanics [39] and has also been generalised to quantum mechanics by John von Neumann [65, 191]. Later, this led to the invention of entropy as a term in probability and information theory by the American mathematician Claude Shannon in 1948 [176]. The dynamical entropy in dynamical systems was created by the Russian mathematician Andrei Kolmogorov [117, 118] and later improved by his student Yakov Sinai [179].

The disorder in a system is a consequence of the increase of its entropy. The increase in thermal motion after heat is added to a working substance changes the highly structured and orderly system to disorderly one in which molecules have no fixed positions. This will create more disordered distributions and arrangements of molecules and subsequently leads to an increase in the measure of entropy [39]. The concept of entropy is an integral part of thermodynamics and it has played a central role in dynamical systems, but in recent years this long-standing use of the term “disorder” to discuss entropy has met with some criticism [123, 141]. Today, entropy stands as an open concept still undergoing a continuous evolution [155].

### 5.1.1 Clausius entropy

The historical development of the concept of entropy started as a response to the observation that a certain amount of functional energy released from heat-powered engines is not transformed into useful work and instead is lost to dissipation or friction. In 1803, the French mathematician Lazare Carnot published his work on the *Fundamental Principle of Equilibrium and Movement* which includes a discussion on the efficiency of fundamental machines. After his death, his son Sadi Carnot published the *Reflections on the Motive Power of Fire* [50]. He envisaged an ideal engine in which any heat converted into work

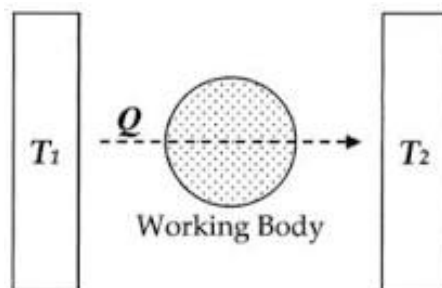


Figure 5.1: Diagram of Sadi Carnot's heat engine, 1824 [5].

and could be reinstated by reversing the motion of the cycle. Later, Rudolf Clausius re-discovered Carnot's works and in his mathematical presentation of the *First Fundamental Theorem* [60], he presented the first-ever mathematical formulation of entropy, although at this point he called it “*equivalence-value*”.

Clausius used the concept of entropy in his attempt to tackle the problem of finding a mathematical expression to describe all transformations of a body through heat exchange between that body and another one or the environment [76]. For two transformations which can mutually replace one another, the generations of the amount of heat  $Q$  from work at temperature  $T$ , has the equivalence-value  $\frac{Q}{T}$ . The passage of the amount of heat  $Q$  from temperature  $T_1$ , through the “working body” which was typically a body of steam (see Fig. 5.1) to temperature  $T_2$  (with  $T_2 > T_1$ ) has the equivalence-value

$$Q\left(\frac{1}{T_2} - \frac{1}{T_1}\right),$$

where  $T$  is a function of the temperature which is independent of the nature of the process by which the transformation is effected. Equivalence-value is thought to be “entropy” in modern terminology and symbolised by  $S$ . We can compute the change in entropy  $\Delta S$  when increasing the temperature from  $T_1$  to  $T_2$ . If we make  $S = \frac{Q}{T}$ , it is equivalent to the amount of heat at temperature  $T$  produced by (external) work [76]. Then, the change in entropy for this transformation is

$$\Delta S = S_{final} - S_{initial},$$

which equals to the form that was derived by Clausius

$$\Delta S = Q\left(\frac{1}{T_2} - \frac{1}{T_1}\right). \quad (5.1.1)$$

In 1862, Clausius stated the “*theorem respecting the equivalence-value of the transformations*” [59] what is now known as *the second law of thermodynamics*.

Let  $dQ$  be an element of heat given up by the body to any reservoir of heat during its own changes. The heat that may be absorbed from the reservoir is negative.  $T$  represents the absolute temperature of the body which does not depend on the properties of its material, at the moment of giving up this amount of heat. Then,

$$\int \frac{dQ}{T} = 0, \quad (5.1.2)$$

must be true for every reversible cyclical process (i.e. the system is without entropy production), and the relation

$$\int \frac{dQ}{T} \geq 0, \quad (5.1.3)$$

must hold for every non-compensated relation (irreversible cyclical process) [76]. This early formulation of the second law of thermodynamics is one of the original forms of the concept of entropy. The second law of thermodynamics implies that entropy of closed systems always increases and for systems that are not closed, entropy can decrease with time. In processes of living systems, local entropy reduces but at the same time the entropy of the surrounding increases, resulting in a net increase in entropy. The concept of *arrow of time* which was developed by Arthur Eddington in 1927, implies that time flows in “one-way direction” [159]. At microscopic level, physical processes are believed to be time-symmetric (i.e. the theoretical statements that describe them would remain true under time reversal). However, at the macroscopic level it appears that time moves at one-way direction. The arrow of time and the second law of thermodynamic show that the thermodynamic arrow of time points in the direction of increase in entropy. It is important to recognise that there are two types of changes in entropy, we have to consider at all times. The entropy change of the system and the entropy change of its surroundings and their sum represents the entropy change of the universe

$$\Delta S_{univ} = \Delta S_{sys} + \Delta S_{surr} = \frac{Q_{sys}}{T} + \frac{Q_{surr}}{T}. \quad (5.1.4)$$

In an isothermal reversible expansion, the heat  $Q$  absorbed by the system from the surroundings is

$$Q_{rev} = nRT \ln \frac{V_2}{V_1},$$

where  $R$  is the ideal gas constant,  $n$  is the amount of substance of gas,  $V_1$  the initial volume,  $V_2$  the final volume and  $T$  is the absolute temperature. Since the heat absorbed

by the system is the amount lost from the surroundings,  $Q_{sys} = -Q_{surr}$ . Therefore, for a truly reversible process, the change in entropy is

$$\Delta S_{univ} = \frac{nRT \ln \frac{V_2}{V_1}}{T} + \frac{-nRT \ln \frac{V_2}{V_1}}{T} = 0.$$

However, for irreversible process, the change in entropy is

$$\Delta S_{univ} = \frac{nRT \ln \frac{V_2}{V_1}}{T} > 0.$$

From the equations of  $\Delta S_{univ}$  for both types of processes, we get the second law of thermodynamics

$$\Delta S_{univ} = \Delta S_{sys} + \Delta S_{surr} \geq 0, \quad (5.1.5)$$

where  $\Delta S_{univ}$  equals zero for truly reversible process and is greater than zero for an irreversible process. The second law of thermodynamics stated that it is impossible to perform a process whose only final effect is the transfer of heat from a cooler medium to a warmer one. Any such transfer must involve an external work, the elements participating in the work will also change their states and the overall entropy will rise [65].

In 1876, physicist Josiah Willard Gibbs, building on the work of Clausius and others, derived a measurement of “the available energy to do useful work” also known as *Gibbs free energy*,  $\Delta G$  in a thermodynamic system. For a process at constant temperature  $T$  and pressure  $p$

$$\Delta G = \Delta H - T\Delta S, \quad (5.1.6)$$

where  $\Delta H$  represents the total energy change of the system and  $T\Delta S$  the energy loss [86]. The second law of thermodynamics can also be stated that “all spontaneous processes produce an increase in the entropy of the universe”. If  $\Delta G < 0$ , then the process is spontaneous. If  $\Delta G > 0$ , then the process is non-spontaneous. In a closed system, if  $T\Delta S \geq \Delta G$  that means the system is not in equilibrium and its Gibbs energy will continue to decrease and when it is in equilibrium (i.e. no longer changing),  $\Delta G$  will be zero. In state of equilibrium, the entropy of the system cannot increase (because it is already at a maximum) and it cannot decrease (because that would violate the second law of thermodynamics). The only changes allowed are those in which the entropy remains constant.

In thermodynamic interpretation of evolution of life, both concepts of entropy and free energy are used. The Austrian physicist Erwin Schrödinger in his book *What is life?*

published in 1944, theorises that life dictated by the second law of thermodynamics, decreases or maintains its entropy by consuming negative entropy [174]. In 1982, American biochemist Albert Lehninger argues in his book, *Principles of Biochemistry* that the order produced within cells as they grow and divide is more than compensated for by the disorder they create in their surroundings in the course of division and growth. He stated that “living organisms preserve their internal order by taking from their surroundings free energy, in the form of nutrients or sunlight, and returning to their surroundings an equal amount of energy as heat and entropy” [145].

### 5.1.2 Entropy in Statistical Mechanics

In 1877, Ludwig Boltzmann developed a statistical mechanical evaluation of the concept of entropy  $S$  [39]. The macroscopic state of a system is characterised by a distribution of its microstates. A thermodynamical state  $A$  or macrostate can be realised in many different ways at the microscopic level and corresponding to many points  $v$  (called microstates) in a phase space  $\Omega$ . The Boltzmann entropy of  $A$  is defined to be proportional to the logarithm of the phase space volume of the set  $M_A$  of all  $v$  that realise the state  $A$

$$S(A) = S_0 + k \log_2(\text{vol}(M_A)), \quad (5.1.7)$$

where the constant  $S_0$  depends on the unit of phase space volume and the proportionality factor  $k$  is known as Boltzmann’s constant. If we take to be  $\Omega$  a finite set and  $\#M_A$  to denote the number of elements in the set  $M_A$ , then Boltzmann entropy can be defined by

$$S(A) = k \log_2(\#M_A). \quad (5.1.8)$$

Formulae (5.1.7) and (5.1.8) can be written in probabilistic terms if we choose one element of the phase space  $\Omega$  at random with uniform distribution. Then, if the set  $\Omega$  of all microstates has  $M$  elements and the set  $M_A$  of those realising the macrostate  $A$  has  $N$  elements, we can assign probabilities  $\frac{1}{M}$  to each microstate and  $\frac{N}{M}$  to state  $A$ . Then, Boltzmann’s formula becomes

$$S(A) = S_{max} + k \log_2(\text{Prob}(A)), \quad (5.1.9)$$

where  $S_{max} = k \log_2(\#\Omega)$  represents the maximal possible entropy of a macrostate, since  $M_A$  cannot have more elements than  $\Omega$ . Hence, the probability of the maximal state is almost equal to 1, while the probabilities of states of lower entropy are exponentially small. This approach provides another interpretation of the second law of thermodynamics, the system spontaneously assumes the state of the maximal entropy, not any of the other states' entropies. [65].

The second law of thermodynamics states that a spontaneous process increases the entropy of the universe,  $\Delta S_{univ} > 0$  and non-spontaneous one decreases it,  $\Delta S_{univ} < 0$ . If  $\Delta S_{univ} = 0$ , the system is at equilibrium. Consider a system which can be described by a single microstate ( $A = 1$ ), a perfect crystallinity and complete lack of motion that means there is only one possible location for each identical atom or molecule comprising the crystal. According to the Boltzmann equation, the entropy of such system with only one possible microstate is zero. This limiting condition for a system's entropy represents *the third law of thermodynamics*: the entropy of a pure, perfect crystalline substance at a temperature of absolute zero (0 Kelvin) is zero.

Later, Josiah Gibbs extended formula (5.1.9) to the case where microstates  $v$  realising the macrostate  $A$  may have different probabilities  $p_v$

$$S(A) = -k \sum_{v \in M_A} p_v \log_2(p_v). \quad (5.1.10)$$

For the continuous probability distribution with density function  $p$ , Gibbs entropy is defined as

$$S(A) = -k \int p(v) \log_2(p(v)) dv. \quad (5.1.11)$$

### 5.1.3 Shannon entropy

The concept of entropy, as it is now used in information theory, was introduced by Claude Shannon in 1948 [176]. As he was working to quantify mathematically the statistical nature of “lost information” in phone-line signals, Shannon developed the very general concept of information entropy which represents a fundamental cornerstone in information theory. In his work, Shannon made use of the two different but related measures, entropy and mutual information. Entropy is really a notion of self-information (i.e. the entropy of a random process is the amount of information in it) while mutual

information is a measure of the information contained in one process about another one [85]. Shannon's information entropy, which is originally an idea inherited from thermodynamics, is a much more general concept than the statistical thermodynamic entropy, while the information entropy is present whenever there are unknown quantities that can be described only by a probability distribution. Statistical thermodynamic entropy can be seen as a particular application of Shannon's information entropy to the probabilities of particular microstates of a system that occur in order to produce a particular macrostate.

Suppose we have an experiment with  $n$  possible outcomes, such as rolling a dice with  $n$  faces and let  $p_1, p_2, \dots, p_n$  be the probabilities of the different outcomes. Then, a measure of the amount of uncertainty about which outcome will turn out,  $H(p)$  is

$$H(p) = - \sum_{i=1}^n p_i \log_2 p_i, \quad (5.1.12)$$

where  $p$  is the probability vector of finitely many nonnegative numbers  $p_1, p_2, \dots, p_n$  whose sum equals 1 [18, 167]. Equation (5.1.12) represents the *Shannon entropy* of a probability vector  $p$  which is a straightforward adaptation of the Gibbs entropy Eq. (5.1.10) but leaving out the proportionality factor  $k$ .

#### 5.1.4 Kolmogorov-Sinai entropy

The definition of *Kolmogorov-Sinai entropy* (*K-S entropy*) also known as the *metric entropy* of a dynamical system is based on the notion of entropy that was developed by Claude Shannon.

Let's consider a measure-preserving dynamical system consisting of two fundamental mathematical objects: a *measure space*  $(X, W, \mu)$  and a *measure-preserving transformation*  $T : X \rightarrow X$ .  $X$  is a set and  $W$  is a collection of subsets of  $X$  such that:

1.  $X \in W$ .
2. If  $A \in W$ , then the complement of  $A$ ,  $X \setminus A \in W$ . So,  $\emptyset \in W$ .
3. Given a finite sequence  $A_i$  of subsets of  $X$  such that  $A_i \in W$  then their union  $\cup_i A_i \in W$ .
4.  $\cap_i A_i \in W$ ,  $W$  is closed under the operation of intersection [138, 202].

If  $W$  satisfies the above properties then it is called a  $\sigma$ -algebra set. The third element  $\mu$  of the triple  $(X, W, \mu)$  is a measure which belongs to a class of set functions, i.e. functions assigning numerical values to sets.  $\mu$  must satisfy the following requirements:

1.  $\mu(A) \geq 0$  for all  $A \in W$ ,
2.  $\mu(\emptyset) = 0$ , i.e. the empty set has zero measure,
3. If  $\{A_i\}$  is a sequence of pairwise disjoint sets, then  $\mu(\bigcup_{i=1}^{\infty} A_i) = \sum_{i=1}^{\infty} \mu(A_i)$ .

The quantity  $\mu(A)$  is called *the measure of A* and the sets  $A_i \in W$  are called *measurable sets* as for them the measure is defined. If  $\mu(X) = 1$ , the measure space is said to be “probabilistic” and  $0 \leq \mu \leq 1$  is called a probability measure [138].

The transformation  $T$  is said to be *measurable* if  $A \in W \rightarrow T^{-1}(A) = \{x|T(x) \in A\} \in W$ .  $T$  is called a *measure-preserving map* with respect to  $\mu$  and  $\mu$  is said to be *T-invariant*, whenever  $\mu(A) = \mu(T^{-1}(A))$  for all sets  $A \in W$ . For flows, we can say that a family  $\phi_t(x)$  of measurable maps preserves the measure  $\mu$  if  $\mu(A) = \mu(\phi_t^{-1}(A))$  for all  $t$  and all measurable subsets  $A \subset X$  [138, 202]. For the invariant probability measure  $\mu$  of the measure-preserving map  $T$  on the defined space  $X$ , the KS entropy can be denoted by  $H_{KS}(\mu)$ . Let's consider a bounded region  $M \subseteq X$  such that  $\mu(M) = 1$  and be invariant under the transformation of the map  $T(x)$ . Let  $M$  consists of  $k$  disjoint partitions such that

$$M = M_1 \cup M_2 \cup \dots \cup M_k.$$

We use this partition to define the entropy function using the Shannon entropy form

$$h(M_i) = \sum_{i=1}^k \mu(M_i) \log(\mu(M_i)^{-1}).$$

We need to construct a series of partitions  $\{M_i^n\}$  that must get finer and finer (i.e. the set size gets smaller and smaller). Since the map  $T(x)$  evolves in time, it produces a series of intersections of the form  $M_j \cap T^{-1}(M_i)$ ,  $j, i = 1, 2, \dots, k$  such that for  $n$  iterations the refined  $\{M_i^n\}$  are given as

$$M_{i1} \cap T^{-1}(M_{i2}) \cap T^{-2}(M_{i3}) \cap \dots \cap T^{-(n-1)}(M_{in}).$$

Then, we can write the entropy equation as

$$H(\mu, \{M_i\}) = \lim_{n \rightarrow \infty} \frac{1}{n} h(\{M_i^n\}). \quad (5.1.13)$$

The KS entropy can be formally defined as the supremum of Eq. (5.1.13) over all initial partitions of  $M_i$ .

$$H_{KS}(\mu) = \sup_{\{M_i\}} (H(\mu, M_i)), \quad (5.1.14)$$

which is the entropy of the system with respect to the partition  $M$  [18, 77, 180, 202].

The entropy of a system with respect to a partition can be given an alternative formulation by making use of the auxiliary concept of *conditional entropy* for the two partitions  $A$  and  $B$ , defined by

$$H(A|B) = - \sum_{a,b} \mu(a,b) \log \mu(a|b), \quad (5.1.15)$$

where  $a, b$  denote elements of the partitions  $A$  and  $B$ , respectively. We can think of a partition as an experiment whose outcome is uncertain. The conditional entropy represents the amount of uncertainty of the experiment  $A$  when the outcome of the experiment  $B$  is known [138].  $H(A|B) = 0$  if and only if the value of  $A$  is completely determined by the value of  $B$ . The mutual information between  $A$  and  $B$ ,  $I(A; B)$  measures how much the entropy of  $A$  is reduced (i.e. reduction in the amount of uncertainty about  $A$ ) if we know the realisation of  $B$  [18]

$$I(A; B) = H(A) - H(A|B) \quad (5.1.16)$$

### 5.1.5 Pesin identity

By definition [176], the entropy of a dynamical system is the measure of the amount of uncertainty about the outcome of an experiment with  $n$  possible outcomes. This uncertainty is caused by the exponential separation of nearby points or trajectories due to their sensitivity to initial conditions in chaotic systems. Since positive Lyapunov exponents characterise this exponential divergence, one should expect that the entropy must be related to the positive Lyapunov (characteristic) exponents [18]. This divergence leads to a change in the information we have about the state of the system. If we consider that the two initial conditions are different (i.e. indistinguishable within certain precision), then they will evolve into distinguishable states after a finite time and that change leads to the creation of information [138, 167]

Consider an  $m$ -dimensional ball of radius  $\epsilon$  in a measure space. If we let this ball evolve according to a transformation  $f$ , we see that the ball will be deformed into an ellipsoid, since a positive Lyapunov exponent signifies the growth along the orthogonal

direction of the ellipsoid. The semi-axes of the ellipsoid are stretched by the transformation and we have

$$\epsilon_i \rightarrow \epsilon_i e^{n\lambda_i}.$$

The two indistinguishable points lying on an expanding axis (i.e. an unstable direction) become distinguishable after a finite time [167]. Although the total volume of the ellipsoid generally shrinks due to dissipation, the uncertainty about the future position of the trajectories grows with lengths of the expanding semi-axes. If there are several positive exponents  $\lambda_i$ , each of the related unstable directions contributes to this effect. Then, the relation between the Kolmogorov-Sinai entropy and the positive Lyapunov exponents which has been established by *Ruelle theorem* [166] is

$$H_{KS} \leq \sum_{\lambda_i > 0} \lambda_i. \quad (5.1.17)$$

The sum of all positive Lyapunov exponents represents an upper bound of the Kolmogorov-Sinai entropy [18, 112, 166]. This inequality holds as equality often, but not always for natural measures. However, Yakov Pesin proved that the equality holds for Lebesgue absolutely continuous invariant measure and in a closed system where no trajectories escape to infinity when the motion is bounded and is called *Pesin identity* [157],

$$H_{KS} = \sum_{\lambda_i > 0} \lambda_i. \quad (5.1.18)$$

Equations (5.1.17) and (5.1.18) suggest that entropy is created by the exponential divergence of nearby trajectories.

### Definition 7

Given a set  $N \subset \mathbb{R}$ ,  $\mu(N)$  will denote its Lebesgue measure if it satisfies the following properties:

- 1- *Extends length*: For every interval  $I$ ,  $\mu(I) = l(I)$ , where  $l(I) = b - a$  for the bounded interval  $I$  with endpoints  $a$  and  $b$  ( $a < b$ ),
- 2- *Monotone*: If  $A \subset B \subset \mathbb{R}$ , then  $0 \leq \mu(A) \leq \mu(B) \leq \infty$ ,
- 3- *Translation invariant*: For every subset  $A$  of  $\mathbb{R}$  and for every point  $x_0 \in \mathbb{R}$ , we define  $A + x_0 := \{x + x_0 : x \in A\}$ . Then,  $\mu(A + x_0) = \mu(A)$ ,

4- *Countably additive: If  $A$  and  $B$  are disjoint subsets of  $\mathbb{R}$ , then  $\mu(A \cup B) = \mu(A) + \mu(B)$ . If  $\{A_i\}$  is a sequence of disjoint sets, then  $\mu(\bigcup_{i=1}^{\infty} A_i) = \sum_{i=1}^{\infty} \mu(A_i)$  [139].*

The Pesin identity (5.1.18) is the formula that relates Kolmogorov-Sinai entropy to positive Lyapunov exponents and represents a suitable tool to compute the increase or the decrease of the entropy in a dynamical system. In our work with the Hindmarsh-Rose system for neuronal activity, we need to evolve a network of HR neurons by maximising the flow of information in the network. The increase of the entropy in the network which equals to the sum of the positive Lyapunov exponents can give us a good indication of the maximisation of the flow of information in the evolved network.

## 5.2 Brain entropy

Entropy is an important property for life as well as the human brain. It is a measure of uncertainty about the state of a system but it also reflects the degree of randomness or disorder in a system [49]. Characterising *brain entropy* (BEN) can provide an informative tool to assess brain states and brain functions [196]. Recently, the concept of brain entropy has been defined as the number of neural states a given brain can access [52, 171]. Low entropy is characterised by orderliness, repetition and less long-range network synchrony. The lowest levels of entropy can be observed in deep sleep or, at the extreme, in coma. Higher levels of entropy is marked by greater long-distance correlations in brain network activities which leads to higher information processing capacity [52].

The human brain has an imperative need for sustaining its entropy for normal functioning [196]. Entropy can be used as a measure of the complexity and irregular variability in brain activity from one moment to the next. That means more entropy in the brain's connectivity can lead to better adaptation to dynamically changing environment rich with unpredictable events. Hence, brain entropy can be understood as a measure of the brain's overall flexibility or readiness to encounter unpredictable stimuli and predict the outcomes of our complex and chaotic world [52].

Many researchers investigate the relationship between brain entropy, consciousness and human intelligence. Consciousness arises naturally as a result of a brain maximising its information content. They found that the greatest number of possible configurations of interactions between brain networks is associated with conscious states and represent-

ing the highest level of brain entropy. However, lower entropy is associated with unconscious or altered states which results from fewer configurations of interactions. Therefore, one can suggest that consciousness could be the result of an optimisation of information processing [69]. Human intelligence comprises comprehension of and reasoning about infinitely variable external events. Brain has large variability in neural configurations, or states, and that provides better ability in understanding and predicting these external events. Entropy, is the measure of the variety of these possible configurations within a brain [171]. Researchers suggest that entropy can be a reliable predictor of human intelligence, and can provide us with unique information not captured by either developmental status or educational status [52, 69, 171].

Entropy-derived measures can represent a physical means for characterising brain status as well as its alterations in diseases [196]. Entropy measures the rate of increase in dynamical complexity as the system evolves with time [202]. Therefore, these entropy-derived measures have been used for evaluating the physiological complexity in neuroscience. Complexity measured by entropy evaluates the amount of information needed to predict the future state of the system, more complex dynamics means that the system has higher entropy. Physiological signals obtained from a healthy individual should contain rich information about their complex behaviours. Whereas aging and diseased status, usually implying decrease of the richness of physiological information, show reduced entropy values and loss of complexity within the dynamics of physiological output [56].

The *functional magnetic resonance imaging* (fMRI) and *resting-state* fMRI (rsfMRI) scanners are two entropy-based metrics used in mapping brain entropy [56, 171, 196]. They measure brain activity by detecting changes associated with blood flow depending on the fact that cerebral blood flow and neuronal activation are coupled. The blood flow to an area of the brain is remarkably sensitive to any change in brain activity and that leads to the blood being more oxygenated when neural activities increase, which is called the *blood oxygenation level-dependent* (BOLD) effect. Brain activity can also be seen as a time series and the *electroencephalogram* (EEG) applies the concept of entropy to time series. There are relations between EEG time series and the functioning of the vast number of neurons within the human brain [107]. As entropy is a measure of irregularity or randomness in a signal, EEG recordings can be used for quantifying, in a statistical sense, the amount of uncertainty or randomness in the pattern, which is also roughly equivalent

to the amount of information contained in the signal. The entropy-derived measures have been widely employed as a noninvasive clinical tool for examining normal and pathologic, neurophysiological temporal dynamics. They have been applied to understand the physiological processes in patients with *neurodegenerative disorder diseases*, a range of conditions primarily affect the neurons in the human brain. Examples of neurodegenerative diseases include Alzheimer's, Parkinson's and Huntington's diseases. Entropy measures have also been applied in many other pathological states, including autism, epilepsy and schizophrenia [56] and widely used during anaesthesia to quantify the anaesthetic drug effect [126].

### 5.3 Evolution of brain dynamical networks

Static networks lack two fundamental characteristics that are displayed by many complex systems: the dynamic nature of the components and their interactions, and the possible evolution of the underlying network structure. Real-world networks evolve over time, either by adding or removing nodes or links (for example, the addition or removal of neurons or synapses during the growth and development of the neural network). In evolving dynamical networks; topology, dynamics and evolution are all affecting one another. The dynamical processes that take place over the network structure are coupled to the evolutionary rules of the network itself. Therefore, the network dynamics influence its evolution and vice versa. Deep understanding of network evolution can reveal the rich interplay between network topology and its dynamics [17].

The human brain which consists of approximately 86 billion neurons and 150 trillion synapses [23, 127] represents perhaps one of the most complex systems in the world. The brain undergoes profound anatomical changes during the first two decades of life. These developmental changes in neuronal connectivity parallel the maturation of social, cognitive, and motor skills from birth to young adulthood and alterations of normal development can also increase the risks for neurodevelopmental disorder diseases such as autism and schizophrenia [153]. Recently, the brain has been modelled using small-world networks that consist of neural units (e.g. neurons and brain regions) linked by structural and functional connectivity [127]. Brain possesses the small-world topology immediately after birth and becomes more stable within two years [78]. Its anatomical connectivity

is sparse, locally clustered, and with a few long-range connections mediating short path-lengths between any pair of regions [33], that leads to excellent local and global wiring efficiency for information transfer [78].

In the human brain, the complete network of neuronal connections is called the *connectome*. Connections within this intricate network are distributed unevenly with certain network elements possessing a relatively large number of connections, marking them as network hubs. Brain hubs facilitate the integration of functionally specialised and anatomically diverse neural systems [153]. In complex networks, flow is distinct from network connectivity. The network connectivity describes the static structure of a network (i.e. its wiring diagram). In contrast, network flow describes the dynamic utilisation of a network as a communication medium and anatomical connections in the brain all relate to network connectivity. Determining how information flows along anatomical brain pathways is a fundamental requirements for understanding how brain dynamical networks (BDNs) perceive and learn about their environments [182].

Mutual information is a fundamental quantity to understand the development and function of the brain. It is a measure of how much information two systems or two data sets exchange. However, the calculation of mutual information in dynamical networks faces many difficulties because it is based on probabilities of significant events. An alternative way is to calculate the mutual information rate (MIR) which represents the amount of information exchanged per unit of time between two nodes in a dynamical network. We can compute the upper bound for the MIR in terms of the positive Lyapunov exponents, i.e.  $I_c = \lambda_1 - \lambda_2$  (see Eq. (4.4.1)) instead of relying on probabilities [27]. In Ref. [20], the authors have used the upper bound for MIR to propose a working hypothesis that brain networks evolve based on the principle of the maximisation of their internal information flow capacity. The amount of the increase of the entropy of the system is another approach that we used to evolve HR networks in this thesis.

## 5.4 Evolution of Hindmarsh-Rose neurons in brain dynamical networks

To evolve a network of Hindmarsh-Rose neurons, we used the Kolmogorov-Sinai entropy  $H_{KS}$  which is equal to the sum of positive Lyapunov exponents, as an evolutionary

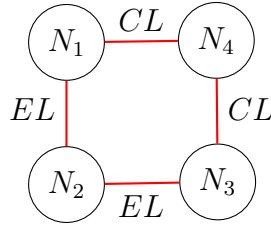


Figure 5.2: An elementary example of 4 neurons connected simultaneously by two undirected electrical ( $EL$ ) and two undirected chemical ( $CL$ ) links.

rule for a coupled Hindmarsh-Rose system. First, we developed a Matlab code to compute the Kolmogorov-Sinai entropy  $H_{KS}$  using the Pesin identity (5.1.18), for a network of 4 neurons connected simultaneously by two undirected electrical and two undirected chemical links for a coupled Hindmarsh-Rose system (see Fig. 5.2). We used the same parameter values and initial conditions as in subsection 4.2.2 in the Matlab code but with different values for the chemical coupling  $g_n$  and electrical coupling  $g_l$  to compute the Lyapunov exponents and the  $H_{KS}$  of the network at each case in the time interval:  $[0, 10^4]$  with time-step 0.01. The coupled HR system for an undirected brain dynamical network of  $N_n$  neurons is given by

$$\begin{aligned}
 \frac{dx_i}{dt} &= y_i - ax_i^3 + bx_i^2 - z_i + I_{ext} - g_n(x_i - V_{syn}) \sum_{j=1}^{N_n} B_{ij}S(x_j) \\
 &\quad - g_l \sum_{j=1}^{N_n} G_{ij}H(x_j), \\
 \frac{dy_i}{dt} &= c - dx_i^2 - y_i, \\
 \frac{dz_i}{dt} &= r[s(x_i - x_o) - z_i], \\
 \frac{d\phi_i}{dt} &= \frac{\dot{y}_i x_i - \dot{x}_i y_i}{x_i^2 + y_i^2}, \quad i = 1, \dots, N_n,
 \end{aligned} \tag{5.4.1}$$

where  $x_i$  is the membrane potential,  $y_i$  the spiking variable,  $z_i$  the bursting variable and  $\phi_i$  the phase variable.  $B_{ij}$  is the adjacency matrix of the chemical connections.  $G_{ij}$  is the Laplacian matrix accounts for the way neurons are electrically coupled,  $G_{ij} = K_{ij} - A_{ij}$  with  $A$  is the adjacency matrix of the electrical connections and  $K$  the degree identity matrix based on  $A$  [20].

For  $g_n = 0.8$  and  $g_l = 0.1$ , the entropy of the system is positive:  $H_{KS} = 0.275$  as the dynamics of the system is chaotic. For  $g_n = 1.2$  and  $g_l = 1.6$ , the entropy of the system is close to zero:  $H_{KS} = 0.001$  as the trajectory of the system converges to one of the fixed

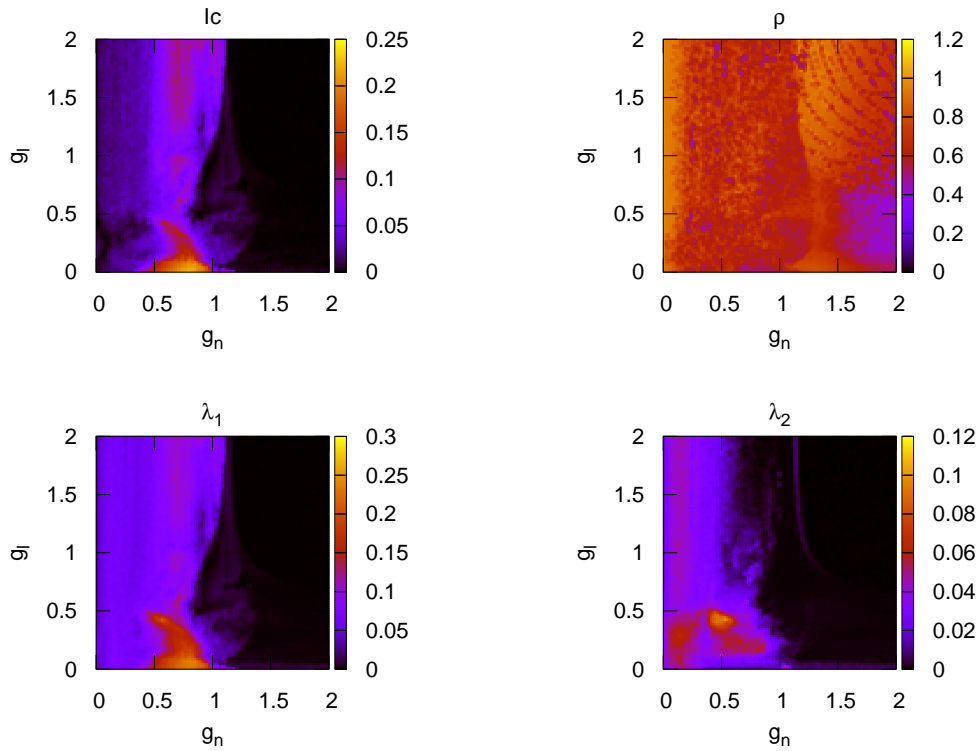


Figure 5.3: Plots of the upper bound  $I_c$ , the order parameter  $\rho$  and the two largest Lyapunov exponents  $\lambda_1$  and  $\lambda_2$  versus the chemical coupling  $g_n$  and electrical coupling  $g_l$  for an elementary example of 4 neurons connected simultaneously by two undirected electrical and two undirected chemical links.

points and loses energy.

We also plot the upper bound  $I_c$  for MIR (4.4.1), the synchronisation measure  $\rho$  (4.3.1) and the two largest Lyapunov exponents  $\lambda_1$  and  $\lambda_2$  versus the chemical coupling  $g_n$  and electrical coupling  $g_l$  for the network of 4 neurons.

In the parameter spaces in Fig. 5.3, we used  $(g_n, g_l) \in [0, 2] \times [0, 2]$  for 100 x 100 points. The plot for the upper bound  $I_c$  versus  $g_n$  and  $g_l$  shows that the highest value for  $I_c$  is between  $g_n = 0.6$  and 1 and  $g_l = 0$  and 0.2. The dynamics of neurons in this area of the plot is chaotic. In the order parameter  $\rho$  plot, the highest value for  $\rho$  is between  $g_n = 0$  and 0.2 and for all the values of  $g_l$  and that indicates the behaviour of the neurons is periodically synchronised. The two other plots represent the two largest Lyapunov exponents  $\lambda_1$  and  $\lambda_2$  versus  $g_n$  and  $g_l$ . The upper bound  $I_c = \lambda_1 - \lambda_2$ , with the value of  $\lambda_1$  positive and  $\lambda_2$  either positive or very close to 0 (e.g., for  $g_n = 0.8$  and  $g_l = 0.1$ ,  $\lambda_1 = 0.234$  and  $\lambda_2 = 0.035$ ) the plot for  $\lambda_1$  is more similar to the  $I_c$  plot.

Then, we used the Kolmogorov-Sinai entropy  $H_{KS}$  of Eq. (5.1.18) as the evolutionary

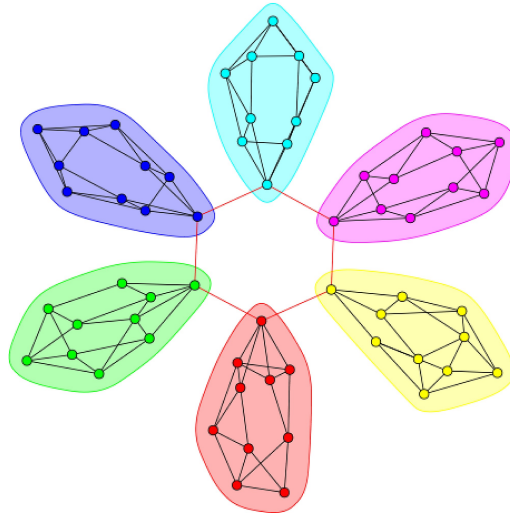


Figure 5.4: A network of 6 clusters composed of 10 neurons each. Neurons in each cluster are connected only by electrical links (black connections) and their connections form small-world networks. The six clusters connect to each other only by chemical links (red connections) [20].

rule for a coupled Hindmarsh-Rose system to evolve a network of 6 clusters of 10 neurons each (see Fig. 5.4). Neurons in each cluster are connected only by electrical links and their connections form a small-world networks as the neural network exhibits a small-world topology. The small-world topology implicates networks that exhibit a densely connected local neighbourhoods to achieve a higher clustering of connections than the random network and exert direct long-range connections to distant regions to achieve a shorter path-length than the regular network, that provide excellent wiring efficiency for information transmission [33, 78]. The six clusters connect to each other only by chemical links, where each link connects two neurons in different clusters.

In the Matlab code, we used two binary adjacency matrices. The first adjacency matrix  $A$  is a block diagonal matrix for the electrical connections in the six clusters. We construct each network in the six clusters using Watts-Strogatz algorithm (rewiring method) so their connections form a small-world networks as the neural network exhibits a small-world topology. The second binary adjacency matrix  $B$  is for the chemical connections among the clusters. The adjacency matrix for the whole network  $C$  is the sum of these two adjacency matrices  $A$  and  $B$ . We start the evolution of the network by computing the Lyapunov exponents ( $\lambda_i$ ) for initial network using the method in subsection 2.2.2 for whole time interval. Then, we compute the values for the upper bound of MIR:  $I_c = \lambda_1 - \lambda_2$  and the Kolmogorov-Sinai entropy using Pesin identity formula:  $H_{KS0} = \sum_{\lambda_i > 0} \lambda_i$

for the initial network.

After that, we add a new chemical link to simulate the creation of new chemical synapses between neurons of different clusters. The idea is that the new chemical link should connect two randomly chosen neurons without any chemical connection between them and should belong to two different clusters. We again run the code and compute the Lyapunov exponents,  $I_c$  and the  $H_{KS1}$  values for the evolved network (i.e. the initial network plus the new chemical link). If the newly added chemical connection leads to an increase of  $H_{KS}$  (i.e.  $H_{KS1} > H_{KS0}$ ), we keep the new connection. If not, it is deleted from the network and another random search for a new one starts. This procedure will be repeated until the maximum number of possible pairs of neurons from different clusters is exhausted.

To compute the maximum number of possible pairs of neurons, we used the following combinations which provide us with all possible combinations of pairs between any two neurons  $i$  and  $j$  in each cluster and in the whole network. These possible combinations of pairs are equal to the maximum number of possible pairs of neurons in the network, since the connections in the network are undirected. As each cluster in the network has 10 neurons, the number of pairs of neurons in each cluster is

$$\binom{10}{2} = \frac{10!}{2!(10-2)!} = 45,$$

and for the whole network with 60 neurons is

$$\binom{60}{2} = \frac{60!}{2!(60-2)!} = 1770.$$

Then,  $1770 - (45 \times 6) = 1500$  represents the maximum number of possible pairs of neurons for chemical connections. The code needs to run 1500 times to exhaust all possibilities of adding new chemical links to connect two randomly chosen neurons with no chemical link between them and belong to two different clusters. At each time, we first add a new chemical link and after the run of the system we compute the values of  $I_c$  and  $H_{KS}$ . We compare the value of  $H_{KS}$  with all previous ones and keep the added link only if it leads to increase in the  $H_{KS}$  entropy. At the end, the sum of the two adjacency matrices for the electrical and chemical connections  $C = A + B$ , which represents the

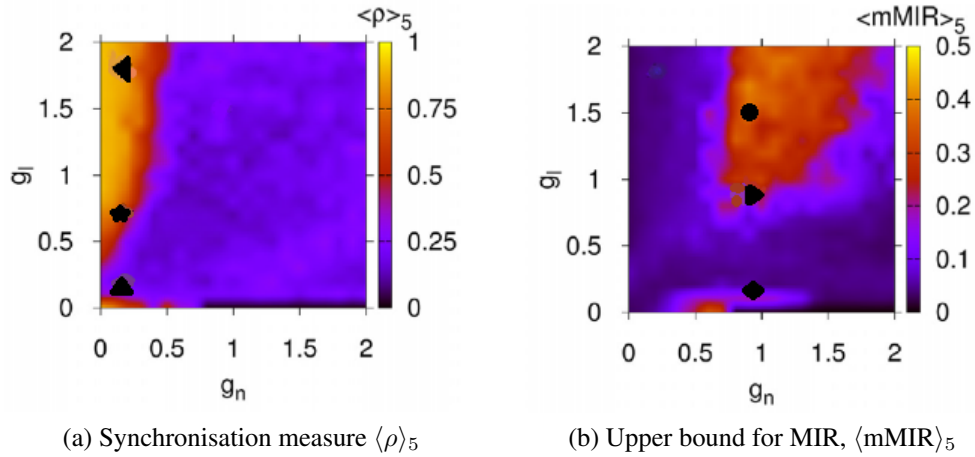


Figure 5.5: (a) Parameter space for the synchronisation measure  $\langle \rho \rangle_5$ . Selected chemical coupling  $g_n$  and electrical couplings  $g_l$ : with low synchronisation measure  $\rho$  and low information flow capacity  $I_c$ ,  $g_n = 0.2$ ,  $g_l = 0.2$  ( $\blacktriangle$ ) and with high  $\rho$  and low  $I_c$ ,  $g_n = 0.2$ ,  $g_l = 0.7$  ( $\star$ ) and  $g_n = 0.2$ ,  $g_l = 1.9$  ( $\blacktriangleleft$ ). (b) Parameter space for the averaged upper bound for MIR,  $\langle \text{mMIR} \rangle_5$ , from the five realisations of a network of 60 neurons with six, equally sized, small-world clusters. Selected  $g_n$  and  $g_l$  values: with low  $\rho$  and low  $I_c$ ,  $g_n = 0.9$ ,  $g_l = 0.2$  ( $\blacklozenge$ ) and with low  $\rho$  and high  $I_c$ ,  $g_n = 0.9$ ,  $g_l = 0.9$  ( $\blacktriangleright$ ) and  $g_n = 0.9$ ,  $g_l = 1.5$  ( $\bullet$ ) [20].

adjacency matrix for the finally evolved network has the highest  $H_{KS}$  value.

The information flow capacity is an important property of the dynamics in brain dynamical networks. The authors in Ref. [20], have used the upper bound  $I_c$  for the amount of information exchanged per unit of time between two nodes in a dynamical network to propose a working hypothesis that the brain networks evolve based on the principle of the maximisation of their information flow capacity  $I_c$ . We will use a similar principle in evolving a network of 6 clusters of 10 neurons each by increasing the Kolmogorov-Sinai  $H_{KS}$  entropy of the network and compare between the combined effect of chemical and electrical coupling with the two concepts, the upper bound  $I_c = \lambda_1 - \lambda_2$  and  $H_{KS} = \sum_{\lambda_i > 0} \lambda_i$ . First, we select 6 characteristic values for the chemical coupling  $g_n$  and electrical coupling  $g_l$  from the two parameter space plots (Fig. 5.5) for the Model for Brain Network Evolution in Ref. [20] which has the same network structure. From the parameter space plot for the average of the global synchronisation of the evolved BDNs for the five realisations [20], the three coupling pairs are:  $g_n = 0.2$ ,  $g_l = 0.2$  ( $\blacktriangle$ ) that corresponds to low  $\rho$  and  $I_c$ ,  $g_n = 0.2$ ,  $g_l = 0.7$  ( $\star$ ) and  $g_n = 0.2$ ,  $g_l = 1.9$  ( $\blacktriangleleft$ ), that correspond to high  $\rho$  and low  $I_c$  (Fig. 5.5a). We select the remaining 3 coupling pairs of  $\langle \text{mMIR} \rangle_5$ :  $g_n = 0.9$ ,  $g_l = 0.2$  ( $\blacklozenge$ ) that corresponds to low  $\rho$  and  $I_c$ ,  $g_n = 0.9$ ,  $g_l = 0.9$

(►) and  $g_n = 0.9, g_l = 1.5$  (●) that correspond to low  $\rho$  and high  $I_c$  (Fig. 5.5b) [20].

Then, we use the values of the 6 coupling pairs in the coupled Hindmarsh-Rose system (5.4.1) to evolve a network of 6 clusters of 10 neurons each. We used the same parameter values and initial conditions as in subsection 4.2.2, the time interval was set  $[0, 10^3]$  and the time-step to 0.01. Each of the 6 realisations of the code run 1500 times to exhaust all possibilities of adding new chemical links following the evolutionary rule described before.

We plot  $H_{KS}$  and  $I_c$  versus the number of added links for each coupling pair (Fig. 5.6) to compare how  $H_{KS}$  and  $I_c$  behave as the networks evolve by using the evolutionary rule. We analyse the behaviours of  $H_{KS}$  and  $I_c$  for the plots of all pairs of  $g_n$  and  $g_l$  values in Fig. 5.5:

At the first row: plots of points with low synchronisation measure  $\rho$  and low information flow capacity  $I_c$ . The plot in Fig. 5.6a, for the coupling pair  $g_n = 0.2, g_l = 0.2$  (▲) from Fig. 5.5a shows that  $H_{KS}$  increases slowly as we evolve the network by increasing  $H_{KS}$ , while  $I_c$  decreases to even smaller values with the adding of new chemical connections. The plot in Fig. 5.6b, for the coupling pair  $g_n = 0.9, g_l = 0.2$  (◆) from Fig. 5.5b shows that  $H_{KS}$  increases slowly and  $I_c$  fluctuates and later remains almost constant.

At the second row: plots of points with high  $\rho$  and low  $I_c$ . The plot in Fig. 5.6c, for the coupling pair  $g_n = 0.2, g_l = 0.7$  (★) from Fig. 5.5a shows that  $H_{KS}$  increases and  $I_c$  increases with some drops for smaller number of added links. The plot in Fig. 5.6d, for the coupling pair  $g_n = 0.2, g_l = 1.9$  (◄) from Fig. 5.5a shows that  $H_{KS}$  increases and that  $I_c$  fluctuates and later decreases.

At the third row: plots of points with low  $\rho$  and high  $I_c$ . The plot in Fig. 5.6e, for the coupling pair  $g_n = 0.9, g_l = 0.9$  (►) from Fig. 5.5b shows that both  $H_{KS}$  and  $I_c$  increase. The plot in Fig. 5.6f for the coupling pair  $g_n = 0.9, g_l = 1.5$  (●) from Fig. 5.5b shows that  $H_{KS}$  and  $I_c$  increase.

Brain networks evolve over time by adding or removing large number of connections in short period of time and that evolution produce either increase or decrease of their entropies. We note here that we evolve the networks by adding new chemical connections which increase their entropy, therefore we expect to see  $H_{KS}$  increasing for all coupling pairs. Different values of coupling strengths result in different values of  $I_c, H_{KS}$  and numbers of added links. The plots for coupling pairs from regions with low  $\rho$  and low

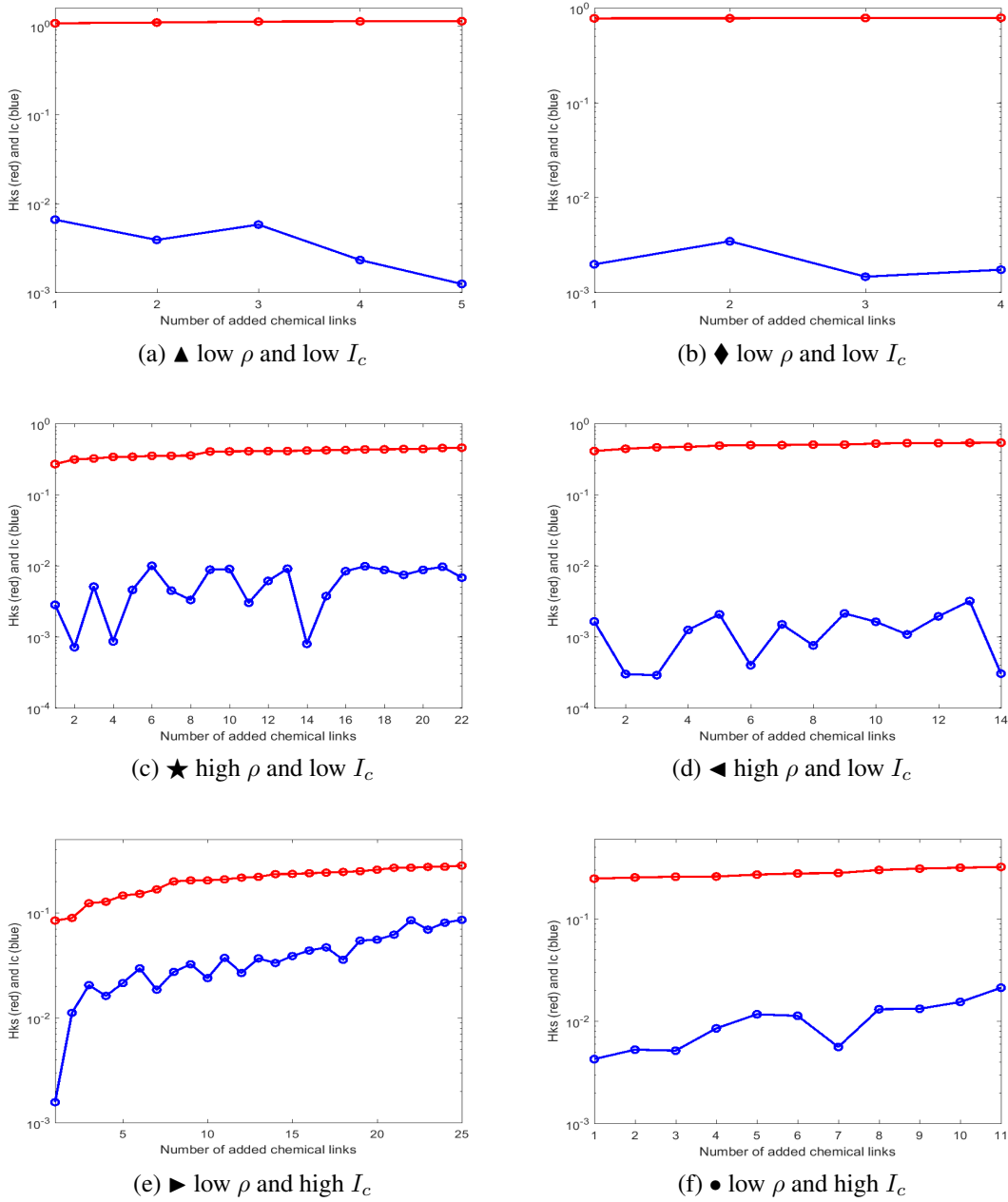


Figure 5.6: The 6 plots of  $H_{KS}$  (red line) and  $I_c$  (blue line) versus the number of added chemical links (red and blue dots) using different coupling pairs (Fig. 5.5) to evolve a network of 6 clusters of 10 neurons each by increasing  $H_{KS}$ . (a)  $g_n = 0.2$ ,  $g_l = 0.2$  ( $\blacktriangle$ ):  $H_{KS}$  increases slowly and  $I_c$  decreases to smaller values with adding new chemical connections. (b)  $g_n = 0.9$ ,  $g_l = 0.2$  ( $\blacklozenge$ ):  $H_{KS}$  increases slowly and  $I_c$  fluctuates and then remains almost constant. (c)  $g_n = 0.2$ ,  $g_l = 0.7$  ( $\star$ ):  $H_{KS}$  increases and  $I_c$  increases with some drops for smaller numbers of added links. (d)  $g_n = 0.2$ ,  $g_l = 1.9$  ( $\blacktriangleleft$ ):  $H_{KS}$  increases,  $I_c$  fluctuates and then decreases. (e)  $g_n = 0.9$ ,  $g_l = 0.9$  ( $\blacktriangleright$ ):  $H_{KS}$  and  $I_c$  increase. (f)  $g_n = 0.9$ ,  $g_l = 1.5$  ( $\bullet$ ):  $H_{KS}$  and  $I_c$  increase.

$I_c$  show the highest initial  $H_{KS}$  but with very slow increase in its values and the smallest number of added links. We also notice that the plots for coupling pairs that are either

from regions with high values of synchronisation measure  $\rho$  and low information flow capacity  $I_c$  or regions with low  $\rho$  and high  $I_c$  have the highest number of added chemical connections. We know adding many links to a network can create a synchronised network. But this small portion of added chemical links (out of 1500 possibilities) will not produce a synchronised network instead it will produce a new evolved one with greater entropy.

We used the adjacency matrices of two evolved networks, one with the lowest number of added links and the other with the highest number of added chemical links to compare between the properties of these evolved networks. The two evolved networks have coupling pairs from Fig. 5.5b of the parameter space for the averaged upper bound for MIR. The first adjacency matrix of the evolved network of the plot in Fig. 5.6b, for the coupling pair  $g_n = 0.9, g_l = 0.2$  (◆) with low  $\rho$  and low  $I_c$ . The second adjacency matrix of the evolved network of the plot in Fig. 5.6e, for the coupling pair  $g_n = 0.9, g_l = 0.9$  (►) with low  $\rho$  and high  $I_c$ . We compute the average node degree, average path-length, global clustering coefficient and global efficiency for both evolved networks using the following rules:

The average node degree of an undirected network of  $N$  nodes is

$$\langle k \rangle = \frac{1}{N} \sum_{i=1}^N k_i.$$

and average path-length is

$$L = \frac{2}{N(N-1)} \sum_{i,j=1, i \neq j}^N d_{i,j},$$

where  $d_{i,j}$  is the distance between node  $i$  and node  $j$ , the global clustering coefficient  $C$  is

$$C = \frac{3 \times \text{number of triangles}}{\text{number of connected triples}}.$$

The global efficiency of a network is  $E_{glob} \sim \frac{1}{L}$ .

First, the properties of the evolved network of Fig. 5.6b which has only 4 added chemical links:

$$\langle k \rangle = 4.3333, L = 4.0989, C = 0.4041 \text{ and } E_{glob} = 0.3209.$$

Second, the properties of the evolved network of Fig. 5.6e which has the highest number of added links 25:

$$\langle k \rangle = 5.0333, L = 3.1278, C = 0.2979 \text{ and } E_{glob} = 0.3825.$$

The increase in average node degree for evolved network of Fig. 5.6e related to the increase in the number of added chemical links and that also results in lower value for the average path-length. These added links connect neurons in two different clusters which can explain why the evolved network has lower  $C$  as the neurons in each cluster can have more connected neighbours. The evolved network has the higher network efficiency 0.3825 as the shorter the average path-length, the more efficient the network.

The evolution of network in Fig. 5.6b started with higher  $H_{KS}$  value but then it increases slowly and  $I_c$  fluctuates and later remains almost constant. While the evolution of network in Fig. 5.6e started with lower  $H_{KS}$  value, then both  $H_{KS}$  and  $I_c$  increase steadily with each added link and produce an evolved network with higher network efficiency.

The relation between  $H_{KS}$ ,  $I_c$  and the number of added chemical connections in evolving the network in the plots is evident even when the values of  $I_c$  fluctuate or decrease. However, they still exhibit a higher increase in  $H_{KS}$  as more chemical connections are added when the pairs of  $g_n$  and  $g_l$  values have high  $I_c$ . Both  $H_{KS}$  and  $I_c$  depend on Lyapunov exponents (LEs). The upper bound  $I_c$  for the amount of information exchanged per unit of time between two nodes in a dynamical network has been used to demonstrate evidence that the brain networks might evolve based on the principle of the maximisation of their information flow capacity [20]. The relation that we have investigated here between  $H_{KS}$  and  $I_c$  shows that the evolution of networks by increasing their entropies can be another approach to evolve BDNs.

Working with the three concepts:  $\rho$ ,  $I_c$  and  $H_{KS}$  and their dependence on coupling strengths  $g_n$  and  $g_l$  needs many runs of the codes with different values of  $g_n$  and  $g_l$  which require more time and much faster cluster. We selected constant values to  $g_n$  and different values to  $g_l$ . We need to run the codes with constant values to  $g_l$  and different values to  $g_n$  and compare the results to see which coupling strength has more effect on the dynamics and the increase in  $H_{KS}$  entropy. We first used the code to evolve a network of 6 clusters of 5 neurons each. After that, we increase the number of neurons in each cluster to 10 for each evolved network. Both runs of the code produce same results but still we need to run the code with much bigger size of networks. Then, we can compare the number of adding links and the increase in  $H_{KS}$  and their relation with the increase in  $I_c$ .

# Chapter 6

## Conclusions and future work

In the thesis, we have studied the dynamics and mathematical modelling of biological neurons. The biological neuron model we chose to work with is the Hindmarsh-Rose neuronal model. We will briefly state the main conclusions of our research and the proposed future work.

### 6.1 Conclusions

We started our work by studying the spike-bursting behaviour of the Hindmarsh-Rose model which is exhibited for specific initial conditions and parameter values. Then, we used linear stability analysis to determine the stability of its equilibrium points. We computed the Lyapunov exponents LEs of the model using two different integration schemes, the Runge-Kutta (RK4) and Euler's forward method. We used in the computation of LEs same parameter values, initial conditions, time interval and time-step to compare the execution time and accuracy for both methods. The code for the Euler's forward method was much faster than the one using the RK4 method for the same time-step yielding similar numerical results.

Since the small-world configuration represents an attractive model for the organisation of brain networks, we coupled the HR system to create an undirected brain dynamical network (BDN) of  $N_n$  neurons connected simultaneously by electrical (linear coupling) and chemical (nonlinear coupling) synapses. First, we used the coupled HR system with the same parameter values and slightly different initial conditions to study the dynamics of elementary examples of three and four neurons and plotted the Lyapunov exponents of both examples. The behaviour of the LEs was not clear in the transient period, however after that, the largest Lyapunov exponent  $\lambda_1$  started to converge to a positive value and

represented the maximal Lyapunov exponent (MLE) for each neuron.

Then, we studied the upper bound  $I_c$  for the mutual information rate (MIR), the synchronisation measure  $\rho$  (order parameter) and the two largest Lyapunov exponents  $\lambda_1$  and  $\lambda_2$  and their dependence on the values of electrical and chemical couplings. We analysed the dynamics of neurons in two elementary examples of 3 neurons through the parameter space plots. The first example connected simultaneously by one undirected chemical and two undirected electrical links and the second by one undirected electrical and two undirected chemical links. We plotted the upper bound  $I_c$ , order parameter  $\rho$  and two largest Lyapunov exponents  $\lambda_1$  and  $\lambda_2$  versus the chemical coupling  $g_n$  and electrical coupling  $g_l$ . To further examine the dynamics of the system, we selected different values for electrical and chemical couplings for both examples and plotted the trajectories for all neurons at each value. The resulting dynamics indicates that the two types of coupling produce different patterns of dynamics. Even for small number of neurons, it has been shown that dynamics depends on the number of neurons and the type of coupling strength between them.

We computed the Kolmogorov-Sinai entropy  $H_{KS}$  for a network of 4 neurons connected simultaneously by two undirected electrical links and two undirected chemical links for a coupled Hindmarsh-Rose system. We obtained different entropies with the use of different values for both the chemical and electrical couplings. If the entropy of the system is positive, the dynamics of the system is chaotic and if it is close to zero, the trajectory of the system converges to one of the fixed points and loses energy. Then, we used the Kolmogorov-Sinai entropy as the evolutionary rule for a coupled Hindmarsh-Rose system to evolve a network of 6 clusters of 10 neurons each. Neurons in each cluster are connected only by electrical links and their connections form a small-world network. The six clusters connect to each other by chemical link only, where each link connects with two neurons in different clusters. We ran six realisations of the code evolving 6 networks of coupled HR system with different pairs of chemical and electrical couplings to compare between the combined effect of chemical and electrical couplings with the two concepts, the information flow capacity  $I_c = \lambda_1 - \lambda_2$  and  $H_{KS}$  in evolving the BDNs and show results that brain networks might evolve based on the principle of the maximisation of their entropies.

## 6.2 Future work

The work in this thesis can be extended in two possible directions. First, one can explore further the potentials of the Hindmarsh-Rose model. Fractional-order dynamics of excitable systems can be described as a memory dependent phenomenon and can produce diverse oscillatory patterns for certain types of neuron models. Many single neuron models are analysed by using fractional-order dynamics such as Hodgkin-Huxley, Fitzhugh-Nagumo and Hindmarsh-Rose models [142]. On the other hand, time delays are common in all biological processes. They affect the generation, transmission and processing of information among different components of a living system [134]. Information time delays between neurons have many sources, such as the limited speed of transmitting action potential through the axon, different types of synapses (chemical, electrical), the release of neurotransmitter and the condition of myelin sheaths [125]. In recent years, the stability analysis of neural models with time delays has received considerable attention [121]. Thus, one can consider studying the dynamics of two models: the *fractional-order Hindmarsh-Rose model* and the *time-delay Hindmarsh-Rose model*.

The second direction will be the study of two interesting single neuron models, namely the *simple model of spiking neurons* and the *adaptive exponential integrate-and-fire model*. Accurate, simple and versatile single neuron models are required for the simulations of large spiking neuron networks [40, 144]. We can use the models to construct different sizes of networks of spiking neurons capable of exhibiting collective dynamics. Then, one can evolve the resulting networks by using Kolmogorov-Sinai entropy  $H_{KS}$  as an evolutionary rule to compare the results with our work on coupled Hindmarsh-Rose system. We will discuss these models briefly next.

- The fractional-order Hindmarsh-Rose model.

Fractional calculus is a generalisation of integer-order calculus. The integer-order dynamical models depend on the immediate previous response. Whereas, the fractional-order derivative depends on all the previous responses, so it has a memory effect [142]. We can obtain the fractional-order Hindmarsh-Rose system by replacing its integer-order derivatives in (3.6.1) by fractional-order Caputo-type derivatives [114]. The Caputo fractional-order derivative of order  $q$  of the continuous function

$f(t)$  is defined by

$$D_t^q f(t) = \frac{1}{\Gamma(n-q)} \int_0^t \frac{f^{(n)}(s)}{(t-s)^{q-n+1}} ds, \quad (6.2.1)$$

where  $n$  is the first integer larger than  $q$  (i.e.  $n-1 \leq q < n$ ) and  $\Gamma(\cdot)$  the gamma function [111, 114]. Using the Caputo definition, the HR neuronal model of fractional-order derivative is as follows

$$\begin{aligned} D^q x &= y - ax^3 + bx^2 - z + I_{ext}, \\ D^q y &= c - dx^2 - y, \\ D^q z &= r[s(x - x_o) - z], \end{aligned} \quad (6.2.2)$$

where  $x(t)$  is the *membrane potential*,  $y(t)$  the *spiking variable* and  $z(t)$  the *bursting variable*.  $a, b, c, d, s, r, x_o$  and  $I_{ext}$  are system parameters.  $I_{ext}$  mimics the membrane input current for biological neurons. The integer-order HR neuronal model refers to the case of order  $q = 1$  [111, 114]. The generalization of this integer-order model can provide a wide range of neuronal responses (regular spiking (RS), fast-spiking (FS), bursting, etc.). The models of dynamical equations using fractional derivatives proved to be more accurate in the mathematical modelling of real-world phenomena [114]. Still, it is not completely understood to what extent the fractional-order dynamics may reproduce the firing properties of excitable systems [142].

- The time-delay Hindmarsh-Rose model.

Time delays are usually overlooked in mathematical models, presumably to reduce their complexity. However, neglecting time delay effects in mathematical models has led to discrepancies between theoretical and experimental findings [134]. In the Hindmarsh-Rose neuron model, a time delay can exist when the slow oscillation of  $z$  drives the fast subsystem  $(x, y)$ . To make the single Hindmarsh-Rose neuron model (3.6.1) more realistic, time delays should be included in the slow oscillation

state of  $z$ , as in the following model [121]:

$$\begin{aligned}\frac{dx}{dt} &= y - ax^3 + bx^2 - z(t - \tau) + I_{ext}, \\ \frac{dy}{dt} &= c - dx^2 - y, \\ \frac{dz}{dt} &= r[s(x - x_o) - z],\end{aligned}\tag{6.2.3}$$

where  $\tau > 0$  represents the time delay. One can analyse the chaotic behaviours of the HR neuron either by increasing or fixing the external current and varying the time delay. The increase in external current causes the excitable HR neuron to exhibit periodic or chaotic bursting/spiking behaviours. Using fixed external current and varying the time delay can also affect the stability of the HR neuron. Furthermore, the effects of time delays along with system parameters can be investigated in a coupled HR system [121, 125].

- The simple model of spiking neurons.

The simple model of spiking neurons is a mathematical model developed by Eugene Izhikevich in 2003 [109]. The model has the biological plausibility of Hodgkin-Huxley-type dynamics combined with the computational efficiency of the integrate-and-fire model [109]. We can simulate only a handful of neurons in real time with the use of Hodgkin-Huxley-type models due to its complexity. Whereas, integrate-and-fire models are computationally effective, but much simpler and incapable of producing rich spiking and bursting dynamics exhibited by many types of neurons [109]. We chose the simple model of spiking neurons model because it is relatively simple and can fire spiking patterns that resemble those of biological neurons. Also, we can use the model to simulate large-size networks of spiking neurons [143]. In addition, the mathematical model computation can be done in Matlab as we did with the Hindmarsh-Rose model.

The model consists of two coupled nonlinear first order ordinary differential equa-

tions [109, 143], given by

$$\begin{aligned}\dot{V} &= 0.04V^2 + 5V + 140 - U + I, \\ \dot{U} &= a(bV - U),\end{aligned}$$

If  $V \geq 30$  mV, then (6.2.4)

$$\begin{aligned}V &= c, \\ U &= U + d,\end{aligned}$$

where  $V$  represents the membrane potential of the neuron and  $U$  the recovery variable. The injected currents are delivered through the variable  $I$ . The parameter  $a$  gives the decay rate of the spike, smaller  $a$  values result in slower recovery. The parameter  $b$  gives the sensitivity of the spike.  $c$  represents the after-spike reset value of the membrane potential  $V$  and  $d$  the after-spike reset of the recovery variable  $U$ . Different values of the parameters result in various intrinsic firing patterns [109, 143]. For a single neuron, different choices of functions are more preferable such as the function  $(0.04v^2 + 4.1v + 108)$  with  $b = -0.1$  being a better choice for regular spiking neurons.

- The adaptive exponential integrate-and-fire model.

An exponential model combined with an adaptation variable is called the adaptive exponential integrate-and-fire (AdEx) model which was developed by Brette and Gerstner in 2005 [24]. AdEx is a simple model described by only two differential equations and a reset condition [93, 144]:

$$\begin{aligned}C \frac{dV}{dt} &= -g_L(V - E_L) + g_L \Delta_T \exp\left(\frac{V - V_T}{\Delta_T}\right) + I - w, \\ \tau_w \frac{dw}{dt} &= a(V - E_L) - w,\end{aligned}$$

(6.2.5)

If  $V > 0$  mV, then

$$\begin{aligned}V &\rightarrow V_r, \\ w &\rightarrow w_r = w + b,\end{aligned}$$

where  $V$  is the membrane potential,  $w$  the adaptation current and  $I$  the injected current. The model has nine parameters required to define the evolution of the membrane potential  $V$  and the adaptation current  $w$  [144].  $C$  is the membrane ca-

capacitance,  $g_L$  the leak capacitance,  $E_L$  the leak reversal potential,  $\Delta_L$  the threshold slope factor,  $V_T$  the effective threshold potential. The rest of the parameters are bifurcation parameters,  $a$  the adaptation coupling parameter,  $\tau_w$  the adaptation time constant,  $b$  the spike triggered adaptation and  $V_r$  the reset potential. The AdEx model is capable of producing multiple firing patterns corresponding to different parameter values [144].

Another interesting approach in studying brain dynamical networks is the study of the entropy-based metrics in functional magnetic resonance imaging (fMRI) and electroencephalogram (EEG) (section 5.2). The relations between EEG time series and the functioning of the vast number of neurons within the human brain was first analysed by Norbert Wiener in 1948 [199]. Since entropy is a measure of irregularity or randomness in a signal, EEG recordings can be used for quantifying, in a statistical sense, the amount of uncertainty or randomness in the signal, which is also roughly equivalent to the amount of information contained in it [56]. In recent years, the concept of entropy-derived measures has been widely used in studying brain complexity and analysing physiological signals in biological systems. Numerous entropy algorithms have been developed to quantify different aspects of the complexity of physiological signals such as *sample entropy* (SampEn), *Shannon permutation entropy* (SPE), *distribution entropy* (DistEn) and *approximate entropy* (ApEn) which are based on the estimation of the Kolmogorov-Sinai entropy from a time series [56, 140].

# References

- [1] Action potential. <https://www.moleculardevices.com/applications/patch-clamp-electrophysiology/>. Accessed: 2019-03-15. 69
- [2] Brain hemispheres. <https://brainmadesimple.com/left-and-right-hemispheres>, . Accessed: 2019-03-20. 71
- [3] Types of branching. <https://www.nicks.com.au/vintage-school/vintage-school-1-1-76.1347>, . Accessed: 2019-03-10. 67
- [4] Classification of neurons. <https://qbi.uq.edu.au/brain/brain-anatomy/types-neurons>. Accessed: 2019-03-11. 68
- [5] Heat engine. [https://www.wikiwand.com/en/History\\_of\\_entropy](https://www.wikiwand.com/en/History_of_entropy). Accessed: 2019-07-10. 109
- [6] Brain lobes. <https://courses.lumenlearning.com/waymaker-psychology/chapter/reading-parts-of-the-brain>. Accessed: 2019-03-20. 71
- [7] Neuron. <https://training.seer.cancer.gov/anatomy/nervous/tissue.html>, . Accessed: 2019-03-10. 67
- [8] Neurotransmitters. <https://opentextbc.ca/anatomyandphysiology/chapter/12-4-the-action-potential>, . Accessed: 2019-03-15. 69
- [9] Undamped pendulum. <https://iopscience.iop.org/article/10.1088/1361-6404/aa8961>. Accessed: 2018-11-10. 12
- [10] Period doubling bifurcation. [https://courses.maths.ox.ac.uk/node/view\\_material/35614](https://courses.maths.ox.ac.uk/node/view_material/35614). Accessed: 2018-11-20. 22

- [11] Phase space. [https://commons.wikimedia.org/wiki/File:Pendulum\\_phase\\_portrait.svg](https://commons.wikimedia.org/wiki/File:Pendulum_phase_portrait.svg). Accessed: 2018-11-10. 13
- [12] Increase in randomness. <http://jasss.soc.surrey.ac.uk/12/2/3.html.bak>. Accessed: 2018-12-20. 52
- [13] Neuron distinct shapes. <https://www.sciencedirect.com/topics/medicine-and-dentistry/pyramidal-cell>. Accessed: 2019-03-11. 68
- [14] Synapse. <https://www.biologyonline.com/dictionary/axon-terminal>. Accessed: 2019-03-11. 68
- [15] R. Albert and A.-L. Barabási. Statistical mechanics of complex networks. *Reviews of modern physics*, 74(1):47, 2002. 59
- [16] K. T. Alligood, T. D. Sauer, and J. A. Yorke. *Chaos*. Springer, 1996. 27, 28, 32, 34
- [17] K. Anand and G. Bianconi. Entropy measures for networks: Toward an information theory of complex topologies. *Physical Review E*, 80(4):045102, 2009. 120
- [18] V. Angelo, C. Fabio, and C. Massimo. *Chaos: From Simple Models To Complex Systems*, volume 17. World Scientific, 2009. 12, 13, 15, 17, 22, 23, 26, 27, 30, 33, 114, 116, 117
- [19] C. G. Antonopoulos. Dynamic range in the *C. elegans* brain network. *Chaos: An Interdisciplinary Journal of Nonlinear Science*, 26(1):013102, 2016. 74
- [20] C. G. Antonopoulos, S. Srivastava, S. E. d. S. Pinto, and M. S. Baptista. Do brain networks evolve by maximizing their information flow capacity? *PLOS computational biology*, 11(8):e1004372, 2015. 7, 64, 78, 82, 83, 91, 94, 97, 99, 121, 122, 124, 126, 127, 130
- [21] C. G. Antonopoulos, A. S. Fokas, and T. C. Bountis. Dynamical complexity in the *C. elegans* neural network. *The European Physical Journal Special Topics*, 225(6-7):1255–1269, 2016. 78, 91
- [22] C. G. Antonopoulos, E. Bianco-Martinez, and M. S. Baptista. Evaluating performance of neural codes in model neural communication networks. *Neural Networks*, 109:90–102, 2019. 73

- [23] F. A. Azevedo, L. R. Carvalho, L. T. Grinberg, J. M. Farfel, R. E. Ferretti, R. E. Leite, W. J. Filho, R. Lent, and S. Herculano-Houzel. Equal numbers of neuronal and nonneuronal cells make the human brain an isometrically scaled-up primate brain. *Journal of Comparative Neurology*, 513(5):532–541, 2009. [70](#), [120](#)
- [24] L. Badel, S. Lefort, R. Brette, C. C. Petersen, W. Gerstner, and M. J. Richardson. Dynamic iv curves are reliable predictors of naturalistic pyramidal-neuron voltage traces. *Journal of Neurophysiology*, 99(2):656–666, 2008. [136](#)
- [25] J. Banks, V. Dragan, and A. Jones. *Chaos: a mathematical introduction*. Number 18. Cambridge University Press, 2003. [26](#)
- [26] B. Bao, A. Hu, H. Bao, Q. Xu, M. Chen, and H. Wu. Three-dimensional memristive Hindmarsh–Rose neuron model with hidden coexisting asymmetric behaviors. *Complexity*, 2018, 2018. [88](#)
- [27] M. S. Baptista, R. M. Rubinger, E. R. Viana, J. C. Sartorelli, U. Parlitz, and C. Gregori. Mutual information rate and bounds for it. *PLoS One*, 7(10):e46745, 2012. [7](#), [98](#), [99](#), [121](#)
- [28] Y. Bar-Yam. General features of complex systems. *Encyclopedia of Life Support Systems (EOLSS)*, UNESCO, EOLSS Publishers, Oxford, UK, page 1, 2002. [41](#)
- [29] A.-L. Barabási and R. Albert. Emergence of scaling in random networks. *science*, 286(5439):509–512, 1999. [58](#)
- [30] A.-L. Barabási et al. *Network science*. Cambridge university press, 2016. [40](#), [45](#), [46](#), [47](#), [49](#), [50](#), [55](#), [56](#), [58](#), [59](#), [60](#)
- [31] C. F. Barenghi. *Chaos: theoretical and numerical methods*. 2008. [17](#)
- [32] V. J. Barranca, D. C. Johnson, J. L. Moyher, J. P. Sauppe, M. S. Shkarayev, G. Kovačič, and D. Cai. Dynamics of the exponential integrate-and-fire model with slow currents and adaptation. *Journal of computational neuroscience*, 37(1):161–180, 2014. [76](#)
- [33] D. S. Bassett and E. Bullmore. Small-world brain networks. *The neuroscientist*, 12(6):512–523, 2006. [64](#), [73](#), [74](#), [121](#), [124](#)

- [34] E. A. Bender and E. R. Canfield. The asymptotic number of labeled graphs with given degree sequences. *Journal of Combinatorial Theory, Series A*, 24(3):296–307, 1978. [56](#)
- [35] E. Bianco-Martinez, N. Rubido, C. G. Antonopoulos, and M. Baptista. Successful network inference from time-series data using Mutual Information Rate. *Chaos: An Interdisciplinary Journal of Nonlinear Science*, 26(4):043102, 2016. [82](#), [93](#), [98](#)
- [36] R. C. Bishop. Chaotic dynamics, indeterminacy and free will. 1999. [26](#)
- [37] E. Bodenschatz. Complex systems. *Max Planck Gesellschaft*, pages 3–6, 2009. [40](#), [41](#)
- [38] P. Bogacki and L. F. Shampine. A 3 (2) pair of Runge-Kutta formulas. *Applied Mathematics Letters*, 2(4):321–325, 1989. [39](#)
- [39] L. Boltzmann. *Lectures on gas theory*. Courier Corporation, 2012. [13](#), [108](#), [112](#)
- [40] F. Borges, P. Protachevicz, R. Pena, E. Lameu, G. Higa, A. Kihara, F. Matias, C. Antonopoulos, R. de Pasquale, A. Roque, et al. Self-sustained activity of low firing rate in balanced networks. *Physica A: Statistical Mechanics and its Applications*, 537:122671, 2020. [133](#)
- [41] R. R. Borges, F. S. Borges, E. L. Lameu, A. M. Batista, K. C. Iarosz, I. L. Caldas, C. G. Antonopoulos, and M. S. Baptista. Spike timing-dependent plasticity induces non-trivial topology in the brain. *Neural Networks*, 88:58–64, 2017. [72](#), [96](#)
- [42] A. Bose. Bifurcations dynamics of single neurons and small networks. *Encyclopedia of Computational Neuroscience*, pages 371–380, 2015. [87](#)
- [43] M. Breakspear and J. Terry. Nonlinear interdependence in neural systems: motivation, theory, and relevance. *International Journal of Neuroscience*, 112(10):1263–1284, 2002. [96](#)
- [44] R. Brette and W. Gerstner. Adaptive exponential integrate-and-fire model as an effective description of neuronal activity. *Journal of neurophysiology*, 94(5):3637–3642, 2005. [76](#)

- [45] A. Buehlmann and G. Deco. Optimal information transfer in the cortex through synchronization. *PLoS computational biology*, 6(9):e1000934, 2010. [96](#)
- [46] A. N. Burkitt. A review of the integrate-and-fire neuron model: I. homogeneous synaptic input. *Biological cybernetics*, 95(1):1–19, 2006. [76](#), [77](#)
- [47] J. C. Butcher. *Numerical methods for ordinary differential equations*. John Wiley & Sons, 2016. [38](#)
- [48] S. Camazine, J.-L. Deneubourg, N. R. Franks, J. Sneyd, E. Bonabeau, and G. Theraula. *Self-organization in biological systems*, volume 7. Princeton University Press, 2003. [43](#), [44](#)
- [49] R. L. Carhart-Harris, R. Leech, P. J. Hellyer, M. Shanahan, A. Feilding, E. Tagliazucchi, D. R. Chialvo, and D. Nutt. The entropic brain: a theory of conscious states informed by neuroimaging research with psychedelic drugs. *Frontiers in human neuroscience*, 8:20, 2014. [118](#)
- [50] S. Carnot. Reflections on the motive power of fire, and on machines fitted to develop that power. *Paris: Bachelier*, 1824. [108](#)
- [51] J. R. Cash and A. H. Karp. A variable order Runge-Kutta method for initial value problems with rapidly varying right-hand sides. *ACM Transactions on Mathematical Software (TOMS)*, 16(3):201–222, 1990. [39](#)
- [52] D. Chang, D. Song, J. Zhang, Y. Shang, Q. Ge, and Z. Wang. Caffeine caused a widespread increase of resting brain entropy. *Scientific reports*, 8(1):2700, 2018. [118](#), [119](#)
- [53] P. Checco, M. Righero, M. Biey, and L. Kocarev. Synchronization in networks of Hindmarsh–Rose neurons. *IEEE Transactions on Circuits and Systems II: Express Briefs*, 55(12):1274–1278, 2008. [90](#), [96](#)
- [54] G. Chen, J. L. Moiola, and H. O. Wang. Bifurcation control: theories, methods, and applications. *International Journal of Bifurcation and Chaos*, 10(03):511–548, 2000. [17](#), [23](#)

- [55] G. Chen, X. Wang, and X. Li. *Fundamentals of complex networks: models, structures and dynamics*. John Wiley & Sons, 2014. [14](#), [15](#), [17](#), [44](#), [48](#), [52](#), [53](#), [56](#), [58](#), [59](#), [60](#), [62](#), [63](#), [97](#)
- [56] C. Chen-Chih, J.-H. Kang, and C.-J. Hu. Measuring entropy in functional neuroscience: pathophysiological and clinical applications. *Neuroscience and Neuroeconomics*, 5:45, 2016. [119](#), [120](#), [137](#)
- [57] A. Clauset. 1 models of network structure. [57](#)
- [58] R. Clausius. I. on the moving force of heat, and the laws regarding the nature of heat itself which are deducible therefrom. *The London, Edinburgh, and Dublin Philosophical Magazine and Journal of Science*, 2(8):1–21, 1851. [108](#)
- [59] R. Clausius. Xiii. on the application of the theorem of the equivalence of transformations to the internal work of a mass of matter. *The London, Edinburgh, and Dublin Philosophical Magazine and Journal of Science*, 24(159):81–97, 1862. [109](#)
- [60] R. Clausius. *The mechanical theory of heat: with its applications to the steam-engine and to the physical properties of bodies*. J. van Voorst, 1867. [109](#)
- [61] L. K. Comfort. Self-organization in complex systems. *Journal of Public Administration Research and Theory: J-PART*, 4(3):393–410, 1994. [42](#), [43](#)
- [62] N. Corson and M. Aziz-Alaoui. Dynamics and complexity of Hindmarsh-Rose neuronal systems. *Encyclopedia of Mathematical Physics: Elsevier*, 5:213–226, 2006. [96](#)
- [63] N. Corson and M. Aziz-Alaoui. Asymptotic dynamics of Hindmarsh-Rose neuronal system. *Dynamics of Continuous, Discrete and Impulsive Systemes, Series B: Applications and Algorithms*, (16):p–535, 2009. [70](#), [87](#)
- [64] P. Cvitanovic, R. Artuso, R. Mainieri, G. Tanner, G. Vattay, N. Whelan, and A. Wirzba. Chaos: classical and quantum. *ChaosBook.org (Niels Bohr Institute, Copenhagen 2005)*, 69, 2005. [25](#), [26](#)
- [65] T. Downarowicz. *Entropy in dynamical systems*, volume 18. Cambridge University Press, 2011. [108](#), [111](#), [113](#)

- [66] H. Dulac. Solutions d'un système d'équations différentielles dans le voisinage de valeurs singulières. *Bulletin de la Société mathématique de France*, 40:324–383, 1912. [18](#)
- [67] G. T. Einevoll, A. Destexhe, M. Diesmann, S. Grün, V. Jirsa, M. de Kamps, M. Migliore, T. V. Ness, H. E. Plesser, and F. Schürmann. The scientific case for brain simulations. *Neuron*, 102(4):735–744, 2019. [3](#)
- [68] P. Erdos and A. Rényi. On the evolution of random graphs. *Publ. Math. Inst. Hung. Acad. Sci.*, 5(1):17–60, 1960. [52](#)
- [69] R. G. Erra, D. M. Mateos, R. Wennberg, and J. Velazquez. Towards a statistical mechanics of consciousness: Maximization of number of connections is associated with conscious awareness. *arXiv preprint arXiv:1606.00821*, 2016. [119](#)
- [70] E. Estrada, P. A. Knight, and P. Knight. *A first course in network theory*. Oxford University Press, USA, 2015. [46](#), [47](#), [49](#), [51](#), [52](#)
- [71] L. Euler. *Institutionum calculi integralis*. 1768. [36](#)
- [72] E. Fehlberg. Low-order classical Runge-Kutta formulas with stepsize control and their application to some heat transfer problems. 1969. [39](#)
- [73] Y. Feng and W. Li. Analysis on the synchronized network of Hindmarsh-Rose neuronal models. In *Journal of Physics: Conference Series*, volume 604, page 012006. IOP Publishing, 2015. [96](#)
- [74] S. E. Fienberg. Stochastic models for single neuron firing trains—a survey. *Advances in Applied Probability*, 7(2):259–260, 1975. [66](#)
- [75] R. FitzHugh. Impulses and physiological states in theoretical models of nerve membrane. *Biophysical journal*, 1(6):445–466, 1961. [77](#)
- [76] F. Flores Camacho, N. Ulloa Lugo, and H. Covarrubias Martínez. The concept of entropy, from its origins to teachers. *Revista mexicana de física E*, 61(2):69–80, 2015. [109](#), [110](#)

- [77] R. Frigg. In what sense is the Kolmogorov-Sinai entropy a measure for chaotic behaviour?-bridging the gap between dynamical systems theory and communication theory. *The British journal for the philosophy of science*, 55(3):411–434, 2004. [116](#)
- [78] W. Gao, J. H. Gilmore, K. S. Giovanello, J. K. Smith, D. Shen, H. Zhu, and W. Lin. Temporal and spatial evolution of brain network topology during the first two years of life. *PLoS one*, 6(9):e25278, 2011. [120](#), [121](#), [124](#)
- [79] P. Gaspard. Rössler systems. *Encyclopedia of nonlinear science*, 231:808–811, 2005. [29](#)
- [80] A. Geminiani, C. Casellato, F. Locatelli, F. Prestori, A. Pedrocchi, and E. D’Angelo. Complex dynamics in simplified neuronal models: reproducing Golgi cell electroresponsiveness. *Frontiers in neuroinformatics*, 12:88, 2018. [3](#)
- [81] W. Gerstner. Hebbian learning and plasticity. *From neuron to cognition via computational neuroscience*, pages 0–25, 2011. [72](#)
- [82] W. Gerstner and W. M. Kistler. *Spiking neuron models: Single neurons, populations, plasticity*. Cambridge university press, 2002. [69](#)
- [83] J. W. Gibbs. *Elementary principles in statistical mechanics*. Courier Corporation, 2014. [14](#)
- [84] E. N. Gilbert. Random graphs. *The Annals of Mathematical Statistics*, 30(4):1141–1144, 1959. [53](#)
- [85] R. M. Gray. *Entropy and information theory*. Springer Science & Business Media, 2011. [114](#)
- [86] W. Gibbs. A methods of geometrical representation of the thermodynamic properties of substances by means of surfaces. *On the equilibrium of heterogeneous substabces*, pages 34–85, 1873. [111](#)
- [87] C. Gros. *Complex and adaptive dynamical systems: A primer* 2010. [24](#)

- [88] K. Guan. Important notes on Lyapunov exponents. *arXiv preprint arXiv:1401.3315*, 2014. [26](#), [27](#)
- [89] D. O. Hebb. *The organization of behavior: a neuropsychological theory*. Science Editions, 1962. [72](#)
- [90] D. Heeger. Poisson model of spike generation. *Handout, University of Stanford*, 5:1–13, 2000. [76](#)
- [91] T. Heinbockel. Introductory chapter: Mechanisms and function of synaptic plasticity. *Synaptic Plasticity*, page 1, 2017. [72](#)
- [92] M. Hénon. A two-dimensional mapping with a strange attractor. In *The Theory of Chaotic Attractors*, pages 94–102. Springer, 1976. [30](#)
- [93] L. Hertäg, J. Hass, T. Golovko, and D. Durstewitz. An approximation to the adaptive exponential integrate-and-fire neuron model allows fast and predictive fitting to physiological data. *Frontiers in computational neuroscience*, 6:62, 2012. [136](#)
- [94] A. V. Herz, T. Gollisch, C. K. Machens, and D. Jaeger. Modeling single-neuron dynamics and computations: a balance of detail and abstraction. *science*, 314(5796):80–85, 2006. [75](#), [76](#)
- [95] F. Heylighen. Complexity and self-organization. *Encyclopedia of library and information sciences*, 3:1215–1224, 2008. [40](#)
- [96] W. D. Hillis. Why physicists like models and why biologists should. *Current Biology*, 3(2):79–81, 1993. [2](#)
- [97] J. Hindmarsh and P. Cornelius. The development of the Hindmarsh-Rose model for bursting. In *Bursting: the genesis of rhythm in the nervous system*, pages 3–18. World Scientific, 2005. [78](#), [79](#), [80](#)
- [98] J. L. Hindmarsh and R. Rose. A model of neuronal bursting using three coupled first order differential equations. *Proc. R. Soc. Lond. B*, 221(1222):87–102, 1984. [78](#), [79](#), [80](#), [81](#), [82](#)

- [99] M. W. Hirsch, S. Smale, and R. L. Devaney. *Differential equations, dynamical systems, and an introduction to chaos*. Academic press, 2012. [10](#), [14](#), [17](#), [31](#), [33](#)
- [100] J. Hizanidis, N. E. Kouvaris, and C. G. Antonopoulos. Metastable and chimera-like states in the C. elegans brain network. *Cybernetics and Physics*, 4(1):17–20, 2015. [91](#), [93](#), [97](#)
- [101] A. L. Hodgkin and A. F. Huxley. A quantitative description of membrane current and its application to conduction and excitation in nerve. *The Journal of physiology*, 117(4):500–544, 1952. [77](#)
- [102] P. Holman. *Engaging emergence: Turning upheaval into opportunity*. Berrett-Koehler Publishers, 2010. [41](#), [42](#)
- [103] K.-S. Hong et al. Adaptive synchronization of two coupled chaotic Hindmarsh–Rose neurons by controlling the membrane potential of a slave neuron. *Applied Mathematical Modelling*, 37(4):2460–2468, 2013. [96](#)
- [104] S. G. Hormuzdi, M. A. Filippov, G. Mitropoulou, H. Monyer, and R. Bruzzone. Electrical synapses: a dynamic signaling system that shapes the activity of neuronal networks. *Biochimica et Biophysica Acta (BBA)-Biomembranes*, 1662(1-2):113–137, 2004. [90](#)
- [105] A. S. Householder. Unitary triangularization of a nonsymmetric matrix. *Journal of the ACM (JACM)*, 5(4):339–342, 1958. [29](#)
- [106] J. K. Hunter. Introduction to dynamical systems. *UCDavis Mathematics MAT A*, 207:2011, 2011. [12](#), [19](#), [20](#), [21](#)
- [107] M. Ignaccolo, M. Latka, W. Jernajczyk, P. Grigolini, and B. J. West. The dynamics of EEG entropy. *Journal of biological physics*, 36(2):185–196, 2010. [119](#)
- [108] G. Innocenti and R. Genesio. On the dynamics of chaotic spiking-bursting transition in the Hindmarsh–Rose neuron. *Chaos: An Interdisciplinary Journal of Nonlinear Science*, 19(2):023124, 2009. [78](#), [80](#)
- [109] E. M. Izhikevich. Simple model of spiking neurons. *IEEE Transactions on neural networks*, 14(6):1569–1572, 2003. [135](#), [136](#)

- [110] Q. Jia and Z. Chen. Complex data analysis of the Hindmarsh-Rose model at specific parameters. In *Intelligent Control and Automation (WCICA), 2010 8th World Congress on*, pages 1963–1967. IEEE, 2010. [3](#), [78](#)
- [111] D. Jun, Z. Guang-jun, X. Yong, Y. Hong, and W. Jue. Dynamic behavior analysis of fractional-order Hindmarsh–Rose neuronal model. *Cognitive neurodynamics*, 8(2):167–175, 2014. [88](#), [134](#)
- [112] H. Kantz and T. Schreiber. *Nonlinear time series analysis*, volume 7. Cambridge university press, 2004. [117](#)
- [113] C. Ç. Karaaslanlı. Bifurcation analysis and its applications. In *Numerical simulation-from theory to industry*. InTech, 2012. [20](#), [23](#), [24](#)
- [114] E. Kaslik. Analysis of two-and three-dimensional fractional-order Hindmarsh-Rose type neuronal models. *Fractional Calculus and Applied Analysis*, 20(3):623–645, 2017. [81](#), [82](#), [133](#), [134](#)
- [115] A. Kaw. Runge-Kutta 4th order method for ordinary differential equations. *Ordinary Differential Equations*, pages 08–04, 2009. [38](#)
- [116] B. Kolb, R. Gibb, and T. E. Robinson. Brain plasticity and behavior. *Current directions in psychological science*, 12(1):1–5, 2003. [72](#), [73](#)
- [117] A. N. Kolmogorov. A new metric invariant of transient dynamical systems and automorphisms in lebesgue spaces. In *Doklady Akademii Nauk*, volume 119, pages 861–864. Russian Academy of Sciences, 1958. [108](#)
- [118] A. N. Kolmogorov. Entropy per unit time as a metric invariant of automorphisms. In *Dokl. Akad. Nauk SSSR*, volume 124, pages 754–755, 1959. [108](#)
- [119] G. Kovacic. Models of neuronal dynamics. [75](#), [77](#)
- [120] Y. Kuramoto and D. Battogtokh. Coexistence of coherence and incoherence in nonlocally coupled phase oscillators. *arXiv preprint cond-mat/0210694*, 2002. [97](#)

- [121] S. Lakshmanan, C. P. Lim, S. Nahavandi, M. Prakash, and P. Balasubramaniam. Dynamical analysis of the Hindmarsh-Rose neuron with time delays. *IEEE transactions on neural networks and learning systems*, 28(8):1953–1958, 2016. [133](#), [135](#)
- [122] S. Lakshmanan, C. P. Lim, S. Nahavandi, M. Prakash, and P. Balasubramaniam. Dynamical analysis of the Hindmarsh–Rose neuron with time delays. *IEEE transactions on neural networks and learning systems*, 28(8):1953–1958, 2017. [88](#)
- [123] F. L. Lambert. Disorder—a cracked crutch for supporting entropy discussions. *Journal of Chemical Education*, 79(2):187, 2002. [108](#)
- [124] N. Le Novère. *Computational systems neurobiology*. Springer Science & Business Media, 2012. [76](#)
- [125] M. Łeppek and P. Fronczak. Spatial evolution of Hindmarsh-Rose neural network with time delays. *Nonlinear Dynamics*, 92(2):751–761, 2018. [133](#), [135](#)
- [126] Z. Liang, Y. Wang, X. Sun, D. Li, L. J. Voss, J. W. Sleight, S. Hagihira, and X. Li. EEG entropy measures in anesthesia. *Frontiers in computational neuroscience*, 9:16, 2015. [120](#)
- [127] X. Liao, A. V. Vasilakos, and Y. He. Small-world human brain networks: perspectives and challenges. *Neuroscience & Biobehavioral Reviews*, 77:286–300, 2017. [70](#), [120](#)
- [128] K. Lindsay, J. Ogden, D. Halliday, and J. Rosenberg. An introduction to the principles of neuronal modelling. In *Modern techniques in neuroscience research*, pages 213–306. Springer, 1999. [2](#), [75](#)
- [129] E. N. Lorenz. Deterministic nonperiodic flow. *Journal of the atmospheric sciences*, 20(2):130–141, 1963. [26](#)
- [130] E. N. Lorenz. Atmospheric predictability as revealed by naturally occurring analogues. *Journal of the Atmospheric sciences*, 26(4):636–646, 1969. [30](#)
- [131] E. N. Lorenz. Three approaches to atmospheric predictability. *Bull. Amer. Meteor. Soc*, 50(3454):349, 1969. [30](#)

- [132] S. Lowel and W. Singer. Selection of intrinsic horizontal connections in the visual cortex by correlated neuronal activity. *Science*, 255(5041):209–212, 1992. [72](#)
- [133] J. Maaita, C. K. Volos, I. Kyprianidis, and I. Stouboulos. The dynamics of a cubic nonlinear system with no equilibrium point. *Journal of Nonlinear Dynamics*, 2015, 2015. [14](#)
- [134] M. Madadi Asl, A. Valizadeh, and P. A. Tass. Dendritic and axonal propagation delays may shape neuronal networks with plastic synapses. *Frontiers in physiology*, 9:1849, 2018. [133](#), [134](#)
- [135] P. Mateos-Aparicio and A. Rodríguez-Moreno. The impact of the study of brain plasticity. *Frontiers in Cellular Neuroscience*, 13:66, 2019. [72](#)
- [136] L. D. McCarthy. Chaos theory: Towards an alternative perspective of african american leadership, organization, and community systems. *Journal of Alternative Perspectives in the Social Sciences*, 6(2):122–155, 2014. [25](#)
- [137] L. S. McCue and A. W. Troesch. Use of Lyapunov exponents to predict chaotic vessel motions. In *Contemporary Ideas on Ship Stability and Capsizing in Waves*, pages 415–432. Springer, 2011. [27](#)
- [138] A. Medio and M. Lines. *Nonlinear dynamics: A primer*. Cambridge University Press, 2001. [114](#), [115](#), [116](#)
- [139] G. Meisters. Lebesgue measure on the real line. *University of Nebraska, Lincoln*, 1997. [118](#)
- [140] S. S. Menon and K. Krishnamurthy. A study of brain neuronal and functional complexities estimated using multiscale entropy in healthy young adults. *Entropy*, 21(10):995, 2019. [137](#)
- [141] E. E. Michaelides. Entropy, order and disorder. *Open Thermodynamics Journal*, 2(1):7–11, 2008. [108](#)
- [142] A. Mondal, S. K. Sharma, R. K. Upadhyay, and A. Mondal. Firing activities of a fractional-order Fitzhugh-Rinzel bursting neuron model and its coupled dynamics. *Scientific reports*, 9(1):1–11, 2019. [133](#), [134](#)

- [143] S. Murali, J. Kumar, J. Kumar, and R. Bhakthavatchalu. Design and implementation of Izhikevich spiking neuron model on FPGA. In *2016 IEEE International Conference on Recent Trends in Electronics, Information & Communication Technology (RTEICT)*, pages 946–951. IEEE, 2016. [135](#), [136](#)
- [144] R. Naud, N. Marcille, C. Clopath, and W. Gerstner. Firing patterns in the adaptive exponential integrate-and-fire model. *Biological cybernetics*, 99(4-5):335, 2008. [133](#), [136](#), [137](#)
- [145] D. L. Nelson, A. L. Lehninger, and M. M. Cox. *Lehninger principles of biochemistry*. Macmillan, 2008. [112](#)
- [146] M. E. Nelson. Electrophysiological models. *Databasing the brain: from data to knowledge*, pages 285–301, 2004. [77](#)
- [147] M. Newman. *Networks*. Oxford university press, 2018. [2](#), [44](#), [45](#), [48](#), [50](#), [52](#), [53](#), [56](#), [57](#), [58](#), [60](#), [68](#), [75](#)
- [148] E. M. Ngouonkadi, H. Fotsin, P. L. Fotso, V. K. Tamba, and H. A. Cerdeira. Bifurcations and multistability in the extended Hindmarsh–Rose neuronal oscillator. *Chaos, Solitons & Fractals*, 85:151–163, 2016. [80](#), [88](#)
- [149] R. W. Nickalls. A new approach to solving the cubic: Cardan’s solution revealed. *The Mathematical Gazette*, 77(480):354–359, 1993. [82](#)
- [150] D. D. Nolte. The tangled tale of phase space. *Physics today*, 63(4):33–38, 2010. [14](#)
- [151] D. D. Nolte. *Introduction to modern dynamics: Chaos, networks, space and time*. Oxford University Press, USA, 2015. [45](#), [46](#)
- [152] N. Nossenson and H. Messer. Modeling neuron firing pattern using a two state markov chain. In *2010 IEEE Sensor Array and Multichannel Signal Processing Workshop*, pages 41–44. IEEE, 2010. [76](#)
- [153] S. Oldham and A. Fornito. The development of brain network hubs. *Developmental cognitive neuroscience*, 2018. [120](#), [121](#)

- [154] B. Pakkenberg, D. Pelvig, L. Marner, M. J. Bundgaard, H. J. G. Gundersen, J. R. Nyengaard, and L. Regeur. Aging and the human neocortex. *Experimental gerontology*, 38(1-2):95–99, 2003. [70](#)
- [155] E. M. Pellegrino and E. Ghibaudi. Entropy from Clausius to Kolmogorov: historical evolution of an open concept. [108](#)
- [156] A. E. Pereda. Electrical synapses and their functional interactions with chemical synapses. *Nature Reviews Neuroscience*, 15(4):250, 2014. [89](#), [90](#)
- [157] Y. B. Pesin. Characteristic Lyapunov exponents and smooth ergodic theory. *Dynamical Systems: Collection of Papers*, 1:37, 1991. [117](#)
- [158] H. Poincaré. *Les méthodes nouvelles de la mécanique céleste: Solutions périodiques. Non-existence des intégrales uniformes. Solutions asymptotiques.-t. 2. Méthodes de MM. Newcomb, Gylden, Lindstedt et Bohlin.-t. 3. Invariants intégraux. Solutions périodiques du deuxième genre. Solutions doublement asymptotiques*, volume 1. Gauthier-Villars, 1892. [18](#)
- [159] H. Price. The thermodynamic arrow: puzzles and pseudo-puzzles. In *Time and matter*, pages 209–224. World Scientific, 2006. [110](#)
- [160] D. E. Purves, G. J. Augustine, D. E. Fitzpatrick, L. C. Katz, et al. Neuroscience. 1997. [70](#)
- [161] P. Reynaud-Bouret, C. Tuleau-Malot, V. Rivoirard, and F. Grammont. Spike trains as (in) homogeneous poisson processes or hawkes processes: non-parametric adaptive estimation and goodness-of-fit tests. *Journal of Mathematical Neuroscience*, 2013. [76](#)
- [162] D. Rickles, P. Hawe, and A. Shiell. A simple guide to chaos and complexity. *Journal of Epidemiology & Community Health*, 61(11):933–937, 2007. [11](#)
- [163] M. Rosenblum, A. Pikovsky, J. Kurths, C. Schäfer, and P. A. Tass. Phase synchronisation: from theory to data analysis. In *Handbook of biological physics*, volume 4, pages 279–321. Elsevier, 2001. [97](#)

- [164] O. Rossler. An equation for hyperchaos. *Physics Letters A*, 71(2-3):155–157, 1979. [30](#), [34](#)
- [165] O. E. Rössler. An equation for continuous chaos. *Physics Letters A*, 57(5):397–398, 1976. [30](#), [34](#)
- [166] D. Ruelle. Thermodynamic formalism. The mathematical structures of classical equilibrium statistical mechanics, volume 5 of encyclopedia of mathematics and its applications, 1978. [117](#)
- [167] D. Ruelle. *Chaotic evolution and strange attractors*, volume 1. Cambridge University Press, 1989. [114](#), [116](#), [117](#)
- [168] C. Runge. Über die numerische auflösung von differentialgleichungen. *Mathematische Annalen*, 46(2):167–178, 1895. [36](#)
- [169] M. Sandri. Numerical calculation of Lyapunov exponents. *Mathematica Journal*, 6(3):78–84, 1996. [26](#), [28](#), [29](#)
- [170] H. K. Sarmah. Period doubling bifurcation and feigenbaum universality in rössler system. *Journal of Global Research in Mathematical Archives (JGRMA) An UGC Approved Journal*, 1(9), 2013. [23](#), [29](#), [30](#), [33](#)
- [171] G. N. Saxe, D. Calderone, and L. J. Morales. Brain entropy and human intelligence: A resting-state fMRI study. *PloS one*, 13(2):e0191582, 2018. [118](#), [119](#)
- [172] H. Sayama. *Introduction to the modeling and analysis of complex systems*. Open SUNY Textbooks, 2015. [9](#), [11](#), [13](#), [14](#), [15](#), [16](#), [17](#), [18](#), [19](#), [20](#), [40](#), [42](#), [44](#)
- [173] T. Schreiber. Measuring information transfer. *Physical review letters*, 85(2):461, 2000. [96](#)
- [174] E. Schrödinger. *What is life? The physical aspect of the living cell and mind*. Cambridge University Press Cambridge, 1944. [112](#)
- [175] C. E. Shannon. A mathematical theory of communication. *Bell system technical journal*, 27(3):379–423, 1948. [97](#)

- [176] C. E. Shannon. A mathematical theory of communication. *ACM SIGMOBILE Mobile Computing and Communications Review*, 5(1):3–55, 2001. [108](#), [113](#), [116](#)
- [177] B. K. Shivamoggi. *Nonlinear dynamics and chaotic phenomena: An introduction*, volume 103. Springer, 2014. [18](#)
- [178] T. Siau and A. Bayen. *An introduction to MATLAB® programming and numerical methods for engineers*. Academic Press, 2014. [36](#)
- [179] Y. G. Sinai. On the notion of entropy of a dynamical system. In *Dokl. Akad. Nauk. SSSR*, volume 124, page 768, 1959. [108](#)
- [180] Y. G. Sinai. Metric entropy of dynamical system. *Retrieved March*, 20:2013, 2007. [116](#)
- [181] S. S. Skiena. *The algorithm design manual: Text*, volume 1. Springer Science & Business Media, 1998. [51](#)
- [182] V. A. Smith, J. Yu, T. V. Smulders, A. J. Hartemink, and E. D. Jarvis. Computational inference of neural information flow networks. *PLoS computational biology*, 2(11):e161, 2006. [121](#)
- [183] O. Sporns. *Networks of the Brain*. MIT press, 2010. [73](#)
- [184] E. Steur. Parameter estimation in Hindmarsh-Rose neurons. *Traineeship report*, 2006. [79](#), [80](#)
- [185] M. Storace, D. Linaro, and E. de Lange. The Hindmarsh–Rose neuron model: bifurcation analysis and piecewise-linear approximations. *Chaos: An Interdisciplinary Journal of Nonlinear Science*, 18(3):033128, 2008. [3](#), [75](#), [78](#), [79](#), [87](#), [88](#)
- [186] C. Teeter, R. Iyer, V. Menon, N. Gouwens, D. Feng, J. Berg, A. Szafer, N. Cain, H. Zeng, M. Hawrylycz, et al. Generalized leaky integrate-and-fire models classify multiple neuron types. *Nature communications*, 9(1):709, 2018. [76](#)
- [187] W. Teka. The fractional order leaky integrate-and-fire model: Fractional differentiation-spiking properties. [76](#)

- [188] R. F. Thompson. *The brain: A neuroscience primer*. Macmillan, 2000. 1, 66, 67, 70, 71
- [189] S. K. Thottil and R. P. Ignatius. Nonlinear feedback coupling in Hindmarsh–Rose neurons. *Nonlinear Dynamics*, 87(3):1879–1899, 2017. 88
- [190] J. Travers and S. Milgram. The small world problem. *Psychology Today*, 1(1): 61–67, 1967. 60
- [191] J. Von Neumann. *Mathematische grundlagen der quantenmechanik*, volume 38. Springer-Verlag, 2013. 108
- [192] P. Wallisch, M. E. Lusignan, M. D. Benayoun, T. I. Baker, A. S. Dickey, and N. G. Hatsopoulos. *MATLAB for neuroscientists: an introduction to scientific computing in MATLAB*. Academic Press, 2014. 77
- [193] H. Wang, Q. Wang, Q. Lu, and Y. Zheng. Equilibrium analysis and phase synchronization of two coupled hr neurons with gap junction. *Cognitive neurodynamics*, 7(2):121–131, 2013. 96
- [194] H. Wang, Q. Wang, and Y. Zheng. Bifurcation analysis for Hindmarsh-Rose neuronal model with time-delayed feedback control and application to chaos control. *Science China Technological Sciences*, 57(5):872–878, 2014. 87
- [195] H. Wang, Y. Zheng, and Q. Lu. Stability and bifurcation analysis in the coupled hr neurons with delayed synaptic connection. *Nonlinear Dynamics*, 88(3):2091–2100, 2017. 88
- [196] Z. Wang, Y. Li, A. R. Childress, and J. A. Detre. Brain entropy mapping using fMRI. *PloS one*, 9(3):e89948, 2014. 118, 119
- [197] Watts, Duncan J and Strogatz, Steven H. Collective dynamics of ‘small-world’ networks. *nature*, 393(6684):440, 1998. 60, 63, 74
- [198] W. Weaver. Recent contributions to the mathematical theory of communication. *ETC: a review of general semantics*, pages 261–281, 1953. 98

- 
- [199] N. Wiener. *Cybernetics or control and communication in the animal and the machine* (vol. 25). *MIT Press*, 10:13140–000, 1961. [137](#)
- [200] A. Wilmer, M. de Lussanet, and M. Lappe. Time-delayed mutual information of the phase as a measure of functional connectivity. *PloS one*, 7(9):e44633, 2012. [96](#)
- [201] Y. Wu, Y. Gong, and Q. Wang. Random coupling strength-induced synchronization transitions in neuronal network with delayed electrical and chemical coupling. *Physica A: Statistical Mechanics and its Applications*, 421:347–354, 2015. [90](#)
- [202] L.-S. Young. Entropy in dynamical systems. *Entropy*, 313, 2003. [114](#), [115](#), [116](#), [119](#)
- [203] F. Zaidi. Small world networks and clustered small world networks with random connectivity. *Social Network Analysis and Mining*, 3(1):51–63, 2013. [62](#)
- [204] J. E. Zull. *From brain to mind: Using neuroscience to guide change in education*. Stylus Publishing, LLC., 2012. [2](#)